



HAL
open science

Lithospheric folding and sedimentary basin evolution: a review and analysis of formation mechanisms

Sierd Cloething, Evgenii E.B. Burov

► To cite this version:

Sierd Cloething, Evgenii E.B. Burov. Lithospheric folding and sedimentary basin evolution: a review and analysis of formation mechanisms. *Basin Research*, 2011, 23 (3), pp.257-290. 10.1111/j.1365-2117.2010.00490.x . hal-00640964

HAL Id: hal-00640964

<https://hal.science/hal-00640964v1>

Submitted on 24 Nov 2011

HAL is a multi-disciplinary open access archive for the deposit and dissemination of scientific research documents, whether they are published or not. The documents may come from teaching and research institutions in France or abroad, or from public or private research centers.

L'archive ouverte pluridisciplinaire **HAL**, est destinée au dépôt et à la diffusion de documents scientifiques de niveau recherche, publiés ou non, émanant des établissements d'enseignement et de recherche français ou étrangers, des laboratoires publics ou privés.



Lithospheric folding and sedimentary basin evolution: a review and analysis of formation mechanisms

Journal:	<i>Basin Research</i>
Manuscript ID:	BRE-070-2009.R1
Manuscript Type:	Original Article
Date Submitted by the Author:	
Complete List of Authors:	Cloetingh, Sierd; VU University, Earth & Life Sciences Burov, Evgenii; Université Pierre et Marie Curie, Laboratoire de Tectonique
Keywords:	tectonics and sedimentation, geodynamics, rift basins, foreland basins, Intracratonic basins, strike-slip basins, tectonic geomorphology

Only

1
2
3
4 1 **Lithospheric folding and sedimentary basin evolution:**
5
6 2 a review and analysis of formation mechanisms
7
8
9 3
10 4
11
12 5
13

14 6 **Sierd Cloetingh^{a,*} and Evgenii Burov^b**
15
16 7

18 8 ^aNetherlands Research Centre for Integrated Solid Earth Sciences, Faculty of Earth and Life
19 9 Sciences, VU University Amsterdam, De Boelelaan 1085, 1081 HV Amsterdam, The Netherlands.
20
21 10

23 11 ^bUniversité Pierre et Marie Curie, Laboratoire de Tectonique, 4 Place Jussieu,
24 12 75252 Paris Cedex 05, France.
25
26 13
27
28 14
29

30 15 **Basin Research**
31
32 16

34 17 Submitted: August 17, 2009
35
36 18

37 19 Revised: March 18, 2010
38
39 20
40
41 21
42
43 22
44
45 23
46
47
48
49
50
51
52

54 * Corresponding author: Fax: +31-20- 598 99 43

55 *E-mail addresses:* sierd.cloetingh@falw.vu.nl (Sierd Cloetingh), evgenii.burov@upmc.fr (Evgenii Burov)
56
57
58
59
60

24 **ABSTRACT**

25 Lithospheric folding is an important mode of basin formation in compressional intraplate settings.
26 Basins formed by lithospheric folding are characterized by distinct features in subsidence history. A
27 comparison with extensional basins, foreland basins, intracratonic basins and pull-apart basins
28 provides criteria for the discrimination between these modes of basin formation. These findings are
29 important in deciphering the feed-backs between tectonics and surface processes. In addition,
30 inferences on accommodation space and thermal regime have important consequences for
31 hydrocarbon maturity. Lithospheric folding is coupled to compressional basin and fault reactivation
32 and, therefore, strongly affects reservoir characteristics of sedimentary basins.

35 **INTRODUCTION**

37 Over the last few years much progress has been made in understanding the mechanisms of the
38 formation of sedimentary basins (Cloetingh & Ziegler, 2007; Roure et al., 2010). Quantitative
39 models for several basin types have significantly advanced the understanding of extensional
40 (McKenzie, 1978; Van Wees *et al.*, 2009) and foreland basins (Beaumont, 1981; Naylor & Sinclair,
41 2008). The mechanisms of basin formation as a result of lithospheric folding have received
42 considerably less attention (Cloetingh & Ziegler, 2007) except for some clear-cut cases, in particular
43 in central Asia (Burov & Molnar, 1998; Thomas *et al.*, 1999a,b). Many data exist on the geometry of
44 sedimentary basins affected by large-scale compressional intraplate deformation (Cobbold *et al.*,
45 1993; Lefort & Agarwal, 1996, 2000, 2002; Burov & Molnar, 1998). These observations and results
46 of analytical, numerical (Martinod & Davy, 1992; Burov *et al.*, 1993; Gerbault *et al.*, 1998; Cloetingh
47 *et al.*, 1999) and analogue modelling (Martinod & Davy, 1994; Sokoutis *et al.*, 2005) demonstrate
48 that the thermo-mechanical age of the lithosphere exerts a prime control on the wavelength of
49 lithospheric folds. These studies focused on the role of tectonic stress in lithospheric folding

1
2
3 50 (Stephenson *et al.*, 1990; Burov & Molnar, 1998; Stephenson & Cloetingh, 1991; Perez-Gussinye &
4
5 51 Watts, 2005). However, surface processes also play a significant role in the mechanics of
6
7 52 lithospheric folding. Erosion enhances the development of folding and has a pronounced effect on
8
9
10 53 its wavelengths (Cloetingh *et al.*, 1999; Burov & Toussaint, 2007), specifically in the short-
11
12 54 wavelength domain. In addition, both sedimentation and erosion are likely to significantly prolong
13
14 55 the lifetime of folding. Sedimentation decreases the effect of gravity by filling the downward flexed
15
16 56 basins and thus reducing the isostatic restoring force, whereas erosion of the upward flexed
17
18 57 basement unloads the lithosphere on the basins' uplifted flanks. Lithospheric folding has significant
19
20 58 effects for the geometry of sedimentary sequences deposited on folded lithosphere. However, the
21
22 59 effect has been studied little for several reasons (Cobbold *et al.*, 1993). The hanging walls of
23
24 60 emerging low-angle thrust faults tend to collapse rapidly, blurring the structural relationships at
25
26 61 basin edges. Further, ongoing sedimentation may onlap and bury the hanging walls, whereas scarp
27
28 62 erosion may destroy them. Seismic images of basin edges may not be well resolved where footwall
29
30 63 conglomerates contain few reflecting horizons or when low-angle thrusts reflect and refract seismic
31
32 64 waves, thus hampering the imaging of deeper parts of the basin. Downwarping of folded basins
33
34 65 renders surface geological mapping difficult. At the same time, high plateaux are not at first sight
35
36 66 linked with basins of high hydrocarbon potential, leaving them in many places without well control or
37
38 67 seismic constraints on basin architecture.

39
40
41
42 68 In this paper we review evidence from a number of basins in Eurasia, where folding has been
43
44 69 documented and alternative basin formation mechanisms such as lithospheric extension or foreland
45
46 70 flexure cannot fully explain key features of basin geometry and evolution. We restrict ourselves to
47
48 71 cases where independent evidence points to a major role for lithospheric folding in the basin
49
50 72 development. We demonstrate that an interpretation in terms of folding can sometimes resolve
51
52 73 inconsistencies resulting from interpreting basins origin via other mechanisms. For example
53
54 74 (Ritzmann & Faleide, 2009), the formation mechanism of intracratonic basins is still a matter of
55
56 75 debate. A striking feature of these basins is the prolonged intervals of low rate subsidence
57
58
59
60

1
2
3 76 alternating with episodic accelerations in subsidence rates, often coeval with orogenic activity at
4
5 77 plate boundaries. Due to the frequent absence of evidence for thinned lithosphere below these
6
7 78 basins, alternative models have been proposed. Stel *et al.* (1993) propose that non-extensional
8
9 79 crustal thinning is induced by basaltic underplating, which causes thermal uplift and erosional
10
11 80 thinning. Tectonic loading at plate boundaries is also proposed as a cause of or contributor to large-
12
13 81 scale sag-type subsidence in plate interiors (Cloetingh, 1988; Leighton & Kolata, 1990; Quinlan,
14
15 82 1987) as well as phase transformations (Artyushkov, 2007). Ritzmann & Faleide (2009) point out
16
17 83 that intraplate stresses and crustal inhomogeneities coupled with loading scenarios provide the best
18
19 84 explanation for the Barents Sea Basin and other intracratonic basin evolution. The basins reviewed
20
21 85 here, however, do not include cases such as the Barents Sea where the effect of stresses on
22
23 86 topography and accommodation space has been considerably complicated by other basin formation
24
25 87 processes.

26
27
28
29 88 We present inferences from thermo-mechanical models of lithospheric folding and a comparison
30
31 89 with the results of analogue modelling of folding. We concentrate on the overall geometry of basins
32
33 90 formed by lithospheric folding, the typical timescales intrinsic to their development and the brittle
34
35 91 deformation patterns in the underlying lithosphere. We then discuss subsidence patterns and heat
36
37 92 flow characteristics for such basins. We conclude by comparing key features of basin
38
39 93 accommodation shape, vertical motions, thermal history and brittle deformation patterns of basins
40
41 94 formed on folded lithosphere, foreland basins, intracratonic basins, extensional basins and pull-
42
43 95 apart basins.

44
45
46 96
47
48
49 97 **LITHOSPHERIC FOLDING: AN IMPORTANT MODE OF INTRAPLATE BASIN FORMATION AND**
50
51 98 **DEFORMATION**

52
53 99
54
55 100 Folding of the lithosphere, involving positive and negative deflections (**Fig. 1**), appears to be of
56
57 101 more importance in the large-scale deformation of intraplate domains than hitherto realized
58
59
60

1
2
3 102 (Cloetingh *et al.*, 1999). As has been shown (Burov *et al.*, 1993; Nikishin *et al.*, 1993; Cloetingh *et*
4
5 103 *al.*, 1999; Gerbault *et al.*, 1998; Schmalholtz & Podladchikov, 2000), visco-elastic folding starts to
6
7 104 develop from the onset of compression and in contrast to elastic folding, does not require
8
9
10 105 specifically large intraplate stresses. Folding may continue until the back-ground strain-rate drops,
11
12 106 for example due to the localization of deformation in a specific area or to reduction of far-field
13
14 107 forces. Such intraplate deformation results from transmission of intraplate stress fields away from
15
16 108 plate boundaries into continental forelands (Ziegler *et al.*, 1998; Van der Pluijm *et al.*, 1997; Tesauro
17
18 109 *et al.*, 2005).

19
20 110 In continental lithosphere, several wavelengths of folding are expected to develop as result of the
21
22 111 presence of several rheologically competent layers decoupled from each other by weak layers (**Fig.**
23
24 112 **1, Fig. 3**). Crustal folding can be traced from the surface topography, neotectonic movements and
25
26 113 free air gravity. The crust-mantle boundary (Moho) topography reflects mantle folding, because the
27
28 114 mantle strength is highest at this interface and thus the geometry of Moho deflection is most likely to
29
30 115 correspond to that of mantle folding. This wavelength can be traced from Bouguer gravity anomalies
31
32 116 because the crust-mantle boundary represents also the main density contrast in the lithosphere. It is
33
34 117 to be expected that the base of the Mechanical Lithosphere (MLB) has roughly the same geometry
35
36 118 as the Moho deflection. Likely, the lithosphere-asthenosphere boundary (LAB) has little to do with
37
38 119 mantle lithosphere folding except some specific cases, as the MLB (roughly corresponding to 700°C
39
40 120 depth) is found well above the LAB (1330°C) . Consequently, the low viscosity zone between MLB
41
42 121 and LAB may damp the deformation in a way that the LAB remains even flat. Due to the low
43
44 122 viscosity of gravitating mantle between the LAB and MLB, the LAB is not necessarily advected or
45
46 123 down-warped with deflection of the MLB, or at least the relations between the deformation of the
47
48 124 MLB and LAB are not straightforward. In particular, gravity instabilities or convective movements not
49
50 125 related to folding can perturb the LAB without impact on the MLB.
51
52
53
54
55 126

1
2
3 127 Folding has important implications for vertical motions, sedimentary basin architecture and the
4
5 128 evolution of hydrocarbon systems (Ziegler *et al.*, 1995; 1998). The large wavelength of vertical
6
7 129 motions associated with lithospheric folding necessitates the integration of data from large areas
8
9
10 130 (Elfrink, 2001; Allen & Davies, 2007), often beyond the scope of regional structural and geophysical
11
12 131 studies that target specific structural provinces. Recent studies on the North German Basin show
13
14 132 neotectonic reactivation by lithospheric folding (Marotta *et al.*, 2000). Similarly, acceleration of the
15
16 133 Plio-Pleistocene subsidence in the North Sea Basin is attributed to stress-induced buckling of its
17
18 134 lithosphere (Van Wees & Cloetingh, 1996). Folding of the Variscan lithosphere has been
19
20 135 documented for Brittany (Bonnet *et al.*, 2000; Lagarde *et al.*, 2000), the adjacent Paris Basin (Lefort
21
22 & Agarwal, 1996) and the Vosges-Black Forest arch (Dèzes *et al.*, 2004; Ziegler & Dèzes, 2007;
23
24 136 Bourgeois *et al.*, 2007). Lithospheric folding, therefore, appears to be an effective mechanism for the
25
26 137 propagation of tectonic deformation from active plate boundaries far into intraplate domains (e.g.
27
28 138 Stephenson & Cloetingh, 1991; Burov *et al.*, 1993; Ziegler *et al.*, 1995, 1998).
29
30 139
31 140 Folding can be observed at different spatial scales. At the scale of a micro-continent that was
32
33 141 affected by a succession of collisional events, Iberia illustrates lithospheric folding and interplay
34
35 142 between neotectonics and surface processes (Cloetingh *et al.*, 2002). An important factor favouring
36
37 143 a lithosphere-folding scenario for Iberia is the compatibility of the thermo-tectonic age of its
38
39 144 lithosphere and the wavelength of observed deformations.
40
41
42 145 Other well-documented examples of continental lithospheric folding occur in other cratons (**Fig. 2**).
43
44 146 Prominent examples occur in the Western Gobi area, in the Ferghana basin, but also probably in
45
46 147 the Tadjik basin of Central Asia, involving a lithosphere with thermo-tectonic ages from 150 Ma
47
48 148 (Kazakh shield, Ferghana, Tadjik basins and likely Dzhungaria basin) to 400 Ma (Tarim basin). In
49
50 149 this area, mantle and crustal wavelengths are 360 km and 50 km, respectively, with a shortening
51
52 150 rate of ~10-20 mm/yr and 200-250 km of shortening during 10-15 Myr (Burov *et al.*, 1993; Burov &
53
54 151 Molnar, 1998). Three-dimensional fold structures in the Tibetan Plateau have been inferred from
55
56
57
58
59
60

1
2
3 152 GRACE satellite gravity data, demonstrating prevailing fold wavelengths of 300 to 420 km (Shin *et*
4
5 153 *al.*, 2009).

6
7
8 154 The inferred wavelength of these neotectonic lithosphere folds is consistent with the general
9
10 155 relationship between the wavelength of lithospheric folds and the thermo-tectonic age of the
11
12 156 lithosphere shown by a global inventory of lithospheric folds (**Fig. 3**) (Cloetingh & Burov, 1996;
13
14 157 Cloetingh *et al.*, 2005). In some other areas of continental lithosphere folding, smaller wavelength
15
16 158 crustal folds have also been detected (Burov *et al.*, 1993; Nikishin *et al.*, 1993). Thermal thinning of
17
18 159 the mantle lithosphere, often associated with volcanism and doming, enhances lithospheric folding
19
20 160 and appears to affect the wavelengths of folds (Burov & Cloetingh, 2009).

21
22
23 161

24 25 162 **OBSERVATIONS**

26
27 163 Basins developed on folded continental lithosphere have characteristic features. We illustrate this
28
29 164 by largely concentrating on the basins of Central Asia, the folded lithosphere of Iberia, the NW
30
31 165 European platform, the Pannonian Basin and the South Caspian Basin.

32
33
34 166

35 36 167 **Compressional basins of Central Asia (Tianshan, Ferghana)**

37
38 168 The young Ferghana and Tadjik basins are compressional basins northwest and north of the Pamir
39
40 169 and south of the Tien Shan ranges (Burov & Molnar, 1998). In this area lithosphere underwent
41
42 170 Jurassic reactivation and is characterized by relatively young thermo-mechanical ages (175 Ma)
43
44 171 (Burg *et al.*, 1994; Burov & Molnar, 1998). In addition to having undergone thermal weakening, the
45
46 172 lithosphere underlying these basins also probably has a weak, quartz-dominated lower crustal
47
48 173 rheology. This has resulted in low values for the effective elastic plate thickness (EET) of the order
49
50 174 of 15 km (Burov & Molnar, 1998).

51
52
53 175 The Central Tien Shan consists of an alternation of ranges and basins separated by reverse faults.

54
55 176 The Tien Shan terminates west of the right-lateral Talas-Ferghana fault by splaying into two narrow
56
57
58
59
60

1
2
3 177 mountain chains that surround the Ferghana Valley. A narrow belt of mountains parallel to the
4
5 178 central section of the fault slopes downward to the Ferghana Valley, underlain by a deep basin with
6
7 179 as much as 8 km of Cretaceous-Cenozoic sediments (Cobbold *et al.*, 1993). Gravity data suggest
8
9 180 that the Ferghana and Tadjik basins are gravitationally overcompensated. The negative Bouguer
10
11 181 gravity anomalies indicate a Moho several km deeper than predicted by models of local Airy
12
13 182 isostasy (Burov & Molnar, 1998). This points to Moho down-warping due to non-isostatic processes
14
15 183 and most probably, in this compressional context, to lithospheric folding. As demonstrated by
16
17 184 numerical-thermomechanical experiments (Burov & Molnar, 1998), the approximately north-south
18
19 185 shortening of the relatively thin lithosphere could have created central down-warping and anticline
20
21 186 mountains north and south of the basin. According to this model, this shortening has produced a
22
23 187 folding instability in the mantle lithosphere that has warped the basement immediately surrounding
24
25 188 the basin upward, and has forced the basin floor down beneath the Ferghana Valley (with an
26
27 189 estimate for the folding wavelength of the order of 200-250 km), possibly also producing deep
28
29 190 mantle faulting (seen as Moho offsets in seismic reflection data).

30
31
32
33 191 Pre-existing thermal structure and variations in crustal thickness have played a major control on the
34
35 192 styles and distribution of faulting in this region (**Fig. 4**), (see also Burov & Molnar 1998; Cobbold *et*
36
37 193 *al.*, 1993). Primary faults appear before the folding develops with a spacing that is proportional to
38
39 194 brittle layer thickness. Subsequently the two processes, faulting and folding, co-exist in such a way
40
41 195 that faults localize at the inflection points of folds. At this stage, the appearance of faults does not
42
43 196 significantly influence the wavelength of folding. Because of the weakness of the lower crust, the
44
45 197 upper crust should be completely decoupled from the mantle and interact with it only by flow in the
46
47 198 lower crust. Lower crustal flow changes the wavelength and amplitude of the surface folding, which
48
49 199 is terminated by the development of a single down-warped megafold (Cloetingh *et al.*, 1999). Liu *et*
50
51 200 *al.* (2007) reported evidence for lithospheric folding in the Central/ North China Tarim Basin region,
52
53 201 initiated during Pliocene times, with good time constraints provided by Ar/Ar dating. Two
54
55 202 wavelengths are found of 30 and 400 km. The thermo-mechanical age of the lithosphere is
56
57
58
59
60

1
2
3 203 estimated to be 250 Ma, as the main thermal perturbation was associated with a major orogenic
4
5 204 phase at 250 Ma ago. These findings are consistent with models in which decoupled lithosphere
6
7 205 folds with 30 km and 400 km wavelength correspond to, respectively, crustal and mantle folding.
8
9
10 206 Deep seismic data for basins north of and within the Tibetan plateau (Li *et al.*, 2006; Liu *et al.*, 2006;
11
12 207 Zhao *et al.*, 2006) show that folding is not limited to the Tibetan plateau (see also Shin *et al.*, 2009).
13
14 208

16 209 **Folded lithosphere of Iberia**

17
18 210 As reviewed by Cloetingh *et al.* (2002), Tertiary lithospheric folding of Iberia occurs in Variscan
19
20 211 lithosphere with wavelengths of 300 km, leading to the development of a system of parallel trending
21
22 212 basins and highs (**Fig. 5a**). This folding generated the distribution of basins and mountain chains,
23
24 213 bounded by folds and faults (Cloetingh *et al.*, 2002; De Vicente *et al.*, 2007). The regularity of the
25
26 214 fluvial network pattern of the central-western part of Iberia also indicates large-scale lithospheric
27
28 215 folding. Alpine (mainly Cantabrian-Pyrenean related) compressional tectonics was the principal
29
30 216 factor for closing internally drained sedimentary basins, including the Ebro, Duero and Tagus basins
31
32 217 (Casas-Sainz & De Vicente, 2009).
33
34

35
36 218 A large body of geophysical and geological observations is available on the crustal geometries and
37
38 219 stress regimes of Iberia (De Vicente *et al.*, 2007, 2008). This is supplemented by thermo-
39
40 220 geochronology data (De Bruijne & Andriessen, 2002; Ter Voorde *et al.*, 2004), demonstrating
41
42 221 accelerated uplift of the highs during Late Miocene-Pliocene times. In spite of the existence of
43
44 222 recent localized volcanism in the inner part of the Iberian plate, an important contribution from
45
46 223 thermal uplift is questionable due to the distribution of crustal thickness (Casas-Sainz & De Vicente,
47
48 224 2009). Fernandez-Lozano *et al.* (2010) have constructed a three-layer analogue model consisting of
49
50 225 brittle upper crust, ductile lower crust and ductile upper mantle for Iberia. These models show that
51
52 226 folding is associated with deformation of narrow mountain ranges separated by basins (see **Fig.**
53
54
55 227 **5b**). The narrow mountain ranges representing upper crustal pop-ups form the main topographic
56
57 228 reliefs. Shortening is accommodated within the viscous crust beneath the pop-ups leading to lateral
58
59
60

1
2
3 229 thickness variations of the ductile crust. These results are consistent with seismic and gravity data
4
5 230 collected in the Cantabrian mountains, the Spanish Central System, and the Toledo Mountains (see
6
7 231 also **Fig. 5a**).

8
9 232 The earliest sediments in the terrestrial basins (Calvo et al., 1993) were deposited during the
10
11 233 Eocene, with very well developed continuous successions, dominated by continental facies with
12
13 234 high sedimentation rates. The Duero and Tagus basins began to be individualized at the onset of
14
15 235 uplift and the formation of a topographic range in the Central System (Casas-Sainz & De Vicente,
16
17 236 2009). In contrast with this early more homogeneous stage, the Oligocene-Lower Miocene
18
19 237 stratigraphy of the basins is characterized by several tectono-stratigraphic units, separated by
20
21 238 unconformities representing short periods of time. The number and specific ages of these units
22
23 239 varies between basins, indicating variable activity at basin borders. The fact that the largest number
24
25 240 of breaks in the sedimentary succession is concentrated during this time interval points to a tectonic
26
27 241 control (De Vicente & Vegas, 2009).

28
29 242 The final stages in the evolution of these onshore basins are characterized by widespread Miocene
30
31 243 lacustrine sedimentation in the endorheic basins and during Pliocene and Quaternary times, by the
32
33 244 beginning of river capture and exorheism in the Duero, Ebro and Tagus basins (Garcia-Castellanos
34
35 245 *et al.*, 2003). Alluvial deposits were deposited by the fluvial network developed on the ancient,
36
37 246 internally drained basins (Casas-Sainz & De Vicente, 2009). During the endorheic-exorheic
38
39 247 transition, paleo-karstification processes and erosion occurred in the Late Miocene lacustrine
40
41 248 limestones. Two main types of high plains can be distinguished on the Iberian Peninsula. The
42
43 249 coupled origin of both types of surfaces can be related to uplift/sedimentation histories along the
44
45 250 Tertiary compressional basin margins in the Iberian Peninsula (Casas-Sainz & De Vicente, 2009).
46
47 251 The first are high plains with Tertiary sedimentary basins, containing well preserved Late Miocene to
48
49 252 Pliocene strata with subhorizontal bedding. Typical examples are the Duero and Tagus basins. The
50
51 253 second consists of eroded sediments of Mesozoic and Paleozoic rocks with planation surfaces
52
53 254 developed on the Paleogene-Lower Miocene ranges created by fold and thrust systems and
54
55
56
57
58
59
60

1
2
3 255 basement uplifts. Different patterns in evolution and stratigraphy between the eastern and western
4
5 256 Tagus basin may be related to the mechanical decoupling between Iberia and Africa during the
6
7 257 Miocene emplacement of the Alboran Domain in the southern part of the plate. This generated
8
9
10 258 extensional stresses in the eastern Iberian plate, coeval with compression and lithospheric folding in
11
12 259 the western part of the plate (De Vicente *et al.*, 2008; De Vicente & Vegas, 2009).

13
14 260 In general the dimensions of peneplains linked to extensional basins and passive margins are
15
16 261 larger, and their evolution involves time scales much longer than those characteristic for high plains
17
18 262 of the Iberian plate (Casas-Sainz & De Vicente, 2009). Peneplains associated with compressional
19
20 263 or convergent regimes (e.g. Anatolia, Central Iran and Morocco) are characterized by spatial
21
22 264 dimensions comparable with Iberia. In addition, their tectonic setting in the hanging wall of the
23
24 265 African-Eurasian convergence zone is also similar. Thus the Iberian plate may be an analogue for
25
26 266 other present-day intra-mountain basins.

27
28
29 267

30 31 268 **The European Alpine foreland**

32
33 269 Geophysical and geomorphological studies (e.g. Lefort & Agarwal, 1996; 2000; 2002; Marotta *et al.*,
34
35 270 2000) indicate large-scale compressional deformation of the European Alpine foreland lithosphere.
36
37 271 Although different in structural grain and rheological structure (Tesauro *et al.*, 2007; Cloetingh *et al.*,
38
39 272 2005) inherited from differences in their Paleozoic-Mesozoic history, different segments of the
40
41 273 lithosphere in the northern Alpine European foreland share many similarities in their Cenozoic
42
43 274 intraplate deformation. Seismic and geological evidence shows that the North German Basin cannot
44
45 275 be explained by classical models of basin formation (Marotta *et al.*, 2000). The basin underwent a
46
47 276 polyphase history (Scheck & Bayer, 1999; Littke *et al.*, 2008) of extension in the late Triassic
48
49 277 followed by lithospheric scale folding in the late Cretaceous-Early Cenozoic (Mazur *et al.*, 2005;
50
51 278 Marotta *et al.*, 2000). 3D volumetric analysis shows that the compressional event was followed by
52
53 279 faster subsidence during the Cenozoic (Scheck & Bayer, 1999). A similar observation was made by
54
55 280 Van Wees & Cloetingh (1996) for the North Sea Basin. Lithospheric folding modified a basin formed
56
57
58
59
60

1
2
3 281 initially by deep seated thermal perturbations (Scheck & Bayer, 1999) with a thinned crust and
4
5 282 shallow Moho. The Moho updoming with a high of 3 km for the height of the bulge in the southern
6
7 283 part of the North German basin appears to be the consequence of flexural buckling of the previously
8
9 284 thinned lithosphere by a compressive stress perpendicular to the strike of the basin.

10 285 From earliest Triassic to Late Jurassic, the Paris Basin (**Fig. 6a**) subsided in an extensional
11
12 286 framework and was larger than the present basin (Guillocheau *et al.*, 2000). The western margin of
13
14 287 the Paris Basin and the rifted Atlantic margin of France were subject to thermal rejuvenation during
15
16 288 Mesozoic extension related to North Atlantic rifting (Ziegler & Dèzes, 2006; Robin *et al.*, 2003).
17
18 289 Subsequent compressional intraplate deformation (Ziegler *et al.*, 1995) also affected the Paris Basin
19
20 290 (Lefort & Agarwal, 1996). Numerical modelling indicates that the amplitude of the compression
21
22 291 induced vertical deflection in the Paris Basin is relatively small, requiring additional mechanisms
23
24 292 such as flexure due to the load by the Alpine system (Bourgeois *et al.*, 2007; Ziegler & Dèzes,
25
26 293 2007). However, periodic deformation at the same wavelength occurs northwest of the Paris Basin
27
28 294 (**Fig. 6 a**, Bourgeois *et al.*, 2007), which would not be the case if the north-eastern part of the basin
29
30 295 was flexed down by the load of the Alps. Bourgeois *et al.* (2007) carefully analysed basement
31
32 296 geometry and timing of vertical motions in the NW European platform. They separate the
33
34 297 contributions from the European Cenozoic Rift System (ECRIS) and the contributions from long-
35
36 298 wavelength folding striking NE and located between the Alpine front and the North Sea. According
37
38 299 to their analysis, the ECRIS developed mostly between 37 and 17 Ma, whereas lithospheric folds
39
40 300 developed between 17 Ma and present, with a wavelength of 270 km and amplitude of 1500 m (see
41
42 301 **Fig. 6b**).

43
44 302 Quaternary folding of the Variscan lithosphere in the area of the Armorican Massif (Bonnet *et al.*,
45
46 303 2000) developed folds with a wavelength of 250 km, pointing to a mantle-lithospheric control on
47
48 304 deformation. The timing and spatial pattern of uplift inferred from river incision studies in Brittany is
49
50 305 incompatible with a glacio-eustatic origin. Therefore, Bonnet *et al.* (2000) related the vertical
51
52 306 motions to deflection of the lithosphere by the present-day NW-SE directed compressional intraplate
53
54
55
56
57
58
59
60

1
2
3 307 stress field. Stress-induced uplift of the area appears to control fluvial incision rates and the position
4
5 308 of the main drainage divides. Leveling studies (LeNotre *et al.*, 1999) indicate its ongoing
6
7 309 deformation.
8
9

10 310

11 311 **Pannonian Basin System**

12 312 Recent studies of the Pannonian Basin system - formed as a Miocene back-arc basin behind the
13
14 313 Carpathian arc - show that active crustal deformation resulted in significant differential vertical
15
16 314 motions during Late Neogene times (Horvath & Cloetingh, 1996; Cloetingh *et al.*, 2005, 2006;
17
18 315 Horvath *et al.*, 2006; Matenco *et al.*, 2007; **Fig. 7a**). The river network in the area is affected by
19
20 316 differential neotectonic crustal motions (Necea *et al.*, 2005; Dombradi *et al.*, 2010).
21
22

23 317 The Late Neogene evolution of the Pannonian Basin is largely controlled by its interaction with the
24
25 318 Carpathian arc and the Adriatic indenter impinging the Pannonian basin lithosphere (e.g. Bada *et al.*,
26
27 319 2001). As a result of the consumption of subductable lithosphere of the European foreland, the
28
29 320 Pannonian basin became locked. At the same time, the continuous N-NE directed indentation of the
30
31 321 Adriatic microplate built up a high level of compressional stresses in the Pannonian Basin. The
32
33 322 structural inversion of the basin is a direct consequence of the temporal changes in the stress field
34
35 323 from extension to compression. Recent studies of the stress field together with an extensive array of
36
37 324 geological and geophysical data have shown that horizontal stresses are transmitted from the plate
38
39 325 boundaries into the interior of the Pannonian Basin (Bada *et al.*, 2007).
40
41
42
43

44 326 The Pannonian Basin is underlain by what is probably the hottest lithosphere of continental Europe,
45
46 327 characterized by a very low lithospheric strength (Tesauro *et al.*, 2007). Miocene extension resulted
47
48 328 in a high level of mantle stretching, leading to a strength distribution with practically zero strength in
49
50 329 the subcrustal lithosphere and lower crust (Cloetingh *et al.*, 2005), making it prone to tectonic
51
52 330 reactivation. Therefore, in this area relatively low compressional stresses induced mainly by plate
53
54 331 boundary interactions, and further amplified by topography-induced stresses (Bada *et al.*, 2001),
55
56 332 could initiate significant intraplate deformation.
57
58
59
60

1
2
3 333 It should be noted that in the Pannonian basin system, seismic tomography (Wortel & Spakman,
4
5 334 2000) supports slab detachment under the adjacent Romanian Carpathians. At the same time, the
6
7 335 seismic tomography shows the presence of a hot upper mantle below the folded lithosphere in the
8
9 336 Pannonian basin. In this area, therefore, the upper mantle structure reflects more the back-arc
10
11 337 extension prior to the folding than the consequences of folding on the density stratification of the
12
13 338 mantle. The reverse is true for the crustal configuration. The geometries imaged by the crustal scale
14
15 339 deep seismic reflection profiling are clearly dominated by compressional structures resulting from
16
17 340 folding (**Fig. 7b**).

18
19
20 341 Quaternary patterns of differential uplift and subsidence with a timing coeval with an increased level
21
22 342 of compressional stresses are interpreted as caused by lithospheric folding (Horvath & Cloetingh,
23
24 343 1996; Cloetingh *et al.*, 2006; Horvath *et al.*, 2006; Bada *et al.*, 2007). Late-stage compressional
25
26 344 deformation of the Pannonian basin is demonstrated to be of key importance for the geometry of
27
28 345 basin fill (Sacchi *et al.*, 1999, see **Fig. 7b**) and for its reservoir structures, both crucial in
29
30 346 assessment of its hydrocarbon potential (Horváth, 1995). Analogue tectonic experiments by
31
32 347 Dombradi *et al.* (2010) further examine accumulation and transmission of stresses in the hot and
33
34 348 weak back-arc lithosphere of the Pannonian basin and the interplay between lithospheric processes
35
36 349 and the intrabasinal topography development. Based on available rheological and seismotectonic
37
38 350 constraints, the basin system is represented by a two-layer model with a 10-15 km thick brittle upper
39
40 351 crust. The lower crust and the mantle are represented by a low-strength layer of 45 km thickness
41
42 352 (Dombradi *et al.*, 2010). The strain rates applied were constrained by GPS velocities (Grenerczy *et*
43
44 353 *al.*, 2005). In the experiments lithospheric folds develop with wavelengths equivalent to 200-250 km
45
46 354 (**Fig. 7c**). The experiments also show that crustal thickness variations largely determine the
47
48 355 localisation of stresses. Topographic profiles extracted by laser scans of the model show that
49
50 356 surface topography reflects long wavelength buckling of the lithosphere. These results are
51
52 357 compatible with Pliocene-Quaternary subsidence, which occurs in the centre of the Pannonian
53
54 358 basin, simultaneously with accelerated uplift at the basin margins. The latter has lead to elevated
55
56
57
58
59
60

1
2
3 359 topography of up to 1 km in areas at the rim of the Pannonian Basin such as the Styrian, Zala and
4
5 360 Transylvanian basins (Cloetingh *et al.*, 2006).
6

7 361
8

9 362 **The South Caspian Basin**

10 363 The South Caspian Basin with an estimated sedimentary thickness up to 20 km (Brunet *et al.*, 2003;
11
12 364 Egan *et al.*, 2009), is probably one the deepest basins in the world. It is flanked by the Alborz
13
14 365 Mountains to the south, with an elevation of 2-4 km (see **Fig. 8**). The transition between basin and
15
16 366 flanking high is abrupt and coincides with a coastline bounded by a major fault system. The
17
18 367 formation of the South Caspian Basin is enigmatic. Attempts to explain it as an extensional basin or
19
20 368 as a foreland basin have been unsuccessful. There is a lack of evidence for basin extension and
21
22 369 both stretching models and topographic loads and slab pull operating on down flexed lithosphere in
23
24 370 foreland basin systems cannot explain differential vertical motions of this order of magnitude. As a
25
26 371 result, phase changes in continental crust have been proposed as a mechanism for the formation of
27
28 372 this superdeep basin (Artyushkov, 2007). A limitation in conclusively resolving the basin formation
29
30 373 mechanism is the lack of multi-channel seismic reflection data capable of imaging crustal structure
31
32 374 below the thick sedimentary sequences. Over the last few years, however, other constraints on the
33
34 375 area have become available (e.g. Guest *et al.*, 2007).
35
36
37
38
39

40 376 **Figure 8** presents a cross section of northern Iran and the South Caspian Basin (Guest *et al.*,
41
42 377 2007). As shown, wavelengths for compressional folding of the lithosphere are typically in the range
43
44 378 of 400 km. Although the actual basin formation mechanism for the Caspian Basin is not well
45
46 379 resolved (e.g. Artyushkov, 2007), late Neogene folding has been affecting a lithosphere probably
47
48 380 thermally reset by middle Late Jurassic marginal basin formation (Guest *et al.*, 2007) with a thermo-
49
50 381 mechanical age at the onset of collision of 130-150 Ma. Satellite data demonstrate an exceptionally
51
52 382 large gravity anomaly over the basin (Kaban *et al.*, 2002). Seismic tomography shows slab
53
54 383 detachment under the Iranian plateau (Hafkenscheid *et al.*, 2006; Alinaghi *et al.*, 2007) beginning at
55
56 384 about 10-15 Ma.
57
58
59
60

1
2
3 385 Basin analysis has shown that basement inversion has occurred 20 Ma ago, simultaneously with
4
5 386 the slowing of Arabian/Eurasian plate convergence and the onset of accumulation of Neogene
6
7 387 clastics in foreland basins (e.g. Fakhari et al., 2008). By 10 Ma, contraction occurred by
8
9 388 underplating of the Arabian crustal units beneath the Iranian plate. Estimated shortening rates from
10
11 389 current geodetic surveys (Vernant *et al.*, 2004) are 7 mm/yr. Results from geothermochronology
12
13 390 demonstrate rapid uplift of the Alborz mountains, with rates of 0.7 km/my exhumation between 6
14
15 391 and 4 Ma (Axen *et al.*, 2001), implying approximately 10 km of uplift. This uplift was nearly
16
17 392 synchronous with rapid South Caspian subsidence (Nadirov *et al.*, 1997) and subsequent folding
18
19 393 (Devlin *et al.*, 1999). South Caspian sedimentation rates locally increased more than tenfold at ca 6
20
21 394 Ma, with more than 10 km of sediments deposited since then. Axen *et al.* (2001) argue that if
22
23 395 approximately 10 km of post 6 Ma sediments are present in this basin, then as much as 20 km
24
25 396 (equivalent to 80 %) of the structural relief of about 25 km between the high Alborz and the
26
27 397 southernmost Caspian basement may be younger than 6 Ma.

28
29 398 Folds in the southernmost Caspian Basin (Devlin *et al.*, 1999) and in the Neogene of the Northern
30
31 399 Alborz foothills imply contraction. The lack of a crustal root under the Alborz Mountains also points
32
33 400 to a flexural support by the South Caspian basement (Axen *et al.*, 2001). The simultaneous reversal
34
35 401 of Zagros strike slip and extrusion of central Iran, coarse Zagros molasse deposition, Dead Sea
36
37 402 transform reorganisation, Red Sea oceanic spreading (Chu & Gordon, 1998) all initiated around $5 \pm$
38
39 403 2 Ma (e.g. Axen et al., 2001; Smit et al., 2010), was interpreted by these authors in terms of a
40
41 404 widespread tectonic event. Slab detachment could explain part of the recent uplift of Iran, but does
42
43 405 not directly explain the simultaneous dramatic subsidence in the adjacent Caspian Basin. However,
44
45 406 slab detachment could have an indirect effect if reducing slab pull forces acting on the downgoing
46
47 407 lithosphere promote the development of compressional stresses in both the downgoing and
48
49 408 overriding plates (Cloetingh *et al.*, 2004; Matenco *et al.*, 2007).

50
51 409 Guest *et al.* (2007) argue in favour of compressional deformation of the South Caspian Basin/Alborz
52
53 410 mountains. This interpretation was largely based on available industrial seismic reflection data and
54
55
56
57
58
59
60

1
2
3 411 gravity data for the basin and followed a similar proposition made for the late-stage deformation of
4
5 412 the adjacent Black Sea (Nikishin *et al.*, 2003; Cloetingh *et al.*, 2008). Guest *et al.* (2007) present
6
7 413 kinematic models, without addressing the reason for the difference in the order of magnitude of the
8
9 414 basin depression and the adjacent high. Analogue experiments (Sokoutis *et al.* 2005) show that
10
11 415 when compression acts on two blocks with contrasting thickness (and rigidity), a major syncline will
12
13 416 develop on top of the suture zone separating these blocks, flanked by an anticline of much lower
14
15 417 amplitude. These results are consistent with predictions from folding theory that as a result of the
16
17 418 acting gravity field, down-warping is mechanically more effective than up-warping against the action
18
19 419 of gravity forces. The presented numerical experiments illustrate this (see for example **Fig. 9**).
20
21
22
23

24
25 421 **Basins on folded lithosphere in Eurasia: differences and similarities in lithospheric**
26
27 422 **deformation and basin habitat**

28
29 423 Comparison of lithospheric deformation in Central Asia, Iberia, the NW European Alpine foreland,
30
31 424 the Pannonian Basin and the South Caspian Basin demonstrates common features compatible with
32
33 425 an interpretation in terms of basins developed on folded lithosphere. Amongst these are their
34
35 426 symmetrical shape, dimensions and the temporal association of their basin formation history with
36
37 427 the build up of intraplate stresses. Important differences can be observed between the Central
38
39 428 Asian and Iberian basins and the South Caspian Basin on one side and the European Alpine
40
41 429 foreland and the Pannonian Basin on the other side.

42
43
44 430 The Central Asian Basins and the basins of the Iberian plate were initiated by Tertiary folding,
45
46 431 whereas the European Alpine foreland underwent a polyphase history, following Carboniferous
47
48 432 and Triassic stretching (Scheck & Bayer, 1999; Le Solleuz *et al.*, 2004), prior to Late Cretaceous-
49
50 433 Early Cenozoic folding. Similarly, the Pannonian Basin, formed by back-arc extension in Miocene
51
52 434 times, was subsequently compressionaly reactivated (Cloetingh *et al.*, 2008). The origin of the
53
54 435 South Caspian Basin is not well resolved, but km scale vertical motions are compatible with a
55
56 436 megafold as a prime control on present-day basin geometry. These differences in evolution have a
57
58
59
60

1
2
3 437 pronounced impact on basin dimensions and on the nature of basin fill. The Central Asian basins,
4
5 438 the folded basins of Iberia, and the South Caspian Basin have a wavelength compatible with
6
7 439 theoretical predictions. In contrast, the fold wavelengths of the European Alpine foreland and the
8
9 440 Pannonian Basin appear to be primarily controlled by the pre-existing geometry of the sediment-
10
11 441 basement interface and pre-existing Moho topography inherited from the pre-folding stage.
12
13 442 Differences occur also in the development of the ranges flanking the basins. In Central Asia and
14
15 443 Iberia, these highs have amplitudes and widths comparable to the prediction for periodic folding,
16
17 444 whereas in the Paris Basin and the North German Basin these highs are less well developed. The
18
19 445 ratio of the depth of the South Caspian Basin to the height of the flanking Alborz Mountains is
20
21 446 compatible with a megafold under this area of dramatic differential topography. The large
22
23 447 amplitudes of folding at the flanks of the Pannonian Basin system are compatible with its extremely
24
25 448 weak rheology. Differences in the amplitude of the highs might also partly result from the differences
26
27 449 in neotectonic shortening. The highs bounding the basins of Iberia, Pannonian Basin, South
28
29 450 Caspian Basin and Central Asia, located relatively close to the site of ongoing convergence, are still
30
31 451 experiencing active uplift. This is much less the case for the low strain deforming areas of the NW
32
33 452 European platform and the North German basin where the peak compression occurred during Late
34
35 453 Cretaceous-Early Cenozoic. Another difference occurs in the depositional regime prevailing in these
36
37 454 basins. The closed basin systems of Central Asia, Iberia and the intra-Carpathian Pannonian Basin
38
39 455 are dominated by continental and lacustrine deposits, whereas capture is usually a late-stage
40
41 456 feature of these basins. The Paris basin of the NW European platform has a basin fill largely
42
43 457 dominated by marine sediments deposited during the pre-folding stage of their evolution, followed
44
45 458 by marine Tertiary successions in the basin centre with truncated basin margins. The creation of
46
47 459 basin highs in this case was in general not capable of interrupting open connections to marine
48
49 460 environments.

50
51 461 A general observation for all these basin systems is the flatness of sedimentary sequences in the
52
53 462 depocentres. Faulting plays a minor role in the basin development. Faulting appears to be
54
55
56
57
58
59
60

1
2
3 463 concentrated at the basin margins, with a highly variable depth extent, varying from upper crustal
4
5 464 scale faults bounding pop-up structures in the Central System of Iberia and the Pannonian Basin to
6
7 465 minor faulting in the basement of the North German Basin. The thermal regimes of the basins are
8
9
10 466 similar with thermal histories strongly affected by subsidence and sediment deposition on down
11
12 467 flexed lithosphere, pre-conditioned by its thermo-mechanical age.

13
14 468

16 469 **THE ROLE OF LITHOSPHERIC RHEOLOGY**

17
18 470 Folding is commonly associated with periodic deformation of layered structures with contrasting
19
20 471 mechanical properties. As a consequence, the harmonic spatial periodicity is often believed to be its
21
22 472 primary, almost synonymous, identifying factor. However, from a mechanical point of view, constant
23
24 473 wavelength is not a necessary requirement. Folding is a compressional instability developing in stiff
25
26 474 layers embedded in a weaker material. The harmonic solution of the equilibrium and conservation
27
28 475 equations is a possible solution (Muehlhaus *et al.*, 1998; Burov & Molnar, 1998; Cloetingh *et al.*,
29
30 476 1999). The physical mechanism of folding is well understood. In a continuous layered medium the
31
32 477 stresses and strains must be continued across the interfaces between the layers. In multi-layer
33
34 478 systems with contrasting mechanical properties (e.g. strong and weak layers) this requirement may
35
36 479 be difficult to satisfy, because the same amount of shortening in a stiffer layer would require much
37
38 480 larger stress than in the neighbouring weaker layer. The system becomes unstable and, in
39
40 481 attempting to reduce the stress and strain unconformities at the interfaces between the layers, starts
41
42 482 to fold (or buckle) in response to very small perturbations. In non-elastic media with strain-
43
44 483 dependent properties, locally increased flexural strain at the fold limbs can create weakened zones
45
46 484 that significantly facilitate further deformation. These weak or softened plastic or viscous zones are
47
48 485 often referred to as inelastic hinges, since the system easily folds at such weakened zones.
49
50 486 Homogeneous shortening of the lithosphere under horizontal compression requires more work than
51
52 487 required by an equivalent amount of shortening by folding. However, shortening by
53
54 488 underthrusting/subduction of the lithosphere may be more mechanically efficient than folding but
55
56
57
58
59
60

1
2
3 489 may be blocked or unable to start immediately after the onset of shortening. For this reason, folding
4
5 490 is likely to be a primary and common response to tectonic compression. Folding probably may
6
7 491 continue, in an attenuated form, even after the beginning of subduction (Cloetingh *et al.*, 1999), or
8
9 492 re-appear when the subduction channel is locked or during the aftermath of collision (Cloetingh *et*
10
11 493 *al.*, 2004; Matenco *et al.*, 2007).

12
13
14 494 The rheological structure of the lithosphere (Watts & Burov, 2003) is a key factor in lithospheric
15
16 495 folding. Compressional stresses must build up to a level comparable with the integrated strength of
17
18 496 the lithosphere in order to induce folding. Prior to the advent of rheological models based on
19
20 497 extrapolation of laboratory experiments (Goetze & Evans, 1979; Carter & Tsenn, 1987) lithospheric
21
22 498 stresses were thought to be incapable of reaching the failure levels required for folding (Turcotte &
23
24 499 Schubert, 2002).

25
26
27 500 The simplest expression of the folding process is in oceanic lithosphere, characterized by an
28
29 501 absence of a rheological stratification, and with thermo-mechanical ages spanning a limited age
30
31 502 window with a maximum of 200 Myr (Geller *et al.*, 1993; Zitellini *et al.*, 2010). Because weak
32
33 503 lithosphere is easier to fold than strong lithosphere, one would expect the first observations of
34
35 504 lithospheric folding from the rheologically weak continental plate interiors. However, the observation
36
37 505 of folding of the relatively strong lithosphere of the central Indian Ocean with a thermo-mechanical
38
39 506 age of 80 Ma and with wavelengths of 200-250 km (Geller *et al.*, 1983; McAdoo & Sandwell, 1985;
40
41 507 Stein *et al.*, 1989; Bull & Scrutton, 1992) triggered the interest in this mode of deformation. There
42
43 508 may be two reasons for this. First, the recognition of folding, by mapping of basin reflectors and
44
45 509 gravity anomalies requires spatial scales of several hundreds of kilometres. This is feasible with
46
47 510 marine geophysical surveys, but generally in excess of the spatial scales covered by land surveys.
48
49 511 An exception has been the systematic mapping of basins in Central Australia, located on strong
50
51 512 lithosphere with a thermo-mechanical age of approximately 700 Ma (Lambeck, 1983; Stephenson &
52
53 513 Lambeck, 1985). The Indo-Australian plate is under an exceptionally high level of compression
54
55 514 (Stein *et al.*, 1989), as a result of its collision with the Eurasian plate. Under these conditions high
56
57
58
59
60

1
2
3 515 stresses might have been more important than the rheology of the plate interior (Beekman et al.,
4
5 516 1996; Gerbault *et al.*, 1998; Gerbault, 2000).

6
7 517 Secondly, folding in oceanic lithosphere is not affected by surface erosion, making it relatively easy
8
9
10 518 to recognize. The presence of only one dominant folding wavelength characteristic of non-stratified
11
12 519 oceanic lithosphere also facilitated a quantitative interpretation. Following the early studies in the
13
14 520 Indian Ocean and in Central Australia in the rear of the Indian-Eurasian collision, attention shifted to
15
16 521 the other side of the plate contact in Central Asia. Large scale folding patterns were recognized
17
18 522 through analysis of geophysical data, including gravity and topography (Burov *et al.*, 1993; Nikishin
19
20 523 *et al.*, 1993; Burov & Molnar, 1998) as well as detailed geological studies (Cobbold *et al.*, 1993).

21
22 524 On the basis of an inventory of currently available results of studies of folded continental
23
24 525 lithosphere, it appears that in general the observed wavelengths of folding follow theoretical
25
26 526 predictions for wavelengths as a function of thermo-mechanical age remarkably well (see **Fig. 3**).

27
28
29 527

30
31 528

32
33 529 **NUMERICAL EXPERIMENTS FOR SELECTED THERMO-MECHANICAL AGES OF**
34
35
36 530 **LITHOSPHERE**

37
38 531

39
40 532 Folding is an unstable deformation that may develop in stratified media with significant competence
41
42 533 contrasts, as occur in the continental lithosphere, in response to horizontal loading (Biot, 1961;
43
44 534 Ramberg, 1961). These instabilities may develop under compression or basal shear as a result of
45
46 535 strain/stress incompatibility on the interfaces between layers of different competence. In the initial
47
48 536 stages of deformation, compressional instabilities cause periodic folds with an exponential growth
49
50 537 rate and a dominant wavelength λ roughly proportional to 5 -10 times the thickness(es) of the
51
52 538 competent layer(s). In the lithosphere, the layer thickness is that of the competent core h . So, $h =$
53
54 539 10-100 km, gives rise to $\lambda = 50-1000$ km.

1
2
3 540 "Biot's", or linear, folding encompasses the cases where compression of the lithosphere takes place
4
5 541 from the beginning, leading to the formation of alternating (synclinal) basins and (anticlinal) highs,
6
7 542 and where the conditions of the linear theory are more or less satisfied (e.g. thin layer
8
9 543 approximation, no strain-softening, plane layers). For linear folding in a Newtonian medium, an
10
11 544 asymptotic relationship derived from the thin layer equilibrium equation is (Biot, 1961; Ramberg,
12
13 545 1961):

$$\lambda_1 = 2\pi h (\mu_{11}/6\mu_{12})^{1/3} \quad (1)$$

16
17
18 546 Here λ_1 is the "Laplacian" dominant wavelength of folding in the absence of gravity, h is the
19
20 547 thickness of the competent layer (crustal or mantle), and μ_{11} and μ_{12} are the effective viscosities (or
21
22 548 competencies) of the strong layer and weak surrounding material, respectively. The above
23
24 549 equation, derived assuming zero gravity, provides estimates of $\lambda_1/h = 20-40$ for typical competence
25
26 550 contrasts. This does not hold for most lithospheric-scale cases, where $\lambda/h = 4 - 6$ is more common
27
28 551 due to the influence of the gravity-dependent terms. A reduction of the normalized characteristic
29
30 552 wavelength to values around 4 is also predicted for power-law rheology or plastic layers (Smith,
31
32 553 1979). For a single stiff viscous layer on top of an inviscid medium, the dominant gravity-dependent
33
34 554 wavelength is (Burov & Molnar, 1998):

$$\lambda_g \sim 2\pi(2h \dot{\epsilon} \mu_{eff} / (\Delta\rho g))^{1/2} \quad (2)$$

35
36
37
38
39
40
41
42 555 where $\Delta\rho$ is the density contrast, $\dot{\epsilon}$ is the strain rate, μ_{eff} is the layers' effective ductile viscosity
43
44 556 (see Appendix A), n is the power-law exponent, and h is the thickness of the competent layer.

45
46
47 557 At large amounts of shortening this deformation may become a-periodic (Hunt *et al.*, 1996) so that
48
49 558 the wavelength and amplitude of folding vary along the deformed transect. Plume-induced periodic
50
51 559 deformation (Burov & Cloetingh, 2009) also includes folding or boudinage caused by shear on the
52
53 560 base of the lithosphere. However, the prime cause for folding of continental lithosphere is tectonic
54
55 561 loading by horizontal far-field forces. For characteristic parameters of various layers within the
56
57
58
59
60

1
2
3 562 continental lithosphere ($h = 10 - 120$ km, $\mu = 10^{19} - 10^{26}$ Pa s; $\Delta\rho = 10 - 600$ kg m⁻³), equations (1-
4
5 563 2) predict folding wavelengths that may vary from 30 km (upper crustal folding) to as high as 600-
6
7 564 800 km. The findings of numerical models (Cloetingh *et al.*, 1999) are in excellent agreement with
8
9 565 analogue tectonic experiments (Sokoutis *et al.*, 2005). Numerical experiments show that the
10
11 566 wavelength and amplitude of folding is largely controlled by the thermo-mechanical age and less by
12
13
14 567 the rate of shortening (Burov & Cloetingh, 2009). Lithospheres older than 500 Ma develop nearly
15
16 568 the same wavelength of folding as 1000 Ma old lithosphere because of the similar nearly stationary
17
18 569 thermal state. Here, therefore, we restrict ourselves to a set of experiments for ages of 150 and 300
19
20
21 570 Ma and convergence rates of 1.5 and 3 cm/yr.

22
23 571 Surface topography and sedimentary deposition is described through diffusion-like erosion laws and
24
25 572 fluvial transport laws (Gossman, 1976; Kirkby, 1986; Leeder, 1991; Beaumont *et al.*, 1992; Kooi and
26
27 573 Beaumont, 1994):

$$dh/dt = \text{div}(k^*(x,h,\nabla h) \nabla h) \quad (\text{slope erosion})$$

30
31
32 574 where h is topography, t is time, x is the horizontal coordinate, k^* is an experimentally established
33
34 575 scale-dependent coefficient of erosion (500 – 1000 m²/y). For simplicity, we used zero order linear
35
36
37 576 diffusion (k^* constant) for the short-range erosion and flat deposition for long-range fluvial transport
38
39 577 (Avouac & Burov, 1996). The hill-slope erosion law ensures conservation of matter but holds only
40
41 578 for small-scales. At large scales it is no longer applicable, and conservation of matter is not
42
43 579 observed, because some sediments are lost due to transport out of the system by long-range
44
45 580 processes.

46
47
48 581 **Figure 9** shows the results of the experiments for relatively young (150 Ma) lithosphere compressed
49
50 582 at rates of 1.5 and 3 cm/yr. Strongly decoupled low-amplitude short wavelength (mantle wavelength
51
52 583 $\lambda = 250$ km) folding developed leading to crustal thickening above a synclinal mantle fold. At later
53
54
55 584 stages, harmonic folding was followed by mega-folding (Cloetingh *et al.*, 1999; Burg &
56
57 585 Podladchikov, 1999). For higher rates of shortening these mantle synclines developed in a mode

1
2
3 586 resembling symmetric subduction. For lower convergence rates (**Fig. 9a**) folding does not develop
4
5 587 due to the low Peclet number of the system, leading to heat diffusion and weakening of folds.
6
7

8 588 Folding is well developed for medium (300 Ma) age lithosphere (**Fig. 10**). This case is characterized
9
10 589 by long mantle wavelengths ($\lambda=360$ km) and high surface amplitudes (2000 m after 10 Myr). These
11
12 590 compare well with observations from Iberia (Fernandez-Lozano *et al.*, 2010), Western Goby and the
13
14 591 Ferghana basin in Central Asia (Burov *et al.*, 1993; Burov & Molnar, 1998). At late stages (10 - 26
15
16 592 Myr since the onset of shortening for 3 cm/y or 20- 50% of shortening), folding becomes aperiodic,
17
18 593 leading to mega-folding (Cloetingh *et al.*, 1999; Burg & Podladchikov, 1999) and subsequent
19
20 594 formation of high-amplitude crustal down-warps. The amplitude of vertical movements may reach 20
21
22 595 km (± 10 km) or even more. As pointed out earlier, such high amplitudes of vertical motions are
23
24 596 observed in the South Caspian Basin (Guest *et al.*, 2007) and the Barents Sea (Ritzmann &
25
26 597 Faleide, 2009). However, it may be relatively rare for folding to continue for periods in excess of 10
27
28 598 Myr. More typically is that at a certain stage deformation localizes along single major fault zones
29
30 599 (Cloetingh *et al.*, 1999; Gerbault *et al.*, 1998).
31
32
33

34 600 As was discussed by Bird (1991), Avouac & Burov (1996) and Cloetingh *et al.* (1999), large-scale
35
36 601 undulations of the lithosphere cannot be preserved for a long time (longer than 10 Myr) in the
37
38 602 absence of sufficient compression, except for plates with very strong (especially lower crustal)
39
40 603 rheology. Otherwise, the folds either will be flattened by gravity-driven crustal flow associated with
41
42 604 the large crust-mantle density contrast at the Moho, or deformation will localize along some of the
43
44 605 faults created at the inflection points of folds.
45
46

47 606 The fact that folding with wavelengths of 400-500 km and 500-600 km persists long after cessation
48
49 607 of the compression in the presumably high-rigidity Australian craton and Russian platform points to
50
51 608 a strong rheology yielding a high value for the effective elastic thickness EET (in excess of 60 km),
52
53 609 as expected from its thermo-mechanical age (Beekman *et al.*, 1997). The long wavelengths of 400-
54
55 610 600 km of crust-mantle down-warping in the eastern Barents Sea, where Mid-Cenozoic
56
57
58
59
60

1
2
3 611 compression has affected a basin system formed during Late Permian-Triassic time (Ritzmann &
4
5 612 Faleide, 2009), with a total infill of sediments of the order of 15-20 km is another impressive
6
7 613 example of compressional deformation on relatively cold lithosphere.

8
9
10 614 Most of the areas with present-day long-wavelength continental lithosphere folding formed during or
11
12 615 short after the Alpine collision 60 Myr ago. It thus seems that 60 Ma is a characteristic timescale of
13
14 616 gravity collapse of the large-scale folds in such intermediate-age lithospheres. In the case of very
15
16 617 weak quartz-dominated lower crust, folds may disappear rapidly within 8-15 Myr. Experiments
17
18 618 (Cloetingh *et al.*, 1999) for 1000 Ma old lithosphere, with a diabase lower crust, demonstrate that
19
20 619 folding-induced deformation persists for 10-50 Myr following the cessation of compression. During
21
22 620 this period the amplitude of the folds decreased by less than 10 percent. At this stage, crustal faults
23
24 621 may accelerate the gravity collapse of folds, creating inverted basins.

26 622

27 623

30 624 **BASIN GEOMETRY AND ACCOMMODATION SPACE**

31 625

32 626 **Basin shape**

33
34
35
36
37 627 Folding of the lithosphere leads to a symmetrical pattern of down-warped areas (synclines) flanked
38
39 628 by highs (anticlines) of similar amplitude and wavelength, like for instance the Ferghana basin in
40
41 629 Central Asia (Burov & Molnar, 1998).

42
43
44 630 This symmetry is in marked contrast to the asymmetrical shape of foreland basins, formed by
45
46 631 flexure in front of an orogenic wedge, which are flanked by a flexural bulge of an amplitude that is
47
48 632 only up to 10 percent of the maximum depth of the foreland depression (Royden, 1988; Zoetemeijer
49
50 633 *et al.*, 1999). Both types of compressional basins show linear nature alignment of parallel
51
52 634 depocentres and flanking highs. An important difference is the presence of parallel trending
53
54 635 depocentres for lithospheric folding, whereas foreland flexural basins have a single depositional
55
56 636 system. In addition, basins developed on folded lithosphere have a static location of the axis of their
57
58
59
60

1
2
3 637 depocentres, in contrast to foreland basins, where the axis of depocentres can migrate with time
4
5 638 (e.g. Zoetemeijer *et al.*, 1993).

6
7 639 In both cases, the integrated strength of the lithosphere (Watts and Burov, 2003; Tesauro *et al.*,
8
9 640 2007) defines the characteristic width of the basins. For folding, basin width roughly corresponds to
10
11 641 one half of the fold wavelength (λ), which equals 5 to 10 times the thickness of the strong core of
12
13 642 the lithospheric plate, h ($h = 10$ to 100 km, i.e. $\lambda = 50 - 1000$ km). In the case of crust-mantle
14
15 643 decoupling, which occurs in relatively young plates, two dominant folding wavelengths develop
16
17 644 (typically $250 - 400$ km and $50-100$ km). Thus two basin populations may be observed, one
18
19 645 imbricated within the other. In the case of flexural foreland deformation, the width of the basin is
20
21 646 controlled by the flexural parameter and is thus of the same order as the largest fold wavelength.
22
23
24
25 647

26 27 648 **Subsidence patterns**

28
29 649 Lithospheric folding results from an instability in the lithosphere due to stress/strain incompatibilities
30
31 650 that develop in rheologically stratified layers under compressive strain. This process typically
32
33 651 operates with timescales of the order of 1-10 Myr (Cloetingh *et al.*, 1999). The preservation of
34
35 652 lithospheric folds appears to depend strongly on the thermo-mechanical age of the underlying
36
37 653 lithosphere (Cloetingh *et al.*, 1999). Folds in young lithosphere will not be preserved upon relaxation
38
39 654 of the stress field, whereas ones in cratonic lithosphere will be well preserved (Cloetingh *et al.*,
40
41 655 1999).

42
43
44 656 **Figure 11a** displays characteristic basin subsidence patterns predicted by folding of 150 and 300
45
46 657 Ma old lithosphere due to a 3 cm/year shortening rate. As illustrated (**Figure 11b**), the differential
47
48 658 motions occur in three distinct phases:

49
50
51 659 **Stage 1** is the basin formation phase, coinciding with the initiation and development of folding,
52
53 660 which is marked by an acceleration of subsidence in the basin and uplift in the flanking highs. As a
54
55 661 result of the time lag between sediment supply and the creation of accommodation space, during
56
57 662 the few Myr needed to form the basin, deposition cannot keep up with subsidence causing
58
59
60

1
2
3 663 sediment-starved basins. A similar pattern occurs in pull-apart basins (Pitman & Golovchenko,
4
5 664 1983) which are also associated with ultra rapid subsidence in their formation stage also lasting only
6
7 665 a few Myr.
8

9
10 666 **Stage 2** is the basin preservation stage, where equilibrium develops between sediment supply and
11
12 667 sediment deposition. As a result the basin will be rapidly filled to overfilled.
13

14 668 **Stage 3** is the basin destruction phase, characterized by basin capture and removal of sediments to
15
16 669 areas outside the folding system. During this phase, the size of the accommodation space is
17
18 670 reduced and erosion occurs on both flanks and depocentre. Thus, the net effect of these three
19
20 671 stages is that lithospheric folding will lead to the development of distinct depositional-erosional
21
22 672 cycles.
23

24
25 673 Characteristic patterns for vertical motions for folding of continental lithosphere of 150 and 300 Ma
26
27 674 old (**Fig. 11**) demonstrate a remarkably short time scale in which substantial amounts of tectonic
28
29 675 subsidence are induced by the process of lithospheric folding. As shown by **Figure 11**, within 1 Myr
30
31 676 after the initiation of folding induced by shortening the lithosphere at a rate of 3 cm/yr, subsidence
32
33 677 rates are in the order of 5-15 km/Myr, depending on the thermo-mechanical age of the lithosphere.
34
35 678 Thus, folding appears to be more effective in middle aged lithosphere of 300 Ma than in lithosphere
36
37 679 of younger ages (Cloetingh *et al.*, 1999; Burov & Cloetingh, 2009). After 2 Myr, a slow uplift phase
38
39 680 starts of relatively minor magnitude of the order of a few hundreds of meters to a km. The predicted
40
41 681 subsidence in **Figure 11** is for the centre of the syncline. As pointed out above, erosion of the
42
43 682 uplifted flanks is taken into account, adopting a diffusive equation approach to erosion (see Burov &
44
45 683 Cloetingh, 1997; Cloetingh *et al.*, 1999, for further details).
46
47

48
49 684 The alignment of parallel highs and basins of similar dimensions has an important consequence for
50
51 685 the areal extent of the source areas for sediments available for deposition in the folded depressions.
52

53 686 In comparison with foreland basins the distribution of sources is more symmetrical, superseding the
54
55 687 volume of sediments that can be eroded from, for example, the flexural foreland bulge. As noted
56
57 688 earlier, erosion reduces the contribution of gravity-dependent terms and accelerates local
58
59
60

1
2
3 689 deformation. Erosion, therefore, has an important feed-back with the geometry of the
4
5 690 accommodation space in changing the spectrum of wavelengths (Cloetingh *et al.*, 1999). Erosion
6
7 691 acts as a filter, suppressing the shorter wavelengths in folded basin topography. Strong erosion,
8
9 692 insufficiently compensated by tectonic deformation, can even wipe out most of the topography.
10
11 693 However, if the erosion is tuned to the average elevation rates (**Fig. 12**), it may dramatically
12
13 694 accelerate folding (Cloetingh *et al.*, 1999).

14
15
16 695 There has been a rapid development and application of stratigraphic modelling packages to
17
18 696 sequence stratigraphy over the last two decades (e.g. Cross, 1989; Alzaga-Ruiz *et al.*, 2008).
19
20 697 Among the different types of modelling programs, the forward stratigraphic modelling approach has
21
22 698 been applied extensively by basin modellers from academia and petroleum industry (e.g. Lawrence
23
24 699 *et al.*, 1990; Granjeon, 2009). Forward stratigraphic modelling commonly starts with an estimate of
25
26 700 the initial conditions related to an adopted basin formation mechanism and controlling parameters,
27
28 701 followed by a forward prediction in time. Most of these software packages are based on sequence
29
30 702 stratigraphic concepts (Wilgus *et al.*, 1988). Assumptions for initial subsidence are either ad-hoc or
31
32 703 related to stretching (e.g. Lawrence *et al.*, 1990) or foreland flexure (Garcia-Castellanos *et al.*,
33
34 704 1997), but to date do not include lithospheric folding as a basin formation mechanism.
35
36
37
38
39

40 706 **Marine versus continental deposits and closed basins versus capture of drainage**

41
42 707 Erosion of uplifted areas and sedimentation in the depressions created by folded lithosphere is a
43
44 708 self reinforcing process promoting continuing uplift of the highs and subsidence in the depocentres.
45
46 709 Thus, such basins will remain closed during much of their evolution. Folded basins will hence be
47
48 710 predominantly characterized by continental deposits with only minor deposition of marine sediments
49
50 711 during marine incursions or during basin capture. This seems to be the case for folded basins in
51
52 712 Iberia (e.g. Duero Basin) and Central Asia (Ferghana, Tarim Basin, Lake Issyk-Kul) (Cobbold *et al.*,
53
54 713 1993). As has been pointed out for flexural foreland basins (Garcia-Castellanos *et al.*, 2003), the
55
56 714 capture time for opening basins decreases with increasing flexural rigidity. The flexural upwarp to
57
58
59
60

1
2
3 715 restoring the topography removed by erosion will be almost instantaneous for very weak
4
5 716 lithosphere, but requires up to 50-100 Myr for high lithospheric rigidities (Garcia-Castellanos *et al.*,
6
7 717 2003). Thus, basins created by folding of cratonic lithosphere probably have a shorter capture time
8
9 718 than ones formed in younger lithosphere.

11 719

14 720 **THERMAL REGIME, STRESS REGIME AND STYLE OF FAULTING**

16 721

18 722 **Thermal regime**

20 723 Lithospheric folding is controlled by the interplay of lithospheric stresses and inherited strength of
21
22 724 the lithosphere. The thermal regime controls the rheological profile and differs between folded
23
24 725 basins developed in young lithosphere and basins in cratonic lithosphere. The latter are associated
25
26 726 with much lower thermal gradients than basins developed on young continental lithosphere. As for
27
28 727 foreland basins, the initiation of folding is not associated with a thermal instability, unless folding
29
30 728 occurs in conjunction with plume activity (Burov & Cloetingh, 2009). Following the deposition of
31
32 729 radiogenic sediments in the folded depression, sediment blanketing will affect the heat flow
33
34 730 (Stephenson *et al.*, 1990; Lavier & Steckler, 1997; Van Wees *et al.*, 2009), modifying the surface
35
36 731 heat flow in the basin centre. As pointed out by Lavier & Steckler (1997) and Ziegler *et al.* (1998),
37
38 732 the effect of sediment fill is to weaken the lithosphere. The low thermal conductivities of the
39
40 733 sediments lead to high temperatures in the upper lithosphere and consequently low local yield
41
42 734 strength. During basin subsidence sediments deposited in the central parts of the basin might be
43
44 735 exposed to temperature windows corresponding to hydrocarbon generation. At the same time,
45
46 736 sediments pre-dating the folding may have undergone extra burial due to syn-folding sedimentation.
47
48 737 An example is the Paris basin, where source rocks of Toarcian age were folded in Cenozoic time
49
50 738 (Guillocheau *et al.*, 2000; Le Solleuz *et al.*, 2004).

51 739 During basin capture overall cooling takes place. This effect is illustrated by characteristic thermal
52
53 740 evolution for different thermo-tectonic ages of 150 and 300 Ma of the folded continental lithosphere,
54
55
56
57
58
59
60

1
2
3 741 incorporating radioactive heat production in the sediments filling in the synclinal depression, shown
4
5 742 in **Figure 13**. Subsidence induced by folding is calculated for the centre of the basin. Basins
6
7 743 developing on folded lithosphere are characterized by their relatively low heat flow at the onset of
8
9 744 folding, followed by a steady increase with time, doubling the heat flow over a time interval of the
10
11 745 order of 5 Myr following the cessation of shortening. This increase is primarily due to the
12
13 746 contribution of radioactive heat production in the very substantial pile of sediments accumulating in
14
15 747 a relatively short time interval. The patterns of heat flow are similar for different thermo-mechanical
16
17 748 ages of the lithosphere, with the oldest lithosphere having the lower heat flow. Older ages enhance
18
19 749 the accommodation space and the contribution of the sediments to heat flow but are compensated
20
21 750 by a larger decrease in heat flow with aging lithosphere. Another important factor is the mode of
22
23 751 folding. Crustal scale folding, which is characteristic for Lake Issyk-Kul, will be associated with
24
25 752 shorter wavelengths, shallower basin depths and thinner sequences of heat producing sediments
26
27 753 than for mantle lithospheric folding. This effect might explain the relatively low heat flow observed in
28
29 754 Lake Issyk-Kul (Vermeesch *et al.*, 2004).
30
31
32

33 755

34 756 **Modes of brittle deformation and faulting**

35
36 757 The role of pre-existing faults on the development of folding has been investigated through
37
38 758 numerical experiments on folding of brittle-elasto-viscous lithosphere (Beekman *et al.*, 1996;
39
40 759 Gerbault *et al.*, 1998; Cloetingh *et al.*, 1999) and through analogue experiments on plastic-elastic
41
42 760 lithosphere (e.g. Martinod & Davy, 1994; Sokoutis *et al.*, 2005). These studies show that lithospheric
43
44 761 folding and faulting can develop simultaneously and that pre-existing crustal scale faults do not
45
46 762 prevent, but instead promote the development of folding instabilities. The instabilities, in turn, can
47
48 763 initiate the formation of new faults at the inflection points of the folds. Although the usual expectation
49
50 764 is that faulting prevents folding, this view neglects the role of the gravity and friction on faults in the
51
52 765 behaviour of the large-scale fault-and-fold systems. As also observed in analogue experiments
53
54 766 (Martinod & Davy, 1994), this continuous behaviour of faulted lithosphere can be explained by fault
55
56
57
58
59
60

1
2
3 767 locking due to gravity and friction. After some sliding (uplift) on a fault, the potential gravitational
4
5 768 energy working against friction generated by horizontal shortening forces becomes too high. As a
6
7 769 result, the fault locks and the rock mass transmits horizontal stresses as a continuous medium. As
8
9
10 770 the compression continues, one of the folds finally starts to grow faster than others, resulting in a
11
12 771 loss of the periodicity and the formation of a mega-fold (see also the discussion in the context of the
13
14 772 Ferghana and Tadjik basins of Central Asia).

15
16 773 Following the initiation of folding, and the further build up of compressional stresses, folding will,
17
18 774 therefore, usually be accompanied by brittle deformation and faulting in the crust and upper
19
20 775 lithosphere. The surface expression of folding in uniform lithosphere is frequently in the form of
21
22 776 fault-controlled pop-up and pop-down structures and inverted basins (e.g. Cobbold *et al.*, 1993),
23
24 777 accompanied by development of imbrications of bivergent thrust wedges at the areas where
25
26 778 shortening is applied (Sokoutis *et al.*, 2005). These findings (see **Fig. 14**) are corroborated by
27
28 779 observations in the Central System of Iberia, where folding of Variscan lithosphere with a thermo-
29
30 780 mechanical age of 280 Ma occurs (Cloetingh *et al.*, 2002). Here the brittle deformation associated
31
32 781 with crustal scale folding expressed by a folded Moho is mechanically decoupled from folding of the
33
34 782 mantle lithosphere (Fernandez-Lozano *et al.*, 2010; see **Fig. 5b**).

35
36 783 Crustal and mantle faults may develop as a result of folding (Burov & Molnar, 1998) (**Fig. 15**).
37
38 784 Folding can continue after these faults develop and folding and faulting can co-exist for times of
39
40 785 several Myr (**Fig. 5b**). For crust-mantle decoupling, a complex distribution of crustal faults and
41
42 786 surface undulations can be expected, with crustal faults not necessarily connected to mantle faults.
43
44 787 Numerical experiments suggest that mantle faults are unlikely to be longer than a few km in depth
45
46 788 (Burov & Molnar, 1998). Such faults may also not develop at longer wavelengths of folding
47
48 789 connected with stronger lithosphere. However, deep seated faults in mantle lithosphere can develop
49
50 790 when cratonic lithosphere is folded (Cloetingh *et al.*, 1999). The mode of faulting, depth extent and
51
52 791 spacing of faults depend on the thermo-mechanical age of the lithosphere. Once the development
53
54 792 of folding begins in a basin, the intensity and depth penetration of faulting will accelerate. The mode
55
56
57
58
59
60

1
2
3 793 of decoupling between crustal and mantle folding is crucial. Discontinuities within the folded
4
5 794 lithosphere will localize the development of deep synclines, flanked by more modest anticlines
6
7 795 (Sokoutis *et al.*, 2005) and affect the distribution of faulting (**Fig. 14**).

8
9
10 796 During the next phase of basin evolution, when a steady state is reached between the creation of
11
12 797 accommodation space and sediment supply, only minor faulting will occur. This is in marked
13
14 798 contrast with the later phase of basin capture, which is in general characterized by erosion and
15
16 799 narrowing of the basin. Due to erosional unloading, stress relaxation will occur, manifested in
17
18 800 upward propagating faults.

19
20
21 801

22 802 **Interaction of folding with other tectonic processes**

23
24 803 Folding, in addition to being a basin forming mechanism, frequently interacts with other tectonic
25
26 804 processes. As pointed out by Cloetingh (1988), intraplate compression can modify pre-existing
27
28 805 basins. As discussed above, the Pannonian Basin of Central Europe created by Miocene back-arc
29
30 806 extension appears to be an example of such a configuration, characterized by a-typical a-periodic
31
32 807 folding. Other examples are cratonic sag basins where intraplate compression (Cloetingh, 1988) is
33
34 808 thought to occur in interaction with phase changes in the lithosphere (Artyushkov, 2007). Examples
35
36 809 of these might be the Barents Sea (Ritzmann & Faleide, 2009) and possibly the South Caspian
37
38 810 Basin, although in the latter case pre-orogenic extension cannot be ruled out (Guest *et al.*, 2007).
39
40 811 Basins exposed to changes in tectonic regime will have a polyphase record (Cloetingh & Ziegler,
41
42 812 2007), characterized by a superposition of more than two regimes, such as pre-orogenic extension,
43
44 813 foreland flexure and late-stage folding. This sequence appears to be characteristic for some very
45
46 814 deep foreland basins, such as the Focsani depression of the Romanian Carpathians, with more
47
48 815 than 16 km of sediments, which was affected by extension due to the opening of the Black Sea
49
50 816 Basin, followed by foreland flexure and overprinted by Late Miocene compression (Tarapoanca *et*
51
52 817 *al.*, 2003). As pointed out above (Ziegler & Dèzes, 2007), the Northwestern European foreland
53
54 818 indicates folding, overprinting, rifting and foreland flexure. Quantification of the topographies created
55
56
57
58
59
60

1
2
3 819 by rifting and foreland flexure and correcting for them is essential to reconstruct the shape of the
4
5 820 additional accommodation shape created by subsequent lithospheric folding (Bourgeois *et al.*,
6
7 821 2007).

8
9
10 822 The impingement of plumes on the base of continental lithosphere can induce differential
11
12 823 topography similar to the surface deflections characteristic for lithosphere folds (Guillou-Frottier *et*
13
14 824 *al.*, 2007; Burov *et al.*, 2007). Plumes and lithospheric folds frequently interact in space and time in
15
16 825 the geological record (Ziegler & Dèzes, 2007; Burov & Cloetingh, 2009). Therefore, the evolution of
17
18 826 folded lithosphere basins can be overprinted by the signatures of a plume or vice-versa. This will
19
20 827 lead to an amplification of the induced vertical motions, particularly significant for young and
21
22 828 intermediate age lithosphere. Emplacement of hot upper mantle material will raise temperatures in
23
24 829 the lithosphere and increase heat flow. Due to the lag time in the propagation of heat, the effect at
25
26 830 the surface might become manifest only after several tens of Myr. Plume emplacement might also
27
28 831 weaken the lithosphere, making it more prone to compressional fault reactivation after cessation of
29
30 832 the folding.

31
32
33 833 Interplay of lithosphere folding and plume impingement on the continental lithosphere occurred
34
35 834 probably almost simultaneously in late Neogene times in the Northwestern European foreland. Two
36
37 835 examples are the Eifel and Massif Central areas of the Alpine foreland of NW Europe (Cloetingh &
38
39 836 van Wees, 2005; Ziegler & Dèzes, 2007). Both areas are sites of main Late Neogene volcanic
40
41 837 activity in the European Cenozoic rift system (ECRIS). Seismic tomography (Ritter *et al.*, 2001)
42
43 838 shows finger shaped baby plumes with a characteristic spatial diameter of 100 km, extending
44
45 839 downward to 400 km. Ziegler & Dèzes (2007) propose that plume activity occurs simultaneously
46
47 840 with recent compressional deformation in the Massif Central area (Guillou-Frottier *et al.*, 2007) and
48
49 841 the Ardennes/Eifel area. Geomorphological studies constrain the recent uplift of the Ardennes and
50
51 842 the Eifel area. An order in magnitude difference occurs between the uplift of the Eifel area, underlain
52
53 843 by a plume and the adjacent Ardennes area where evidence for a plume is lacking. The patterns of
54
55 844 uplift appear to be radial, superimposed by a linear NE-SW trend perpendicular to the main axis of
56
57
58
59
60

1
2
3 845 compression. Baby plumes primarily develop in the anticlines of lithospheric folds (Burov &
4
5 846 Cloetingh, 2009). The plume activity presumably accelerated the rate of uplift by a factor of 3-5
6
7 847 (Cloetingh & Ziegler, 2007). According to presently available data, the plumes in this segment of the
8
9 848 European Cenozoic Rift System arrived about 1 Myr ago. This activity was preceded and followed
10
11 849 by lithospheric folding that continues to present-day since 17 Myr ago (Bourgeois *et al.*, 2007).
12
13 850 Thermo-mechanical modelling illustrates the relative effectiveness of amplification of lithosphere
14
15 851 deformation and topographic effects induced by plumes through folding and vice-versa. Burov &
16
17 852 Cloetingh (2009) examined the response times and time-lags involved and whether these baby
18
19 853 plumes were more efficient in localizing deformation than large plumes. Plume-affected folding
20
21 854 appears to accelerate surface uplift, whereas folding goes into saturation and stagnates when
22
23 855 plastic hinges form. For the discrimination of plumes and folding it is critical to access constraints on
24
25 856 the presence or absence of radial versus linear symmetry, heat flow anomalies, gravity and geoid
26
27 857 data. Plume activity facilitates folding, by dramatically lowering the stress levels required (Burov &
28
29 858 Cloetingh, 2009). Plume impact also reduces the fold wavelength and localizes folding above the
30
31 859 plume impact area. A general outcome of the modelling and observations is that lithospheric folding
32
33 860 as a mechanism for producing thermal perturbations in the lithosphere/upper mantle system is a
34
35 861 less feasible scenario.
36
37
38
39
40 862

41
42 863 **FOLDING AND OTHER MODES OF BASIN FORMATION: DIFFERENCES AND SIMILARITIES**
43
44 864 **IN STRUCTURE AND EVOLUTION**

45
46 865 Sedimentary basins formed through lithospheric folding have characteristic features including
47
48 866 vertical motions, basin architecture, thermal regime and fault activity, distinguishing them from other
49
50 867 basin types (Cloetingh & Ziegler, 2007; Xie & Heller, 2009). **Figure 1b** and **Table 2** illustrate
51
52 868 differences and similarities between basins developed on folded lithosphere (FLB), foreland basins
53
54 869 (FB), intracratonic basins (ICB), extensional basins (EB), and pull-apart basins (PAB).
55
56
57
58
59
60

1
2
3 870 Sedimentary basin systems are, by their nature, prone to tectonic reactivation and, therefore,
4
5 871 frequently characterised by a poly-phase evolution (Cloetingh & Ziegler, 2007). Extensional basins
6
7 872 are, for example, often formed in areas previously thickened by tectonic compression and
8
9
10 873 subsequently often subject to late-stage compression (Lundin & Dorè, 1997). Examples include the
11
12 874 Pannonian basin of Hungary (Horváth & Cloetingh, 1996) and the North Atlantic rifted margins
13
14 875 (Cloetingh *et al.*, 2008). Similarly, foreland basins are frequently characterised by pre-orogenic
15
16 876 extension. Examples include the Carpathian foredeep (e.g. Tarapouca *et al.*, 2003) and the
17
18 877 Aquitaine basin of Southern France, which was the retro-arc foreland basin of the Pyrenees
19
20 878 (Desegaulx *et al.*, 1991). The actual subsidence patterns of these poly-phase systems are often
21
22 879 more complex than predicted by the end-member models discussed below that only consider the
23
24 880 basin formation mechanism. Retro-arc foreland basins are characterised by a prolonged subsidence
25
26 881 history with a distinct thermal signature including the effects of thermal cooling inherited from pre-
27
28 882 orogenic extension. This is sometimes neglected in comparing pro-arc and retro-arc foreland basins
29
30 883 (Naylor & Sinclair, 2007).

31
32
33 884 Basin infill records allow main features, including geometry, vertical motions and faulting
34
35 885 characteristics to be unravelled (Zoetemeijer *et al.*, 1993). However, heat flow histories need to be
36
37 886 determined through kinematic reconstruction and forward modelling. Results of heat flow history
38
39 887 modelling for FB and EB settings (Van Wees *et al.*, 2009) can be subsequently compared to FLB
40
41 888 results presented in this paper (**Fig. 13**). For ICB and PAB we have refrained from a quantitative
42
43 889 approach for heat flow predictions as vertical motions driving subsidence cannot be linked in a
44
45 890 straightforward way to a single or uniformly distributed lithosphere process. As a consequence, for
46
47 891 these settings tentative heat flow patterns have been drawn.

50 892 *Folded lithosphere basins* (FLB) that develop as a result of periodic folding are highly symmetrical,
51
52 893 with dimensions that can vary from 50 km to 600 km, depending on lithospheric age and shortening
53
54 894 rate. These basins can accumulate thick sedimentary sequences up to the order of 20 km. The time
55
56 895 scales associated with this process of basin formation are very short, typically a few Myr. The
57
58
59
60

1
2
3 896 subsidence is so fast that erosion and sediment supply at the basin formation stage typically lags
4
5 897 behind, leading to the development of starved basins, followed by shallowing upward sequences
6
7 898 after stress relaxation. Subsidence patterns are characteristically convex upward with time. A
8
9 899 noticeable feature is the development of significant topography of the order of several km flanking
10
11 900 the synclinal depression. No initial heating is predicted, with an increase in heat flow with time
12
13 901 following the basin formation. Significant brittle deformation is expected to occur in the folded
14
15 902 basement, accelerating during the folding phase.

16
17
18 903 *Foreland basins* (FB) are strongly asymmetrical, with depths usually less than 10 km, and have
19
20 904 modest flexural bulges of a few hundred meters (Royden, 1993; DeCelles & Gilles, 1996;
21
22 905 Zoetemeijer *et al.*, 1999). Important differences occur in the nature of the subsidence of pro- and
23
24 906 retro-foreland basins (Naylor & Sinclair, 2007). The first are typically associated with short life spans
25
26 907 and convex up subsidence patterns with time, whereas the latter show more prolonged subsidence
27
28 908 histories and concave up subsidence patterns. Subsidence patterns will be interrupted during
29
30 909 thrusting phases, also leading to uplift of the flexural marginal bulge (Quinlan & Beaumont, 1984;
31
32 910 Zoetemeijer *et al.*, 1993). The predicted heat flow pattern of a pro-foreland setting shown for the
33
34 911 Ebro foreland basin (well Jabali from Verges, 1999), marked by rapid basement subsidence and
35
36 912 sedimentary infill of ca 4 km in ca 10 My period (other parameters as in Van Wees *et al.*, 2009).
37
38 913 Flexure and rapid sediment infill is marked by a reduction of heat flow, followed by a progressive
39
40 914 increase related to radiogenic heat production of foreland sediments. Basement fracturing is
41
42 915 concentrated at the points of maximum curvature in the flexed lithosphere, at the maximum points of
43
44 916 upward and downward deflection, respectively, with intensity higher than inferred for FLB.

45
46
47 917 *Intracratonic basins* (ICB) share their symmetrical shape and great thickness of their sedimentary
48
49 918 basin fill with FLB. An important difference is their evolution in time, characteristically associated
50
51 919 with very long time spans (typically of the order of 500-800 Myr) with long phases of low subsidence
52
53 920 rate punctuated by phases of subsidence acceleration. As pointed out above, this is why ICB are
54
55 921 probably affected by short-term phases of enhanced intraplate compression superimposed on other
56
57
58
59
60

1
2
3 922 mechanisms operating on longer time scales. The large dimensions of these basins point to
4
5 923 formation in high rigidity lithosphere, that freezes in basin deformation over long time scales. The
6
7 924 long time scales involved also imply that the highs induced by compressional upwarping will be
8
9 925 commonly eroded. A major difference between ICB and FLB is that current hypotheses for ICB
10
11 926 formation are casted only in terms of the tectonic processes operation at their earlier stage such as
12
13 927 phase changes in the lithosphere. It appears, therefore, that lithospheric stress fields and the
14
15 928 lithosphere rheology (inferred from gravity and flexure) are far more diagnostic than the lithosphere-
16
17 929 asthenosphere boundary, which is only giving information on the thermal state of the lithosphere.
18
19 930 Heat flow patterns of ICB will be dominated by sediment infill. ICB are in general characterized by a
20
21 931 low intensity of faulting. However, in the absence of a rigorous understanding of the formation
22
23 932 mechanisms of ICB, predictions for heat flow are often not available. As a consequence, their heat
24
25 933 flow is most often described primarily in terms of the thermal consequences of their burial history.

26
27 934 *Extensional basins* (EB) have received major attention from basin modellers, both because of their
28
29 935 relative abundance and importance and because of the availability of a relatively simple quantitative
30
31 936 model for their formation (McKenzie, 1978). The latter can be relatively easily be incorporated in
32
33 937 forward modelling of their subsidence and heat flow histories (Van Wees *et al.*, 2009). The basin
34
35 938 shape is symmetrical or asymmetrical depending on a pure shear or simple shear mode of
36
37 939 extension. Rifts can be narrow or wide, depending on the mode of rifting and the rheology of the
38
39 940 extending lithosphere (Huisman and Beaumont, 2002). Dependent on the rigidity of the extending
40
41 941 lithosphere, rift shoulders with asymmetrical shape can be formed and be prone to erosion (Van
42
43 942 Balen *et al.*, 1995, Van der Beek *et al.*, 1995). The development of rift shoulders and their erosion
44
45 943 can lead to feed back with lower crustal flow and faulting in the extending lithosphere (Burov &
46
47 944 Cloetingh, 1997). During the post-rift phase, flexural widening of the basin commonly occurs. A
48
49 945 characteristic feature of EB predicted by simple stretching models (McKenzie, 1978) is the
50
51 946 succession of rapid initial subsidence in the syn-rift phase and exponentially decaying subsidence in
52
53 947 their post-rift phase with a typical thermally controlled time constants of the order of 70 Myr. Feed
54
55
56
57
58
59
60

1
2
3 948 backs between rift shoulder erosion and lower crustal flow (Burov & Cloetingh, 1997; Burov &
4
5 949 Poliakov, 2001), have pronounced effects on subsidence in the final phases of rifting and in the
6
7 950 early post-rift phase. Both can be influenced by changes in the mechanical properties of the
8
9 951 lithosphere and its strengthening upon rifting. Multiple rifting phases is another common feature of
10
11 952 EB. The duration of the syn-rift phase can vary from quasi-instantaneous (shorter than 20 Myr) to
12
13 953 several hundreds of Myr (Cloetingh and Ziegler, 2007). In the latter case basin migration is a
14
15 954 common feature (Corti *et al.*, 2003). Extensional faulting occurs during the rift phase, with absence
16
17 955 of faulting in the post-rift phase. Heat flow reaches a peak during the syn-rift phase, followed by a
18
19 956 rapid decrease in heat flow (Van Wees *et al.*, 2009). The syn-rift peak in heat flow is low or almost
20
21 957 absent in continental extensional settings as a consequence of removal of heat producing elements
22
23 958 in the crust and cooling by sediment infill. **Fig. 16** shows such a setting, which is based on the
24
25 959 benchmark model presented in Van Wees *et al.* (2009), As a consequence of the loss of radiogenic
26
27 960 heat production in the crust at the end of the post-rift stage values, heat flow evolves to values
28
29 961 considerably lower than the initial ones. The EB heat flow pattern is, therefore, the reverse of that in
30
31 962 FB where syntectonic heat flow is first lowered due to sediment infilling (Kombrink *et al.*, 2008), but
32
33 963 eventually increases due to thermal relaxation and additional radiogenic heat production in the
34
35 964 sediments.

36
37
38
39 965 *Pull-apart basins* (PAB) are characterized by a narrow fault bounded geometry (Smit *et al.*, 2008),
40
41 966 developing over a very short time span. Models have been developed to calculate subsidence
42
43 967 histories and heat flow histories for these basins (Pitman & Golovchenko, 1983), incorporating
44
45 968 lateral heat transport in stretching models. These models predict rapid subsidence of several km's
46
47 969 over time intervals of the order of 0.1 – 1 Myr, followed by a decay in the subsidence with a concave
48
49 970 shape upward. Erosion and sediment flux can not keep pace with the subsidence at the basin
50
51 971 formation phase, leading initially to a starved basin, followed by a shallowing upward sequence
52
53 972 (Pitman & Golovchenko, 1983). These basins are intensively faulted, also due to their strike-slip
54
55 973 origin, whereas heat flow decays on very short time scales of the order of a few Myr. Although this
56
57
58
59
60

1
2
3 974 scenario is a good first order description, many PAB show a more punctuated fault controlled
4
5 975 subsidence history, often terminating by late-stage uplift, as observed for Late Neogene pull-apart
6
7 976 basins in the internal zone of the Betics in SE Spain (Cloetingh *et al.*, 1992) and for the flanks of
8
9
10 977 pull-apart basins in the Dead Sea Fault System (Smit *et al.*, 2008, 2010).

11 978 From the above overview, it is apparent that FLB have in common with FB a compressional origin
12
13
14 979 and thermal histories controlled to a large extent by burial histories. At the same time, pronounced
15
16 980 differences occur in the duration of subsidence, varying from ultra short (FLB 1-10's Myr), medium
17
18 981 (FB, tens of Myr) and ultra long (ICB, hundreds of Myr). An important difference occurs in the spatial
19
20 982 scales of the topography generated by folding and foreland fold-and-thrust belt deformation. In the
21
22 983 latter case a much steeper differential topography is generated over typical horizontal differences of
23
24 984 the order of 10 km between peak and trough. In contrast, in the case of lithospheric folding
25
26 985 horizontal distances between the topographic highs and the axes of the depocentres are typically of
27
28 986 the order of hundreds of kilometres. As a result, diffusive transfer of mass will occur at a much
29
30 987 slower rate of sediment supply in the case of folded lithosphere than rates of sediment supply
31
32 988 locally generated by thrusting. This together with a very rapid initial subsidence of folded lithosphere
33
34 989 basins has important consequences for the paleobathymetry of these systems.

35
36
37 990 FLB contrast with extensional and pull-apart basins in the shape of the subsidence curves, being
38
39 991 convex up for FLB and concave for EB and PAB. The heat flow histories differ also. EB and PAB
40
41 992 are characterized by a phase of initial heating, whereas FLB and FB are characterized by an
42
43 993 absence of initial heating. A common feature of FLB and PAB formation is their capability to cause
44
45 994 dramatic differential vertical motions in a short time interval, predicting shallowing upward
46
47 995 sequences. FLB are to some extent unique in terms of the magnitude of the uplifted topography
48
49 996 surrounding the down warped depocentres. Similar magnitudes are only reached at rift shoulders of
50
51 997 basins developing in intracratonic lithosphere (Van der Beek *et al.*, 1995). FLB can be associated
52
53 998 with localized brittle deformation and pop-up structures in the upper crust and widespread brittle
54
55 999 deformation at deeper crustal and upper mantle levels.
56
57
58
59
60

1
2
3 10004
5 10016
7 1002 **CONCLUSIONS**8
9 1003

10 1004 Sedimentary basins controlled by lithospheric folding are characterized by a number of features in
11
12 1005 their basin architecture, subsidence history, thermal evolution and faulting patterns making them
13
14 1006 distinctly different from other basin systems. Of particular importance are the relatively short
15
16 1007 temporal scales involved in their evolution, whereas their spatial scales vary from tens to several
17
18 1008 hundreds of km, depending on the rheological stratification of the lithosphere and its thermo-
19
20 1009 mechanical age. Subsidence patterns are characterized by an acceleration of subsidence in the
21
22 1010 depocentres during compressional basin formation, occurring simultaneously with accelerated uplift
23
24 1011 of and erosion from flanking basin highs. In contrast with asymmetrical foreland basins, basins on
25
26 1012 folded lithosphere are symmetrical with equal dimensions for linearly trending topographic highs and
27
28 1013 lows.

29 1014 Basins on folded lithosphere have a strong tendency to remain closed systems during a major part
30
31 1015 of their evolution, with capture times decreasing with thermo-mechanical age from several tens of
32
33 1016 Myr to less than 10 Myr. The thermal history of these basins is not characterized by an initial
34
35 1017 thermal perturbation, unless folding occurs in interaction with plume activity. In the absence of an
36
37 1018 interplay with lithospheric scale thermal perturbations, their thermal evolution will be primarily
38
39 1019 controlled by the burial history of the sediments deposited in the accommodation space created by
40
41 1020 the folding process.

42 1021 Intrabasinal faulting and the formation of pop-up structures and inverted basins at upper crustal
43
44 1022 levels are important in the structural evolution of these basin systems. The intensity of the brittle
45
46 1023 deformation peaks with ongoing shortening of the lithosphere during folding but faulting activity is
47
48 1024 dramatically reduced after the cessation of folding. At this stage, with an equilibrium between
49
50 1025 sedimentation and erosion, minor faulting occurs as a result of stress relaxation due to erosion of
51
52
53
54
55
56
57
58
59
60

1
2
3 1026 folded highs. During capture and overall uplift of basins on folded lithosphere, their accommodation
4
5 1027 space is further reduced by unflexing and associated stress release through faulting.
6
7
8 1028
9
10 1029

11
12 1030 **ACKNOWLEDGEMENTS**

13
14 1031 This work was initiated during S. Cloetingh's visit to Paris VI as Visiting Professor and finalized
15
16 1032 during a subsequent Visiting Professorship at IFP. Comments and stimulating suggestions by Fred
17
18 1033 Beekman, Jan-Diederik van Wees, Francois Roure, Seth Stein, Jeroen Smit and Didier Granjeon
19
20 1034 are gratefully acknowledged. Thomas Kruijer and Elishevah van Kooten provided valuable technical
21
22 1035 assistance. We benefitted from constructive criticism from Dr. Mary Ford and two anonymous
23
24
25 1036 reviewers.
26

27 1037
28
29
30
31
32
33
34
35
36
37
38
39
40
41
42
43
44
45
46
47
48
49
50
51
52
53
54
55
56
57
58
59
60

1
2
3 1038 **REFERENCES**

- 4 1039
- 5 1040 ALINAGHI, A., KOULAKOV, I. & THYBO, H. (2007) Seismic tomographic imaging of *P*- and *S*-waves velocity
- 6 1041 perturbations in the upper mantle beneath Iran. *Geophys. J. Int.*, 169, 1089-1102.
- 7 1042
- 8 1043 ALZAGA-RUIZ, H., GRANJEON, D., LOPEZ, M., SERANNE, M., ROURE, F. (2008) Gravitational collapse
- 9 1044 and Neogene sediment transfer across the western margin of the Gulf of Mexico: Insights from numerical
- 10 1045 models. *Tectonophysics*, 470, 21-41.
- 11 1046
- 12 1047 ALLEN, M.B. & DAVIES, C.E. (2007) Unstable Asia: active deformation of Siberia revealed by drainage shifts.
- 13 1048 *Basin Res.*, 19, 379–392.
- 14 1049
- 15 1050 ARTYUSHKOV, E. V. (2007) Formation of the superdeep Caspian Basin: subsidence driven by phase change
- 16 1051 in continental crust. *Russ. Geol. Geophys.*, 48, 1102-1014.
- 17 1052
- 18 1053 AVOUAC, J., & BUROV, E. (1996) Erosion as a driving mechanism of intracontinental mountain growth. *J.*
- 19 1054 *Geophys. Res.*, 101, 17747-17769.
- 20 1055
- 21 1056 AXEN, G.J., LAM, P.J., GROVE, M., STOCKLI, D.F. & HASSANZADEH, J. (2001) Exhumation of the west-
- 22 1057 central Alborz Mountains, Iran, Caspian subsidence, and collision-related tectonics. *Geology*, 29, 559-562.
- 23 1058
- 24 1059 BADA, G., HORVÁTH, F., CLOETINGH, S., COBLENTZ, D.D. & TÓTH, T. (2001) The role of topography
- 25 1060 induced gravitational stresses in basin inversion: the case study of the Pannonian basin. *Tectonics*, 20, 343–
- 26 1061 363.
- 27 1062
- 28 1063 BADA G., HORVÁTH F., DÖVÉNYI P., SZAFIÁN P., WINDHOFFER G. & CLOETINGH S. (2007) Present-
- 29 1064 day stress field and tectonic inversion in the Pannonian basin. *Global Planet. Change*, 58, 165-180.
- 30 1065
- 31 1066 BEAUMONT, C. (1981) Foreland basins. *Geophys. J. R. Astron. Soc.*, 65, 291–329.
- 32 1067
- 33 1068 BEAUMONT, C., FULLSACK, P., & J. HAMILTON (1992) Erosional control of active compressional orogens. In:
- 34 1069 *Thrust Tectonics* (Ed. by K.R. McClay), Chapman & Hall, London, 1-18.
- 35 1070
- 36 1071 BEEKMAN, F., BULL, J., CLOETINGH, S., SCRUTTON, R., (1996) Crustal fault reactivation facilitating
- 37 1072 lithospheric folding/buckling in the Central Indian Ocean. In: *Modern developments in structural interpretation*
- 38 1073 *validation and modelling* (Ed. by P. Buchanan and D.A. Nieuwland). *Geol. Soc. Lond. Spec. Publ.*, 99, 251-
- 39 1074 263.
- 40
- 41
- 42
- 43
- 44
- 45
- 46
- 47
- 48
- 49
- 50
- 51
- 52
- 53
- 54
- 55
- 56
- 57
- 58
- 59
- 60

- 1
2
3 1075
4
5 1076 BEEKMAN, F., STEPHENSON, R.A. & KORSCH, R.J. (1997) Mechanical stability of the Redbank Thrust
6 1077 Zone, Central Australia: dynamic and rheological implications. *Australian J. Earth Sci.*, 44, 215-226.
7 1078
8
9 1079 BERCOVICI, D., RICARD, Y. & SCHUBERT, G. (2001) A two-phase model for compaction and damage 3.
10 1080 Applications to shear localization and plate boundary formation. *J. Geophys. Res.*, 106, 8925-8939.
11 1081
12 1082 BIOT, M.A. (1961) Theory of Folding of Stratified viscoelastic media and its implications in tectonics and
13 1083 orogenesis. *Geol. Soc. Am. Bull.*, 72, 1595-1620.
14 1084
15 1085 BIRD, P. (1991) Lateral extrusion of lower crust from under high topography in the isostatic limit. *J. Geophys.*
16 1086 *Res.*, 96, 10275-10286.
17 1087
18 1088 BONNET, S., GUILLOCHEAU, F., BRUN, J-P. & VAN DEN DRIESSCHE, J. (2000) Large-scale relief
19 1089 development related to Quaternary tectonic uplift of a Proterozoic-Paleozoic basement: The Armorican
20 1090 Massif, NW France. *J. Geophys. Res.*, 105, 19273-19288.
21 1091
22 1092 BOURGEOIS, O., FORD, M., DIRAISON, M., LE CARLIER DE VESLUD, C., GERBAULT, M., PIK, R., RUBY,
23 1093 N. & BONNET, S. (2007) Separation of rifting and lithospheric folding signatures in the NW-Alpine foreland.
24 1094 *Int. J. Earth Sci.*, 96, 1003-1031.
25 1095
26 1096 BRUNET, M.-F., KOROTAEV, M.V., ERSHOV, A.V. & NIKISHIN, A.M. (2003) The South Caspian Basin: a
27 1097 review of its evolution from subsidence modelling. *Sediment. Geol.*, 156, 119-148.
28 1098
29 1099 BULL, J.M. & SCRUTTON, R.A. (1992) Seismic reflection images of intraplate deformation, central Indian
30 1100 Ocean, and their tectonic significance. *J. Geol. Soc. London*, 149, 955-966.
31 1101
32 1102 BURG, J.P., DAVY, P. & MARTINOD, J. (1994) Shortening of analogue models of the continental lithosphere:
33 1103 New hypothesis for the formation of the Tibetan plateau. *Tectonics*, 13, 475-483.
34 1104
35 1105 BURG, J.P. & PODLADCHIKOV, Y. (1999) Lithosphere scale folding: numerical modelling and application to
36 1106 the Himalayan syntaxes. *Int. J. Earth. Sci.*, 88, 190-200.
37 1107
38 1108 BUROV, E.B. & POLIAKOV, A. (2001) Erosion and rheology controls on syn- and post-rift evolution: verifying
39 1109 old and new ideas using a fully coupled numerical model. *J. Geophys. Res.*, 106, 16461-16481.
40 1110
41 1111 BUROV, E.B. & CLOETINGH, S. (1997) Erosion and rift dynamics: new thermo-mechanical aspects of post-
42 1112 rift evolution of extensional basins. *Earth Planet. Sci. Lett.*, 150, 7-26.
43
44
45
46
47
48
49
50
51
52
53
54
55
56
57
58
59
60

- 1
2
3 1113
4
5 1114 BUROV, E.B. & CLOETINGH, S. (2009) Controls of mantle plumes and lithospheric folding on modes of intra-
6 1115 plate continental tectonics: differences and similarities. *Geophys. J. Int.*, 178, 1691-1722
7
8 1116
9 1117 BUROV, E.B., NIKISHIN, A.M., CLOETINGH, S. & LOBKOVSKY, L.I. (1993) Continental lithosphere folding in
10 1118 central Asia (Part II): Constraints from gravity and tectonic modelling. *Tectonophysics*, 226, 73-87.
11
12 1119
13 1120 BUROV, E. B. & MOLNAR, P. (1998) Gravity anomalies over the Ferghana Valley (Central Asia) and
14 1121 intracontinental deformation. *J. Geophys. Res.*, 103, 18137-18152.
15
16 1122
17
18 1123 BUROV, E.B., JOLIVET, L., LE POURHIET, L., POLIAKOV, A. (2001) A thermomechanical model of
19 1124 exhumation of HP and UHP metamorphic rocks in Alpine mountain belts. *Tectonophysics*, 342, 113-136.
20
21 1125
22 1126 BUROV, E., GUILLOU-FROTTIER, L., D'ACREMONT, E., LE POURHIET, L. & CLOETINGH, S. (2007)
23 1127 Plume head–lithosphere interactions near intra-continental plate boundaries. *Tectonophysics*, 434, 15-38.
24
25 1128
26
27 1129 BUROV E. & TOUSSAINT, G. (2007) Surface processes and tectonics: forcing of continental subduction and
28 1130 deep processes. *Global Planet. Change*, 58, 141-164.
29
30 1131
31
32 1132 BYERLEE, J. D. (1978) Friction of rocks. *Pure Appl. Geophys.* 116, 615-626.
33
34 1133
35 1134 CALVO, J.P., DAAMS, R., MORALES, J., LÓPEZ MARTÍNEZ, N., AGUSTÍ, J., ANADÓN, P.,
36 1135 ARMENTEROS, I., CABRERA, L., CIVIS, J., CORROCHANO, A., DÍAZ MOLINA, M., ELIZAGA, E., HOIOS,
37 1136 M., MARTÍN, E., MARTÍNEZ, J., MOISSENET, E., MUÑOZ, A., PEREZ GARCÍA, A., PÉREZ GONZÁLEZ, A.,
38 1137 PORTERO, J.M., ROBLES, F., SANTISTEBAN, C., TORRES, T., VAN DER MEULEN, A.J., VERA, J.A. &
39 1138 MEIN, P. (1993) Up-to-date Spanish continental Neogene synthesis and paleoclimatic interpretation. *Rev.*
40 1139 *Soc. Geol. España*, 6, 29-40.
41
42 1140
43
44 1141 CARTER, N.L. & TSENN, M.C. (1987) Flow properties of continental lithosphere. *Tectonophysics*, 136, 27–
45 1142 63.
46
47 1143
48
49 1144 CASAS-SAINZ, A.M & DE VICENTE, G. (2009) On the tectonic origin of Iberian topography. *Tectonophysics*,
50 1145 474, 214-235.
51
52 1146
53
54 1147 CHU, D. & GORDON, R.G. (1998) Current plate motions across the Red Sea. *Geophys. J. Int.*, 135, 313-328.
55
56 1148
57
58
59
60

- 1
2
3 1149 CLOETINGH, S. (1988) Intraplate stresses: a new element in basin analysis. In: *New perspectives in Basin*
4 1150 *Analysis* (Ed. by K.L. Kleinspehn and C. Paola), Springer-Verlag, New York, 205-230.
5
6 1151
7
8 1152 CLOETINGH, S. & BUROV, E. (1996) Thermomechanical structure of European continental lithosphere:
9 1153 constraints from rheological profiles and EET estimates. *Geophys. J. Int.*, 124, 695–723.
10
11 1154
12
13 1155 CLOETINGH, S. & WEES, VAN J-D. (2005) Strength reversal in Europe's intraplate lithosphere: transition of
14 1156 basin inversion to lithospheric folding. *Geology*, 33, 285-288.
15
16 1157
17
18 1158 CLOETINGH, S. & ZIEGLER P.A. (2007). Tectonic Models for the Evolution of Sedimentary Basins. In:
19 1159 *Treatise on Geophysics*, 6 (Ed. by A.B. Watts), Elsevier, Amsterdam, 486-611.
20
21 1160
22 1161 CLOETINGH, S., BEEK VAN DER, P.A., REES VAN, D., ROEP, TH.B., BIERMANN, C. & STEPHENSON,
23 1162 R.A. (1992) Flexural interaction and the dynamics of Neogene extensional basin formation in the Alboran-
24 1163 Betic region. *Geo-Mar. Lett.*, 12, 66-75.
25
26 1164
27
28 1165 CLOETINGH, S., BUROV, E. & POLIAKOV, A. (1999) Lithosphere folding: primary response to compression?
29 1166 (from Central Asia to Paris Basin). *Tectonics*, 18, 1064-1083.
30
31 1167
32 1168 CLOETINGH, S., BUROV, E., BEEKMAN, F., ANDEWEG, B., ANDRIESSEN, P., GARCIA-CASTELLANOS,
33 1169 D., DE VICENTE, G. & VEGAS, R. (2002) Lithospheric folding in Iberia. *Tectonics*, 21, 5,
34 1170 doi:10.1029/2001TC901031.
35
36 1171
37
38 1172 CLOETINGH, S., BUROV, E., MATENCO, L., TOUSSAINT, G., BERTOTTI, G., ANDRIESSEN, P.A.M.,
39 1173 WORTEL, M.J.R. & SPAKMAN, W. (2004) Thermo-mechanical controls on the mode of continental collision in
40 1174 the SE Carpathians (Romania). *Earth Planet. Sci. Lett.*, 218, 57-76.
41
42 1175
43
44 1176 CLOETINGH, S., ZIEGLER, P.A., BEEKMAN, F., ANDRIESSEN, P.A.M., MATENCO, L., BADA, G., GARCIA-
45 1177 CASTELLANOS, D., HARDEBOL, N., DÉZES, P. & SOKOUTIS, D. (2005) Lithospheric memory, state of
46 1178 stress and rheology: neotectonic controls on Europe's intraplate continental topography. *Quat. Sci. Rev.*, 24,
47 1179 241–304.
48
49
50 1180
51
52 1181 CLOETINGH, S., BEEKMAN, F., VAN WEES, J.D., ZIEGLER, P.A. & SOKOUTIS, D. (2008) Post-rift
53 1182 compressional reactivation potential of passive margins and extensional basins. In: *Compressional*
54 1183 *Deformation within Passive Margins: Nature, Causes and Effects* (Ed. by H. Johnson et al.), Geol. Soc.
55 1184 London Spec. Pub., 306, 27-70.
56
57 1185
58
59
60

- 1
2
3 1186 COBBOLD, P.R., DAVY, P., GAPAIS, E.A., ROSSELLO, E.A., SADYBASAKOV, E., THOMAS, J.C., TONDJI
4 1187 BIYO, J.J. & DE URREIZTIETA, M. (1993) Sedimentary basins and crustal thickening. *Sediment. Geol.*, 86,
5 1188 77–89.
6 1189
7 1189
8 1189
9 1190 CORTI, G., VAN WIJK, J., BONINI, M., SOKOUTIS, D., CLOETINGH, S., INNOCENTI, F., MANNETI, P.
10 1191 (2003) Transition from continental break-up to seafloor spreading: how fast, symmetric and magmatic.
11 1192 *Geophys. Res. Lett.*, 30, 12, doi:10.1029/2003GL017374.
12 1192
13 1193
14 1193
15 1194 CUNDALL, P.A. (1989) Numerical experiments on localization in frictional materials, *Ing. Arch.* 59, 148-159.
16 1195
17 1195
18 1196 DECELLES, P.G., & GILES, K.A. (1996) Foreland basin systems. *Basin Res.*, 8, 105-123.
19 1197
20 1197
21 1198 DESEGAULX, P., KOOI, H. & CLOETINGH, S., (1991) Consequences of foreland basin development on
22 1199 thinned continental lithosphere: application to the Aquitaine basin (SW France). *Earth. Planet. Sci. Lett.*, 106,
23 1200 116-132.
24 1200
25 1201
26 1201
27 1202 DE VICENTE, G. & VEGAS, R. (2009) Large-scale distributed deformation controlled topography along the
28 1203 western Africa–Eurasia limit: Tectonic constraints. *Tectonophysics*, 474, 124-143.
29 1203
30 1204
31 1204
32 1205 DE VICENTE, G., VEGAS, R., MUÑOZ MARTÍN, A., SILVA, P.G., ANDRIESEN, P., CLOETINGH, S.,
33 1206 GONZÁLES CASADO, J.M., WEES VAN, J-D., ALVAREZ, J., CARBÓ, A. & OLAIZ, A. (2007) Cenozoic
34 1207 thick-skinned deformation and topography evolution of the Spanish Central System. *Global Planet. Change*,
35 1207 58, 335-381.
36 1208
37 1209
38 1209
39 1210 DE VICENTE G., CLOETINGH, S., MUÑOZ-MARTÍN, A., OLAIZ, A., STICH, D., VEGAS, R., GALINDO-
40 1211 ZALDÍVAR, J., FERNÁNDEZ-LOZANO, J. (2008) Inversion of moment tensor focal mechanisms for active
41 1212 stresses around the Microcontinent Iberia: Tectonic implications. *Tectonics*, 27, TC1009.
42 1212
43 1213
44 1213
45 1214 DEVLIN, W.J., COGSWELLII, J.M., GASKINS, G.M., ISAKSEN, G.H., PITCHER, D.M., PIUS, D.P.,
46 1215 STANLEY, K.O. & WALL, J.R.T. (1999) South Caspian basin: young, cool, and full of promise. *GSA Today*, 9,
47 1215 1-9.
48 1216
49 1217
50 1217
51 1218 DÉZES, P., SCHMID, S. M. & ZIEGLER, P. A. (2004) Evolution of the European Cenozoic Rift System:
52 1219 Interaction of the Alpine and Pyrenean orogens with their foreland lithosphere. *Tectonophysics*, 389, 1-33.
53 1219
54 1220
55
56
57
58
59
60

- 1
2
3 1221 DOMBRADI, E., SOKOUTIS, D., BADA, G., CLOETINGH, S., & HORVATH, F. (2010) Modelling of recent
4 1222 deformation of the Pannoanian lithosphere: lithospheric folding and tectonic topography. *Tectonophysics*, 484,
5 1223 103-118.
6
7 1224
8
9 1225 EGAN, S.S., MOSAR, J., BRUNET, M.-F. & KANGARLI, T. (2009) Subsidence and uplift mechanisms within
10 1226 the South Caspian Basin: insights from the onshore and offshore Azerbaijan region. *Geol. Soc. London Spec.*
11 1227 *Pub.*, 312, 219-240.
12
13 1228
14
15 1229 ELFRINK, N.M. (2001) Quaternary groundwater avulsions: Evidence for large-scale midcontinent folding?
16 1230 *Assoc. Env. Eng. Geol. News*, 44, 60.
17
18 1231
19
20 1232 FAKHARI, M.D., AXEN, G.J., HORTON, B.K., HASSANZADEH, J. & AMINI, A. (2008) Revised age of
21 1233 proximal deposits in the Zagros foreland basin and implications for Cenozoic evolution of the High Zagros.
22 1234 *Tectonophysics*, 451, 170-185.
23
24 1235
25
26 1236 FERNANDEZ-LOZANO, J., SOKOUTIS, D., WILLINGSHOFER, E., DE VICENTE, G. & CLOETINGH, S.
27 1237 (2010) Lithospheric-Scale Folding in Iberia from the perspective of analogue modelling. *Trabajos de Geología.*
28 1238 *Univ. Oviedo. Volumen Especial*, 0474-9588. Coden TBGLA9, in press.
29
30 1239
31 1240 GARCIA-CASTELLANOS, D., FERNANDEZ, M., & TORNE, M. (1997) Numerical modelling of foreland basin
32 1241 formation: a program relating thrusting, flexure, sediment geometry and lithosphere rheology. *Comp. &*
33 1242 *Geosc.*, 23, 993-1003.
34
35 1243
36
37 1244 GARCIA-CASTELLANOS, D., VERGES, J., GASPARESCRIBANO, J. & CLOETINGH, S. (2003) Interplay
38 1245 between the tectonics, climate, and fluvial transport during the Cenozoic evolution of the Ebro Basin (NE
39 1246 Iberia). *J. Geophys. Res.*, 108, 2347.
40
41 1247
42
43 1248 GELLER, C. A., WEISSEL, J. K. & ANDERSON, R. N. (1983) Heat transfer and intraplate deformation in the
44 1249 central Indian Ocean. *J. Geophys. Res.*, 88, 1018-1032.
45
46 1250 .
47
48 1251 GERBAULT, M., BUROV, E., POLIAKOV, A.N.B. & DAIGNIERES, M. (1998) Do faults trigger folding in the
49 1252 lithosphere? *Geophys. Res. Lett.*, 26, 271-274.
50
51 1253
52 1254 GERBAULT, M. (2000) At what stress level is the central Indian Ocean lithosphere buckling? *Earth. Planet.*
53 1255 *Sci. Lett.*, 178, 165-181.
54
55 1256
56
57 1257 GOETZE, C. & EVANS, B. (1979) Stress and temperature in the bending lithosphere as constrained by
58 1258 experimental rock mechanics. *Geophys. J. Roy. Astron. Soc.*, 59, 463-478.
59
60

- 1
2
3 1259
4
5 1260 GOSSMAN, H. (1976) Slope modelling with changing boundary conditions - effects of climate and lithology, *Z.*
6 1261 *Geomorphol. Suppl.*, 25, 72-88.
7
8 1262
9 1263 GRANJEON, D. (2009) 3D stratigraphic modelling of sedimentary basins, from source to sink. *AAPG Annual*
10 1264 *Convention and Exhibition*, June 7-10, 2009, Denver Colorado.
11
12 1265
13 1266 GRENERCZY, Y., SELLA, G.F., STEIN, S. & KENYERES, A. (2005) Tectonic implications of the GPS velocity
14 1267 field in the northern Adriatic region. *Geophys. Res. Lett.*, 32, L16311.
15
16 1268
17
18 1269 GUEST, B., GUEST, A. & AXEN, G. (2007). Late Tertiary tectonic evolution of northern Iran: a case for simple
19 1270 crustal folding. *Global. Planet. Change*, 58, 435-453.
20
21 1271
22 1272 GUILLOCHEAU *et al.* (2000) Meso-Cenozoic geodynamic evolution of the Paris Basin: 3D stratigraphic
23 1273 constraints. *Geodin. Acta*, 13, 189-246.
24
25 1274
26
27 1275 GUILLOU-FROTTIER, L., BUROV, E., NEHLIG, P. & WYNS, R. (2007) Deciphering plume–lithosphere
28 1276 interactions beneath Europe from topographic signatures. *Global Planet. Change*, 58, 119-140.
29
30 1277
31 1278 HAFKENSCHIED, E., WORTEL, M.J.R. & SPAKMAN, W. (2006) Subduction history of the Tethyan region
32 1279 derived from seismic tomography and tectonic reconstructions. *J. Geophys. Res.*, 111, B08401.
33
34 1280
35
36 1281 HORVÁTH, F. (1995) Phases of compression during the evolution of the Pannonian Basin and its bearing on
37 1282 hydrocarbon exploration. *Mar. Petrol. Geol.*, 12, 837-844.
38
39 1283
40 1284 HORVÁTH, F. & CLOETINGH, S. (1996) Stress-induced late-stage subsidence anomalies in the Pannonian
41 1285 basin. *Tectonophysics*, 266, 287–300.
42
43 1286
44 1287 HORVÁTH, F., BADA, G., SZAFIÁN, P., TARI, G., ÁDÁM, A. & CLOETINGH, S. (2006) Formation and
45 1288 deformation of the Pannonian basin: constraints from observational data. *Geol. Soc. London Mem.*, 32, 191-
46 1289 206.
47
48
49 1290
50 1291 HUISMANS, R.S. & BEAUMONT, C.B. (2002) Asymmetric lithospheric extension: the role of frictional plastic
51 1292 strain softening inferred from numerical experiments. *Geology*, 30, 211-214.
52
53 1293
54
55 1294 HUNT, G., MUHLHAUS, H., HOBBS, B., & ORD, A. (1996) Localized folding of viscoelastic layers. *Geol.*
56 1295 *Rundsch.*, 85, 58-64.
57
58 1296
59
60

- 1
2
3 1297 KABAN, M.K. (2002) A gravity model of the north Eurasia crust and upper mantle: 2. The Alpine-
4 1298 Mediterranean fold belt and adjacent structures of the southern former USSR. *Russ. J. Earth. Sci.*, 4, 19-33.
5
6 1299
7
8 1300 KIRBY, S.H. & KRONENBERG, A.K. (1987) Rheology of the lithosphere: selected topics. *Rev. Geophys.* 25,
9 1301 1219-1244.
10 1302
11
12 1303 KIRKBY, M.J. (1986) A two-dimensional model for slope and stream evolution. In: *Hillslope Processes* (Ed. by
13 1304 Abrahams, A.D.) Allen and Unwin, Boston, 203-224.
14
15 1305
16
17 1306 KOHLSTEDT, D.L., EVANS, B. & MACKWELL, S.J. (1995) Strength of the lithosphere: constraints imposed
18 1307 by laboratory experiments. *J. Geophys. Res.*, 100, 17587-17602.
19
20 1308
21 1309 KOMBRINK, H., LEEVER, K.A., VAN WEES, J-D., VAN BERGEN, F., DAVID, P., & WONG, T.E. (2008) Late
22 1310 Carboniferous foreland basin formation and Early Carboniferous stretching in Northwestern Europe:
23 1311 inferences from quantitative subsidence analyses in the Netherlands. *Basin Res.*, 20, 377-395.
24
25 1312
26
27 1313 KOOI, H. & BEAUMONT, C. (1994) Escarpment evolution on high-elevation rifted margins: insights derived
28 1314 from a surface processes model that combines diffusion, advection and reaction, *J. Geophys. Res.*, 99,
29 1315 12191-12210.
30
31 1316
32
33 1317 LAGARDE, J.L. BAIZE, S., AMORESE, D., DELCCAILLAU, B., FORT, M. & VOLANT, V. (2000) Active
34 1318 tectonics, seismicity and geomorphology with special reference to Normandy (France). *J. Quat. Sci.*, 15, 745-
35 1319 758.
36
37 1320
38
39 1321 LAMBECK, K. (1983) The role of compressive forces in intracratonic basin formation and mid-plate orogenies.
40 1322 *Geophys. Res. Lett.*, 10, 845-848.
41
42 1323
43
44 1324 LAVIER, L.L. & STECKLER, M.S. (1997) The effect of sedimentary cover on the flexural strength of the
45 1325 continental lithosphere. *Nature*, 389, 476-479.
46 1326
47 1327 LAWRENCE D.T., DOYLE. M., & AIGNER, T. (1990) Stratigraphic simulation of sedimentary basins:
48 1328 Concepts and calibration. *AAPG Bull.*, 74, 273-295.
49
50 1329
51 1330 LEEDER, M. R. (1991) Denudation, vertical crustal movements and sedimentary basin infill. *Geol. Rundsch.*,
52 1331 80, 441-458.
53
54 1332
55
56 1333 LEFORT, J-P. & AGARWAL, B.N. (1996) Gravity evidence for an Alpine buckling of the crust beneath the
57 1334 Paris Basin. *Tectonophysics*, 258, 1-14.
58
59
60

- 1
2
3 1335
4
5 1336 LEFORT, J.P. & AGARWAL, B.N. (2000) Gravity and geomorphological evidence for a large crustal bulge
6 1337 cutting across Brittany (France): a tectonic response to the closure of the Bay of Biscay. *Tectonophysics*, 323,
7 1338 149-162.
8
9 1339
10 1340 LEFORT, J.P. & AGARWAL, B.N. (2002) Topography of the Moho undulations in France from gravity data:
11 1341 their age and origin. *Tectonophysics*, 350, 193-213.
12 1342
13 1343 LEIGHTON, M.W. & KOLATA, D.R. (1990) Selected interior cratonic basins and their place in the scheme of
14 1344 global tectonics: A synthesis. In: *AAPG Memoir* (Ed. by M.W. Leighton, D.R. Kolata, D.F. Oltz and J.J. Eidel),
15 1345 51, 729-797.
16 1346
17 1347 LENOTRE, N., THIERRY, P., BLANCHIN, R. & BROCHARD, G. (1999) Current vertical movement
18 1348 demonstrated by comparative levelling in Brittany (France). *Tectonophysics*, 301, 333-344.
19 1349
20 1350 LE SOLLEUZ, A., DOIN, M.-P. DOIN, ROBIN, C., & GUILLOCHEAU, F. (2004) From a mountain belt collapse
21 1351 to a sedimentary basin development: 2-D thermal model based on inversion of stratigraphic data in the Paris
22 1352 Basin. *Tectonophysics*, 386, 1-27.
23 1353
24 1354 LI, S., MOONEY, W.D. & FAN, J. (2006) Crustal structure of mainland China from deep seismic sounding
25 1355 data. *Tectonophysics*, 420, 239-252.
26 1356
27 1357 LITTKE, R., BAYER, U., GAJEWSKI, D., & NELSKAMP, S. (2008) Dynamics of Complex Intracontinental
28 1358 Basins, Berlin. Heidelberg, Springer, 520 p.
29 1359
30 1360 LIU, M., MOONEY, W.D., LI, S., OKAYA, N., & DETWEILER, S. (2006) Crustal structure of the northeast
31 1361 margin of the Tibetan plateau from the Songpan-Ganzi terrane to the Ordos basin. *Tectonophysics*, 420, 253-
32 1362 266.
33 1363
34 1364 LIU Y., NEUBAUER, F., GENSER, J., GE, X., TAKASU, A., YUAN, S., CHANG, L., & LI, W. (2007)
35 1365 Geochronology of the initiation and displacement of the Altyn strike-slip fault, western China. *J. Asian Earth*
36 1366 *Sci.*, 29, 243-252.
37 1367
38 1368 LUNDIN, E.R. & DORÉ, A.G. (1997) A tectonic model for the Norwegian passive margin with implications for
39 1369 the NE Atlantic: Early Cretaceous to break-up. *J. Geol. Soc.*, 154, 545-550.
40 1370
41 1371 MAROTTA, A. M., BAYER, U. & THYBO, H. (2000) The legacy of the NE German Basin – Reactivation by
42 1372 compressional buckling. *Terra Nova*, 12, 132-14
43
44
45
46
47
48
49
50
51
52
53
54
55
56
57
58
59
60

- 1
2
3 1373
4
5 1374 MARTINOD, J. & DAVY, P. (1992) Periodic instabilities during compression or extension of the lithosphere: 1.
6 1375 Deformation modes from an analytical perturbation method. *J. Geophys. Res.*, 97, 1999-2014.
7
8 1376
9 1377 MARTINOD, J. & DAVY, P. (1994) Periodic instabilities during compression of the lithosphere: 2. Analogue
10 1378 experiments. *J. Geophys. Res.*, 99, 12057-12069.
11
12 1379
13 1380 MATENCO, L., BERTOTTI, G., LEEVER, K., CLOETINGH, S., SCHMID, S., TĂRĂPOANĂ, M. & DINU, C.,
14 1381 2007. Large-scale deformation in a locked collisional boundary: Interplay between subsidence and uplift,
15 1382 intraplate stress, and inherited lithospheric structure in the late stage of the SE Carpathians evolution.
16 1383 *Tectonics*, 26, TC4011
17
18 1384
19
20 1385 MAZUR, S., SCHECK-WENDEROTH M. & KRZYWIEC, P. (2005) Different modes of the Late Cretaceous –
21 1386 Early Tertiary inversion in the North German and Polish basins. *Int. J. Earth Sci.*, 94, 782-798.
22
23 1387
24 1388 MCADOO, D.C. & SANDWELL, D.T. (1985) Folding of the oceanic lithosphere. *J. Geophys. Res.*, 90, 8563–
25 1389 8569.
26
27 1390
28
29 1391 MCKENZIE, D.P. (1978) Some remarks on the development of sedimentary basins. *Earth. Planet. Sci. Lett.*,
30 1392 95, 53-72.
31
32 1393
33 1394 MUEHLHAUS, H.B., SAHAGUCHI, H., & HOBBS, B.E. (1998) Evolution of three-dimensional folds for a non
34 1395 Newtonian plate in a viscous medium. *Proc. R. Soc. London, series A, Math. Phys. NG. Sci.*, 454, 3121-3143.
35 1396
36 1397 NADIROV, R.S., BAGIROV, E., TAGIYEV, M., & LERCHE, I. (1997) Flexural plate subsidence, sedimentation
37 1398 rates and structural development of the super-deep south Caspian Basin. *Mar. Petrol. Geol.*, 14, 383-400.
38 1399
39 1400 NAYLOR, M. & SINCLAIR, H.D. (2007) Punctuated thrust deformation in the context of doubly vergent thrust
40 1401 wedges: implications for the localization of uplift and exhumation. *Geology*, 35, 559–562.
41 1402
42 1403 NAYLOR, M. & SINCLAIR, H.D. (2008) Pro- vs. Retro foreland Basins. *Basin Res.*, 20, 1365-2117.
43 1404
44 1405 NECEA, D., FIELITZ, W., & MATENCO, L. (2005) Late Pliocene-Quaternary tectonics in the frontal part of the
45 1406 SE Carpathians: Insights from tectonic geomorphology. *Tectonophysics*, 410, 137-156.
46 1407
47 1408 NIKISHIN, A.M., CLOETINGH, S., LOBKOVSKY, L., & BUROV, E.B. (1993) Continental lithosphere folding in
48 1409 Central Asia (Part I): constraints from geological observations. *Tectonophysics*, 226, 59-72.
49 1410
50
51
52
53
54
55
56
57
58
59
60

- 1
2
3 1411 NIKISHIN, A.M., BRUNET, M.F., CLOETINGH, S., & ERSHOV, A.V. (1997) Northern Peri-Tethyan Cenozoic
4 1412 intraplate deformations: Influence of the Tethyan collision belt on the Eurasian continent from Paris to Tian-
5 1413 Shan. *C.R. Acad. Sci., Ser. Ila: Sci. Terre Planets*, 234, 49-57.
6 1414
7
8 1415 NIKISHIN, A.M., KOROTAEV, M.V., ERSHOV, A.V., & BRUNET, M.F. (2003) The Black Sea Basin: tectonic
9 1416 history and Neogene-Quaternary rapid subsidence modelling. *Sediment. Geol.*, 156, 149-168.
10 1417
11 1418 PEREZ-GUSSINYE, M. & WATTS, A.B. (2005) The long-term strength of Europe and its implications for
12 1419 plate-forming processes. *Nature*, 436, 381-384.
13 1420
14 1421 PITMAN, W.C. & GOLOVCHENKO, X. (1983) The effect of sea-level change on the shelf edge and slope of
15 1422 passive margin. In: *The shelf break: critical interface on continental margins* (Ed. by D.J. Stanley and G.T.
16 1423 Moore), SEPM, Spec. Publ., 33, 41-58.
17 1424
18 1425 QUINLAN, G. & BEAUMONT, C. (1984) Appalachian thrusting, lithospheric flexure and the Paleozoic
19 1426 stratigraphy of the eastern interior of North America. *Can. J. Earth Sci.*, 21, 973-996.
20 1427
21 1428 QUINLAN, G. (1987) Models of subsidence mechanisms in intracratonic basins and their applicability to North
22 1429 American examples. *Can. Soc. Pet. Geol. Mem.*, 12, 463-481.
23 1430
24 1431 RAMBERG, H. (1961) Contact strain and folding instability of multilayered body under compression. *Geol.*
25 1432 *Rundsch.*, 51, 405-439.
26 1433
27 1434 RANALLI, G. (1995) *Rheology of the Earth*, 2nd edn., Chapman and Hall, London, 413 pp.
28 1435
29 1436 RITTER, J.R.R., JORDAN, M., CHRISTENSEN, U.R. & ACHAUER, U. (2001) A mantle plume under the Eifel
30 1437 volcanics fields, Germany. *Earth Planet. Sci. Lett.*, 186, 7-14.
31 1438
32 1439 RITZMANN, O. & FALEIDE, J.I. (2009) The crust and mantle lithosphere in the Barents Sea/Kara Sea region.
33 1440 *Tectonophysics*, 470, 89-104.
34 1441
35 1442 ROBIN, C., ALLEMAND, P., BUROV, E., DOIN, M.P., GUILLOCHEAU, F., DROMART, G. & GARCIA, J.P.
36 1443 (2003) Vertical movements of the Paris Basin (Triassic - Pleistocene): from 3D stratigraphic database to
37 1444 numerical models. In: *New insights in structural interpretation and modelling* (Ed. by P. Buchanan and D.A.
38 1445 Nieuwland) Geol. Soc. London Spec. Publ., 212, 225-250.
39 1446
40 1447 ROYDEN, L. (1988) Flexural behaviour of the continental lithosphere in Italy: constraints imposed by gravity
41 1448 and deflection data. *J. Geophys. Res.*, 93, 7747-7766.
42
43
44
45
46
47
48
49
50
51
52
53
54
55
56
57
58
59
60

- 1
2
3 1449
4
5 1450 ROYDEN, L.H. (1993) The tectonic expression of the slab pull at continental convergent boundaries.
6 1451 *Tectonics*, 12, 303-325.
7
8 1452
9 1453 ROURE, F., CLOETINGH, S., SCHECK-WENDEROTH, M., & ZIEGLER, P.A., (2010) Achievements and
10 1454 challenges in sedimentary basin dynamics: a review. In: *New Frontiers in Integrated Solid Earth Sciences* (Ed.
11 1455 by S. Cloetingh and J. Negendank), Springer-Verlag, 145-233.
12
13 1456
14
15 1457 SACCHI, M., HORVATH, F. & MAGYARI, O. (1999) Role of unconformity bounded units in the stratigraphy of
16 1458 the continental record: a casestudy from the Late Miocene of the western Pannonian basin, Hungary. *Geol.*
17 1459 *Soc. London Spec. Publ.*, 156, 357-390.
18
19 1460
20
21 1461 SCHECK, M. & BAYER, U., (1999) Evolution of the Northeast German Basin – inferences of a 3D structural
22 1462 model and subsidence analysis. *Tectonophysics*, 373, 55-73.
23
24 1463
25 1464 SCHMALHOLTZ, S.M. & PODLADCHIKOV, Y.Y. (2000) Finite amplitude folding: transition from exponential
26 1465 to taper length controlled growth. *Earth Planet. Sci. Lett.*, 181, 619 -633.
27
28 1466
29
30 1467 SCHUBERT, G., TURCOTTE, D.L. & OLSON, P. (2001) Mantle convection in the Earth and Planets.
31 1468 *Cambridge University Press*, 956 pp.
32
33 1469
34 1470 SHIN, Y.H., SHUM, C.-K., BRAITENBERG, C., LEE, S.M., XU, H., CHOI, K.S., BAEK, J.H., & PARK, J.U.
35 1471 (2009) Three-dimensional fold structure of the Tibetan Moho from GRACE gravity data. *Geophys. Res. Lett.*,
36 1472 36, L01302.
37
38 1473
39
40 1474 SMIT, J., BRUN, J.P., CLOETINGH, S., & BEN-AVRAHAM, Z. (2008) Pull-apart basin formation and
41 1475 development in narrow transform zones with application to the Dead Sea Basin. *Tectonics*, 27, TC6018.
42
43 1476
44 1477 SMIT, J., BRUN, J.P., CLOETINGH, S. & BEN-AVRAHAM, Z. (2010) The rift-like structure and asymmetry of
45 1478 the Dead Sea Fault. *Earth Planet. Sci. Lett.*, 290, 74-82.
46
47 1479
48
49 1480 SMITH, R.B. (1979) The folding of a strongly non-Newtonian layer. *Am. J. Sci.*, 79, 272-287.
50
51 1481
52 1482 SOKOUTIS, D., BURG, J.P., BONINI, M., CORTI, G. & CLOETINGH, S. (2005) Lithospheric-scale structures
53 1483 from the perspective of analogue continental collision. *Tectonophysics*, 406, 1-15.
54
55 1484
56 1485 SOLOMATOV, V.S. & MORESI, L.N. (2000) Scaling of time-dependent stagnant lid convection; application to
57 1486 small-scale convection on Earth and other terrestrial planets. *J. Geophys. Res.*, 105, 21795-21817.
58
59
60

- 1
2
3 1487
4
5 1488 STEIN, C.A., CLOETINGH, S. & WORTEL, R. (1989) Seasat-derived gravity constraints on stress and
6 1489 deformation in the northeastern Indian Ocean. *Geophys. Res. Lett.*, 16, 823-826.
7
8 1490
9 1491 STEL, H., CLOETINGH, S., HEEREMANS, M., & VAN DER BEEK, P.A. (1993) The kinematics of anorogenic
10 1492 basement tectonics and the origin of sedimentary basins. *Tectonophysics*, 226, 285-299.
11
12 1493
13 1494 STEPHENSON, R.S. & CLOETINGH, S. (1991) Some examples and mechanical aspects of continental
14 1495 lithospheric folding. *Tectonophysics*, 188, 27-37.
15
16 1496
17
18 1497 STEPHENSON, R., & LAMBECK, K. (1985) Isostatic response of the lithosphere with in-plane stress:
19 1498 application to Central Australia. *J. Geophys. Res.*, 90, 8581-8588.
20
21 1499
22 1500 STEPHENSON, R.S., Ricketts, B.D., CLOETINGH, S., & BEEKMAN, F. (1990) Lithosphere folds in the
23 1501 Eurekan orogen, Arctic Canada? *Geology*, 18, 603-606.
24
25 1502
26
27 1503 TARAPOANCA, M., BERTOTTI, G., MATENCO, L., DINU, C. & CLOETINGH, S. (2003) Architecture of the
28 1504 Focsani Depression: A 13km deep basin in the Carpathians bend zone (Romania). *Tectonics*, 22, 1074.
29
30 1505
31 1506 TER VOORDE, M., DE BRUIJNE, C.H., CLOETINGH, S.A.P.L. & ANDRIESEN, P.A.M. (2004) Thermal
32 1507 consequences of thrust faulting: simultaneous versus successive fault activation and exhumation. *Earth*
33 1508 *Planet. Sci. Lett.*, 223, 395-413.
34
35 1509
36
37 1510 TESAURO, M., HOLLENSTEIN, C., EGLI, R., GEIGER, A. & KAHLE, H.-G. (2005) Continuous GPS and
38 1511 broad-scale deformation across the Rhine Graben and the Alps. *Int. J. Earth. Sci.*, 94, 525-537.
39
40 1512
41
42 1513 TESAURO, M., KABAN, M., CLOETINGH, S., HARDEBOL, N. & BEEKMAN, F. (2007) 3D strength and
43 1514 gravity anomalies of the European lithosphere. *Earth Planet. Sci. Lett.*, 263, 56-73.
44
45 1515
46 1516 THOMAS, J.C., COBBOLD, P.R., SHEIN, V.S. & LE DOUARAN, S. (1999a) Sedimentary record of late
47 1517 Paleozoic to Recent tectonism in central Asia - analysis of subsurface data from the Turan and south Kazak
48 1518 domains. *Tectonophysics*, 313, 243-263.
49
50 1519
51
52 1520 THOMAS, J.C., GRASSO, J.R., BOSSU, R., MARTINOD, J., & NURTAEV, B. (1999b) Recent deformation in
53 1521 the Turan and South Kazakh platforms, western central Asia, and its relation to Arabia-Asia and India-Asia
54 1522 collisions. *Tectonics*, 18, 201-214.
55
56 1523
57
58
59
60

- 1
2
3 1524 TIKOFF, B. & MAXSON, J. (2001) Lithospheric buckling of the Laramide foreland during Late Cretaceous and
4 1525 Paleogene, western United States. *Rocky Mt Geol.*, 36, 13-35.
5
6 1526
7
8 1527 TURCOTTE, D.L. & SCHUBERT, G. (2002) *Geodynamics, applications of continuum physics to geological*
9 1528 *problems*, 2nd edn., Cambridge University Press, 456 pp.
10 1529
11
12 1530 VAN BALEN, R.T., VAN DER BEEK, P.A. & CLOETINGH, S. (1995). The effect of rift shoulder erosion on
13 1531 stratal patterns at passive margins: implications for sequence stratigraphy. *Earth Planet. Sci. Lett.*, 134, 527-
14 1532 544.
15
16 1533
17
18 1534 VAN DER BEEK., P., ANDRIESSEN, P.A.M., & CLOETINGH, S. (1995). Morphotectonic evolution of rifted
19 1535 continental margins: inferences from a coupled tectonic-surface processes model and fission track
20 1536 thermochronology. *Tectonics*, 14, 406-421.
21
22 1537
23
24 1538 VAN DER PLUIJM, B., CRADDOCK, J.P., GRAHAM, B.R. & HARRIS, J.H. (1997) Paleostress in cratonic
25 1539 North America: implications for deformation of continental interiors. *Science*, 277, 794-796.
26
27 1540
28 1541 VAN WEES, J-D. & CLOETINGH, S. (1996) 3D flexure and intraplate compression in the North Sea basin.
29 1542 *Tectonophysics*, 266, 343-359.
30
31 1543
32
33 1544 VAN WEES, J.D., VAN BERGEN, F., DAVID, P., NEPVEU, M., BEEKMAN, F. & CLOETINGH, S. (2009)
34 1545 Probabilistic Tectonic heat flow modelling for basin maturation: method and applications. *Mar. Petrol. Geol.*,
35 1546 26, 536-551.
36
37 1547
38
39 1548 VERGES, J, (1999) Estudi Geologic Del Vessant Sud Del Pirineu Oriental I Central. In: *Evolucio Cinematica*,
40 1549 3rd edn. (Ed. by Colleccion Monografies Techniques), Institut Cartografic de Catalunya, Barcelona, 7, 194.
41 1550
42
43 1551 VERNANT, P., NILFOROUSHAN, F., HATZFELD, D., ABBASSI, M.R., VIGNY, C., MASSON, F., NANKALI,
44 1552 MARTINOD, J., ASHTIANI, A., BAYER, R., TAVAKOLI, F., CHERY, J. (2004) Present-day crustal
45 1553 deformation and plate kinematics in the Middle East constrained by GPS measurements in Iran and northern
46 1554 Oman. *Geophys. J. Int.*, 157, 381-398.
47
48 1555
49
50 1556 VERMEESCH, P., POORT, J., DUCHKOV, A.D., KLERKX, J. & DE BATIST, M. (2004) Lake Issyk-Kul (Tien
51 1557 Shan): Unusually low heat flow in an active intramountane basin. *Russ. Geol. Geophys.*, 45, 616-625.
52
53 1558
54
55 1559 WATTS, A.B. & BUROV E.B. (2003) Lithospheric strength and its relationship to the elastic and seismogenic
56 1560 layer thickness. *Earth. Planet. Sci. Lett.*, 213, 113-131.
57
58 1561
59
60

- 1
2
3 1562 WEINBERG, R.F. & PODLADCHIKOV, Y. (1994) Diapiric ascent of magmas through power law crust and
4 1563 mantle. *J. Geophys. Res.*, 99, 9543-9559.
5
6 1564
7
8 1565 WILGUS, C.K., HASTINGS, B.S., KENDALL, C.G.St.C., PASAMENTIER, H.W., ROSS, C.A., VAN
9 1566 WAGONER, J.C. (1988) Sea-level changes – an integrated approach. *Spec. Pub. Soc. Econ. Pal. Min.*, 42,
10 1567 402.
11
12 1568
13 1569 WORTEL, M.J.R. & SPAKMAN, W. (2000) Subduction and slab detachment in the Mediterranean Carpathian
14 1570 region. *Science*, 290, 1910-1917.
15
16 1571
17
18 1572 XIE, X. & HELLER, P.L. (2009) Plate tectonics and basin subsidence history. *Geol. Soc. Am. Bull.*, 121, 55-
19 1573 64.
20
21 1574
22 1575 ZHAO, J., MOONEY, W.D, ZHANG, X., LI, Z., JIN, Z., & OKAYA, N. (2006) Crustal structure across the Atityn
23 1576 Tagh Range at the northern margin of the Tibetan plateau and tectonic implications. *Earth Planet. Sci. Lett.*,
24 1577 241, 804-841.
25
26 1578
27
28 1579 ZIEGLER, P.A., CLOETINGH, S. & VAN WEES, J-D. (1995) Dynamics of intraplate compressional
29 1580 deformation: the Alpine foreland and other examples. *Tectonophysics*, 252, 7–59.
30
31 1581
32 1582 ZIEGLER, P.A., VAN WEES, J-D. & CLOETINGH, S. (1998) Mechanical controls on collision-related
33 1583 compressional intraplate deformation. *Tectonophysics*, 300, 103-129.
34
35 1584
36
37 1585 ZIEGLER, P.A. & DÈZES, P. (2006) Crustal evolution of Western and Central Europe. In: *European*
38 1586 *Lithosphere Dynamics* (Ed. by D.G. Gee and R.A. Stephenson), *Geol. Soc. London Mem.*, 32, 43-56.
39
40 1587
41 1588 ZIEGLER, P.A. & DÈZES, P. (2007) Cenozoic uplift of Variscan Massifs in the Alpine foreland: Timing and
42 1589 controlling mechanisms. *Global Planet. Change*, 58, 237-269.
43
44 1590
45
46 1591 ZITELLINI, N., CLOETINGH, S., D'ORIANO, F., & BUROV, E.B., (2010) Synclinal deformation as prime
47 1592 expression of compressional deformation in the lithosphere: the Atlantic segment of the Iberia-Africa plate
48 1593 boundary. *Geology*, submitted.
49
50 1594
51
52 1595 ZOETEMEIJER, R., CLOETINGH, S., SASSI, W. & ROURE, F. (1993) Modelling of piggy-back basin
53 1596 stratigraphy: record of tectonic evolution. *Tectonophysics*, 226, 253-269.
54
55 1597
56 1598 ZOETEMEIJER, R., TOMEK, C. & CLOETINGH, S. (1999) Flexural expression of European continental
57 1599 lithosphere under the western outer Carpathians. *Tectonics*, 18, 843-861.
58
59
60

1
2
3
4
5
6
7
8
9
10
11
12
13
14
15
16
17
18
19
20
21
22
23
24
25
26
27
28
29
30
31
32
33
34
35
36
37
38
39
40
41
42
43
44
45
46
47
48
49
50
51
52
53
54
55
56
57
58
59
60

For Review Only

1
2
3 1600 **APPENDIX A: MODEL DESCRIPTION**
4
5 1601

6
7 1602 **A1. Equations.** The Flamar-Para(o)voz is a “2.5 D” FLAC-like code (Cundall, 1989). It has a mixed
8
9 1603 finite-difference/finite element numerical scheme, in which the coordinate frame is Cartesian 2D, but
10
11 1604 stress/strain relations are computed in a 3D formulation. The Lagrangian mesh of Paravoz is
12
13 1605 composed of quadrilateral elements subdivided onto 2 couples of triangular sub-elements with tri-
14
15 1606 linear shape functions. Para(o)voz is a large strain fully explicit time-marching algorithm. It locally
16
17 1607 solves full Newtonian equations of motion in continuum mechanics approximation:
18
19

$$\langle \rho \ddot{\mathbf{u}} \rangle - \text{div} \boldsymbol{\sigma} - \rho \mathbf{g} = 0 \quad (\text{A1})$$

20
21
22
23
24 1608 coupled with constitutive equations:
25

$$\frac{D\boldsymbol{\sigma}}{Dt} = F(\boldsymbol{\sigma}, \mathbf{u}, \nabla \dot{\mathbf{u}}, \dots, T \dots) \quad (\text{A2})$$

26
27
28
29
30
31 1609 and with equations of heat transfer (heat advection $\mathbf{u} \nabla T$ in the equation below is solved
32
33 1610 separately):
34

$$\rho C_p D T / D t + \dot{\mathbf{u}} \nabla T - k \text{div}(\nabla T) - H_r = 0 \quad (\text{A3})$$

$$\rho = \rho_0(1 - \alpha T)$$

35
36
37
38
39
40
41 1611 Here \mathbf{u} , $\boldsymbol{\sigma}$, \mathbf{g} , k are the respective terms for the displacement, stress, acceleration due to body
42
43 1612 forces and thermal conductivity. The triangular brackets in (A1) specify conditional use of the related
44
45 1613 term (in quasi-static mode inertial terms are dumped using inertial mass scaling (Cundall, 1989)).
46
47 1614 The terms t , ρ , C_p , T and H_r designate respectively time, density, specific heat, temperature and
48
49 1615 internal heat production. The terms D/Dt , $D\boldsymbol{\sigma}/Dt$, F are a time derivative, an objective (Jaumann)
50
51 1616 stress time derivative and a functional, respectively. In the Lagrangian method, incremental
52
53 1617 displacements are added to the grid coordinates allowing the mesh to move and deform with
54
55 1618 material. This enables solution of large-strain problems locally using a small-strain formulation. On
56
57
58
59
60

1
2
3 1619 each time step the solution is obtained in local coordinates, which are then updated in a large strain
4
5 1620 mode.

6
7
8 1621 Solution of (A1) provides velocities at mesh points used for computation of element strains and of
9
10 1622 heat advection $\mathbf{u} \nabla T$. These strains are used in (A2) to calculate element stresses and equivalent
11
12 1623 forces as input for the computation of the velocities for the next time step. Due to the explicit
13
14 1624 approach, there are no convergence issues, which is rather a common problem of implicit methods
15
16 1625 in case of non-linear rheologies. The algorithm automatically checks and adopts the internal time
17
18 1626 step using 0.1 – 0.5 of Courant's criterion for propagation of information, which warrants a stable
19
20 1627 solution.

21
22
23
24 1628

25 26 1629 **A2. Explicit EVP rheology.**

27
28
29 1630 We use a serial (Maxwell type) body (eq. 1), in which total strain increment in each numeric element
30
31 1631 is defined by a sum of elastic, viscous and brittle strain increments. Consequently, in contrast to
32
33 1632 fluid dynamic approaches, where non-viscous rheological terms are simulated using pseudo-plastic
34
35 1633 and pseudo-elastic viscous terms (e.g. Bercovici *et al.*, 2001; Solomatov & Moresi, 2000), our
36
37 1634 method explicitly treats all rheological terms. The parameters of elastic-ductile-plastic rheology laws
38
39 1635 for crust and mantle come from rock mechanics data (**Tables A1 and A2**; Kirby & Kronenberg,
40
41 1636 1987; Kohlstedt *et al.*, 1995).

42
43
44
45 1637

46 47 1638 **Plastic (brittle) behavior.**

48
49 1639 The brittle behavior of rocks is described by Byerlee's law (Byerlee, 1978; Ranalli, 1995), which
50
51 1640 corresponds to Mohr-Coulomb material with a friction angle $\phi = 30^\circ$ and cohesion $|C_0| < 20$ MPa
52
53 1641 (e.g., Gerbault *et al.*, 1998):

$$\tau = C_0 - \sigma_n \tan\phi \quad (A4)$$

1642 where σ_n is normal stress $\sigma_n = \frac{1}{3}\sigma_1 + \sigma_{II}^{\text{dev}} \sin\phi$, $\frac{1}{3}\sigma_1 = P$ is the effective pressure, σ_{II}^{dev} is the
 1643 second invariant of deviatoric stress, or effective shear stress. The condition of transition to brittle
 1644 deformation (function of rupture f) reads as: $f = \sigma_{II}^{\text{dev}} + P \sin\phi - C_0 \cos\phi = 0$ and $\partial f/\partial t = 0$. In terms of
 1645 principal stresses, the equivalent of the yield criterion (5) reads as:

$$\sigma_1 - \sigma_3 = -\sin\phi (\sigma_1 + \sigma_3 - 2C_0/\tan\phi) \quad (A5)$$

1647 **Elastic behavior.**

1648 The elastic behavior is described by the linear Hooke's law:

$$\sigma_{ij} = \lambda \varepsilon_{ii} \delta_{ij} + 2G \varepsilon_{ij} \quad (A6)$$

1649 where λ and G are Lamé's constants. Repeating indexes mean summation and δ is Kronecker's
 1650 operator.

1652 **Viscous (ductile) behavior.**

1653 Mantle convection and a part of lithospheric deformation is controlled by thermally activated creep
 1654 (Ranalli, 1995; Kirby & Kronenberg, 1987). Within deep lithosphere and underlying mantle regions,
 1655 the creeping flow is non-Newtonian since the effective viscosity can vary within 10 orders of
 1656 magnitude as a function of differential stress:

$$e_{ij}^d = A (\sigma_1 - \sigma_3)^n \exp(-Q/R^*T) \quad (A7)$$

1657 Where $e_{ij}^d = \dot{\varepsilon}_{ij}^d$ is shear strain rate, A is material constant, n is the power law exponent, Q is the
 1658 activation enthalpy, R is Boltzmann's gas constant, and T is temperature in K°, σ_1 and σ_3 are the
 1659 principal stresses. The effective viscosity μ_{eff} for this law is defined as:

$$\tau_{ij} \equiv \mu_{eff} e_{ij}^d$$

1660 which yields:

$$\mu_{eff} = e_{ij}^{d(1-n)/n} A^{-1/n} \exp(Q(nRT)^{-1}) \quad (A8)$$

1661 For non-uniaxial deformation, the law (A8) is converted to a triaxial form, using invariant of strain
1662 rate and geometrical proportionality factors:

$$\mu_{eff} = e_{ij}^{d(1-n)/n} A^{-1/n} \exp(Q(nRT)^{-1})$$

1663 where

$$e_{II}^d = (\ln v_{II}(\mathbf{e}_{ij}))^{1/2} \quad \text{and} \quad A^* = \frac{1}{2}A \cdot 3^{(n+1)/2} \quad (A9)$$

1664 parameters A, n, Q are experimentally determined material constants (**Table A1**). Using olivine
1665 parameters (**Table A1**), one can verify that the predicted effective viscosity at the base of the
1666 lithosphere is $10^{19} - 5 \times 10^{19}$ Pa s matching post-glacial rebound data (Turcotte & Schubert, 2002).
1667 In the depth interval of 200 km - 0 km the effective viscosity grows from 10^{19} to $10^{25} - 10^{27}$ Pa s with
1668 decreasing temperature. Within the adiabatic temperature interval at depth, the dislocation flow law
1669 (A8) is replaced by nearly Newtonian diffusion creep, which results in a quasi-constant mantle
1670 viscosity of $10^{19} - 10^{21}$ Pa s (e.g., Turcotte & Schubert, 2002). Weinberg & Podladchikov (1994)
1671 have also shown that the effective viscosity in close vicinity of an ascending diapir is influenced by
1672 the local strain rate field and partly by heat exchanges between the diapir and surrounding rock,
1673 which suggests possible changes.

1674

1
2
3 1675 **FIGURE CAPTIONS**
4

5 1676
6

7
8 1677 **Figure 1.** Concepts of folding in rheologically stratified lithosphere and feedback with sedimentation
9
10 1678 in downfolded areas and erosion of adjacent highs. Different simultaneously occurring wavelengths
11
12 1679 of crustal and mantle folding are a consequence of the rheological stratification of the lithosphere.
13
14 1680 Surface wavelengths can be affected also by feedback with surface processes.
15

16 1681
17

18 1682 **Figure 2.** Map with examples of well-documented areas affected by lithospheric folding. Areas:
19
20 1683 Central Indian Ocean Basin (CIOB) (Geller *et al.*, 1983 ; Stein *et al.*, 1989) ; NW European platform
21
22 1684 (Bourgeois *et al.*, 2007 ; Lefort & Agarwal, 1996; Marotta *et al.*, 2000); Pannonian Basin (Dombradi
23
24 1685 *et al.*, 2010); Iberia (Cloetingh *et al.*, 2002; De Vicente *et al.*, 2007; Fernandez-Lozano *et al.*, 2010);
25
26 1686 Central Asia (Burov *et al.*, 1993; Nikishin *et al.*, 1993; Burov & Molnar, 1998); Tibet/ Himalayan
27
28 1687 syntaxis belt (Burg & Podlachikov, 1999; Shin *et al.*, 2009); Central Australia (Stephenson &
29
30 1688 Lambeck, 1985; Lambeck, 1983); Arctic Canada (Stephenson *et al.*, 1990); Transcontinental Arch
31
32 1689 of North America (Ziegler *et al.*, 1995); South Caspian Basin (Guest *et al.*, 2007); Laramide
33
34 1690 Foreland (USA) (Tikoff & Maxson, 2001); Barents Sea (Ritzmann & Faleide, 2009) (map credit:
35
36 1691 NASA).
37
38 1692
39

40 1692
41

42 1693 **Figure 3.** Relationship between wavelengths of lithospheric folding and thermo-tectonic age of
43
44 1694 lithosphere. The grey zones correspond to theoretical folding wavelengths derived for the upper
45
46 1695 crust, mantle and coupled whole mantle folding, based on an analytical model that accounts for
47
48 1696 strength variations as a function of thermo-mechanical age (Cloetingh *et al.*, 1999). Black squares
49
50 1697 are estimates for wavelengths of differential topography and thermo-tectonic ages inferred from
51
52 1698 observational studies. Numbers refer to sites listed in Table 1.
53
54

55 1699
56
57
58
59
60

1
2
3 1700 **Figure 4.** (a) Map showing major tectonic features of Tien Shan area of Central Asia , with location
4
5 1701 of folding profiles discussed in Burov *et al.* (1993), Burov & Molnar (1998) and Cloetingh *et al.*
6
7 1702 (1999). (b) Neotectonic movements along the profiles AD and CD (Burov *et al.*, 1993). Modified
8
9 1703 after Cloetingh *et al.* (1999). (c) Measured and calculated Bouguer gravity anomalies for lithosphere
10
11 1704 under horizontal compression along profile F across the Ferghana basin with corresponding
12
13 1705 topography profile (d) (after Burov & Molnar, 1998). Predicted topography and Moho geometry for
14
15 1706 Airy and best fitting folding scenario. During compression the amplitude of plate deflection changed
16
17 1707 significantly while the wavelength of folding stayed constant (Burov & Molnar, 1998). Red lines are
18
19 1708 Bouguer anomaly predicted by folding model and Moho depression, respectively. Solid grey line is
20
21 1709 Airy isostasy. Solid black line is Airy Moho. Triangles indicate observed Bouguer anomaly. Green is
22
23 1710 topography above sea level. FB: Ferghana Basin.
24
25
26

27 1711
28
29 1712 **Figure 5.** First order features of basin geometry of folded lithosphere of Iberia. (a) Topography
30
31 1713 displaying cylindrical patterns of alternating parallel trending highs and lows and corresponding
32
33 1714 gravity anomalies (red line) (see Cloetingh *et al.*, 2002). (b) Results from analogue modelling
34
35 1715 experiments, displaying pop-up structures underlying topographic highs, accompanied by folding of
36
37 1716 the Moho (Fernandez-Lozano *et al.*, 2010). Top panel shows final top view of the analogue model
38
39 1717 and location of the cross-section shown below. Arrow indicates the direction of the moving wall. λ is
40
41 1718 the wavelength of folding.
42
43
44

45 1719
46
47 1720 **Figure 6.** (a) Map of elevation of basement in the NW Alpine foreland with rift signature removed
48
49 1721 from the map of actual basement (from Bourgeois *et al.*, 2007). Dashed lines show axes of Late
50
51 1722 Neogene lithospheric folds, with a succession of anticlines and synclines: the Normandy-
52
53 1723 Vogelsberg anticline (NVA), Sologne-Franconian Basin Syncline (SFS) and the Burgundy-Swabian
54
55 1724 Jura Anticline (BSJA). LBR: London Brabant Ridge with thick crust. BF: Black Forest; FB
56
57 1725 Franconian Basin; E: Eifel; H: Hunsruck; S: Sauerland; T: Taunus; V: Vosges. (b) Cross sections of
58
59
60

1
2
3 1726 top basement in the NW Alpine foreland with rift signatures removed (Bourgeois *et al.*, 2007; see for
4
5 1727 location Fig. 6a). Thin line: actual topography surface. Bold line: elevation of top basement as
6
7 1728 predicted in the absence of rifting. Fold signatures are similar with a wavelength λ of 270 km and
8
9
10 1729 amplitude A of 1500 m in the Franconian Basin (Cross section G-G') and in the upper Rhine Graben
11
12 1730 area (Cross section H-H'). In the Paris basin, development of folds with assumed same wavelength
13
14 1731 and amplitude (stippled bold line in cross section C-C'), implies subsidence of Sologne and uplift of
15
16 1732 Normandy.
17

18
19 1733
20
21 1734 **Figure 7.** (a) Schematic E-W cross section through the Pannonian-Carpathian basin system
22
23 1735 (Cloetingh *et al.*, 2008), displaying anomalous Late Neogene acceleration of the subsidence
24
25 1736 between isochrons 2 and 0 Ma in the centre of the Pannonian basin and the Focsani depression of
26
27 1737 the Southern Carpathian foredeep, flanked by uplifting highs. Wavelengths of the differential vertical
28
29 1738 motions are typically of the order of 250 km. (b) Interpreted seismic section in the central part of the
30
31 1739 Pannonian Basin (Sacchi *et al.*, 1999) showing evidence for late Neogene crustal scale folding at
32
33
34 1740 scales of 20-40 km. Note syn-rift grabens formed during the Miocene back-arc extension of the
35
36 1741 basin. (c) Results of analogue tectonic experiments carried out to examine the patterns of
37
38 1742 differential vertical motions in the northern part of the Pannonian Basin and surrounding areas
39
40 1743 (Dombradi *et al.*, 2010), demonstrating a-typical folding of variable amplitude with a wavelength
41
42 1744 equivalent to 200-250 km.
43

44 1745
45
46 1746 **Figure 8.** Schematic north-south trending cross-section illustrating the basic tectonic setting for
47
48 1747 northern Iran and the South Caspian Basin (Guest *et al.*, 2007), illustrating basin inversion of the
49
50 1748 central Iranian basin, pronounced differential topography at the transition of the Alborz mountains,
51
52 1749 with a topographic high of several km's and the South Caspian Basin with about 20 km of
53
54
55 1750 sedimentary infill.
56

57 1751
58
59
60

1
2
3 1752 **Figure 9.** Characteristic patterns of continental lithosphere deformation induced by folding of the
4
5 1753 lithosphere for with time increasing amounts of horizontal shortening for a 150 Ma old lithosphere
6
7 1754 with convergence rates of **(a)** 1.5 cm/yr and **(b)** 3 cm/yr. From left to right: material phase
8
9
10 1755 distribution (with blue for the crust, orange for the mantle lithosphere and red for the upper mantle
11
12 1756 below the lithosphere), temperature, effective viscosity, and topography.

13
14 1757
15
16 1758 **Figure 10.** Characteristic patterns of continental lithosphere deformation induced by folding of
17
18 1759 lithosphere with time. Increasing amounts of horizontal shortening for a 300 Ma old lithosphere with
19
20 1760 convergence rates of **(a)** 1.5 cm/yr and **(b)** 3 cm/yr. From left to right: phase distribution,
21
22 1761 temperature, effective viscosity, and topography.

23
24 1762
25
26
27 1763 **Figure 11. (a)** Characteristic subsidence patterns in centre of synclinal depression for thermo-
28
29 1764 mechanical age of 150 and 300 Ma, respectively. Shortening rate is 3 cm/year. **(b)** Characteristic
30
31 1765 stages in the evolution of a basin formed by lithospheric folding. Stage 1: Basin formation stage,
32
33 1766 acceleration of subsidence and uplift during folding. Stage 2: Steady-state: equilibrium between
34
35 1767 tectonic subsidence and sediment supply from eroding highs. Stage 3: Capture of folded basin;
36
37 1768 overall uplift and erosion. Wiggled waved blue line marks position of base level.

38
39 1769
40
41
42 1770 **Figure 12.** Illustration of the effect of erosion, which acts as a filter suppressing the short
43
44 1771 wavelengths. In this case, the wavelength and amplitude vary along the cross section at different
45
46 1772 stages of deformation due to a partial crust-mantle coupling and strain localization for a 400 Ma old
47
48 1773 lithosphere with weak quartz -dominated rheology. After 5 percent shortening (top), after 25 percent
49
50 1774 shortening (middle), after 25 percent shortening, strong zero order diffusional erosion (Avouac &
51
52 1775 Burov, 1996) tuned to keep mean elevation at the level of 3000 m. Erosion reduces the contribution
53
54 1776 of gravity-dependent terms (middle wavelength) and accelerates local deformation. Strong erosion,
55
56
57
58
59
60

1
2
3 1777 insufficiently compensated by the tectonic deformation wipes out most of the topography (after
4
5 1778 Cloetingh *et al.*, 1999).

6
7 1779
8
9
10 1780 **Figure 13.** Thermal consequences of lithosphere folding, and associated basin evolution depicted in
11
12 1781 Fig. 11. The heat flow response is marked by an initial decrease in heat flow as a consequence of
13
14 1782 rapid sedimentation, followed by a progressive long-term heat flow increase after termination of
15
16 1783 shortening. Thermal conductivity of sediments is $2.5 \text{ Wm}^{-1}\text{C}^{-1}$. Surface radiogenic heat production
17
18 1784 H_s is $9.5 \times 10^{-10} \text{ Wkg}^{-1}$. Concentration of radiogenic heat sources within sedimentary basin fill is
19
20 1785 homogeneous. Exponential decay of heat production is assumed for underlying crustal rocks. Note
21
22 1786 that the figure shows only 7 Ma of thermal evolution. The heat flow does not increase anymore after
23
24 1787 some tens of Ma and subsequently decreases at later stages.

25
26
27 1788
28
29 1789 **Figure 14.** Results of analogue tectonic experiments for lithospheric folding (after Sokoutis *et al.*,
30
31 1790 2005) (Top): folding of uniform lithosphere. Cross section demonstrating pop-up structures in the
32
33 1791 upper crust above highs induced by lithospheric folding. λ_1 and λ_2 indicate first-order and second-
34
35 1792 order wavelengths, respectively. Imbrication of bivergent thrust wedges is responsible for the
36
37 1793 relatively high topography belt (Σ -belt) at the right-hand of the model and closure of prismatic basins
38
39 1794 with a rather undisturbed bottom. The progressive sinking of the prismatic basin allows transferring
40
41 1795 of the crustal material (i.e. cover sediments) that was initially situated at the surface of the model
42
43 1796 down to significant depth. Left-side (a) final top view of model after 34% of bulk shortening. Right
44
45 1797 side (b) cross-section located on the top view. Arrows indicate the direction of the moving wall. Note
46
47 1798 the similarity to Central Iberia (**Fig. 5**). (Bottom): Geometries predicted by analogue experiment,
48
49 1799 shortening a lithosphere with two contrasting blocks, bounded by suture. A deep synclinal
50
51 1800 depocentre develops over the suture zone, flanked by an anticline of smaller amplitude. Left-side (c)
52
53 1801 final top view of model after 26% of bulk shortening. Right side (d) cross-section located on the top
54
55
56
57
58
59
60

1
2
3 1802 view. λ_1 indicates a first-order wavelength of the folding. Note the striking similarity to the
4
5 1803 configuration of the South Caspian Basin/ Alborz Mountain system displayed in **Fig. 8**.

6
7 1804
8
9
10 1805 **Figure 15.** Numerical experiment on faulting developed in folded continental lithosphere of 150 Ma
11
12 1806 (Burov & Molnar, 1998). Note different wavelengths of the crustal and mantle part of the lithosphere
13
14 1807 and differences in spacing and character of faults that are conditioned by folding. In each layer, two
15
16 1808 fault spacings occur: a shorter one proportional to layer thickness (also controlled by the strength
17
18 1809 contrast between the stiff layer and embeddings), and the longer wavelength controlled by the
19
20 1810 wavelength of folding. The insert shows plastic (brittle) strain localization characterizing initialization
21
22 1811 of mantle faulting.

23
24 1812
25
26
27 1813 **Figure 16.** Comparison of main characteristics of basins developed on folded lithosphere (FLB with
28
29 1814 a shortening rate of 3 cm/yr) with other basin types, including foreland basins (FBr = retro-arc
30
31 1815 foreland basin; FBp = pro-arc foreland basin), intracratonic basins (ICB), extensional basins (EB)
32
33 1816 and pull-apart basins (PAB). Different panels give theoretical predictions. (Top): Basin subsidence
34
35 1817 history in basin centre. (Bottom): Thermal history. See text for explanation.

36 1818
37
38
39
40
41
42
43
44
45
46
47
48
49
50
51
52
53
54
55
56
57
58
59
60

TABLE 1

Wavelengths and ages of folded lithosphere displayed in Fig. 3 (see Fig. 2 for location)

	Area	Thermo-tectonic age (Ma)	Folding wavelength λ (km)	References
1	Tien Shan	175	200-250	Burov & Molnar, 1998; Burg <i>et al.</i> , 1994
2	Western Goby	175-400	300-360	Nikishin <i>et al.</i> , 1993; Burov <i>et al.</i> , 1993
3	Central Asia	370-430	50-70 (crust) 300-400 (litho-mantle)	Nikishin <i>et al.</i> , 1993; Burov <i>et al.</i> , 1993
4	Himalayan syntaxis belt	8-10	150	Burg & Podlachikov, 1999
5	Central Australia	500-900	550-650	Lambeck, 1983; Stephenson & Lambeck, 1985; Beekman <i>et al.</i> , 1997
6	Russian platform	400-600	500-600	Nikishin <i>et al.</i> , 1997
7	South Caspian Basin	125-155	350-450	Guest <i>et al.</i> , 2007
8	Eastern Black Sea	40-80	50-100 (crust) 100-150 (litho-mantle)	Cloetingh <i>et al.</i> , 2008
9	Western Black Sea	75-125	50-100 (crust) 100-200 (litho-mantle)	Cloetingh <i>et al.</i> , 2008
10	Pannonian Basin System	20	200-250	Horvath & Cloetingh, 1996; Matenco <i>et al.</i> , 2007 ; Dombradi <i>et al.</i> , 2010
11	NW European platform	180-230	270	Bourgeois <i>et al.</i> , 2007
12	Brittany	210-290	225-275	Bonnet <i>et al.</i> , 2000
13	Iberia	330-370	40-80 (crust) 125-275 (litho-mantle)	Cloetingh <i>et al.</i> , 2002
14	Barents Sea	215-245	550-650	Ritzmann & Faleide, 2009
15	Canadian Arctic	150-250	170-230	Stephenson <i>et al.</i> , 1990
16	Transcontinental Arch of North America	1000-1400	500-700	Ziegler <i>et al.</i> , 1995
17	Laramide foreland (USA)	175-225	190	Tikoff & Maxson, 2001

TABLE 2. Key characteristic features of different classes of sedimentary basins

Basin type	Basin shape	Dimensions	Subsidence characteristics	Thermal evolution	Faulting history
FLB	Symmetrical	Width: 50-600 km; depth: up to 20 km	Accelerated subsidence, time scales 1-10 Myr; simultaneously uplift at highs	No initial heating; heat flow increases in first 10's Myr with sediment deposition and burial, and subsequently decreases	Intensive deformation, accelerating trough basin formation phase
FB	Asymmetrical	Width: 50-250 km; depth: up to 10 km	Linear subsidence, interrupted by short-lived faster subsidence during thrusting phases; timescales 10-100 Myr; simultaneously uplift from thrust front and foreland bulge	No initial heating; heat flow increases with time with sediment deposition and burial	Faulting and thrusting limited to orogenic wedge; minor deformation through faulting in foreland
EB	Symmetrical (pure shear); asymmetrical (simple shear)	Width: 30-500 km; depth: up to 10 km	Rapid initial subsidence, followed by post-rift decay in subsidence; in case of multiple rifting repeated accelerated subsidence; time scales for post-rift subsidence of the order of 70 Myr; At rifting stage development takes place of asymmetrical rift shoulder topography, flanking the rift	Initial heating event, followed by decaying heat flow	Extensional faulting limited to basin formation phase; during post-rift absence of faulting
PAB	Symmetrical	Width: 20-50 km; depth: up to 10 km	Very rapid initial subsidence, followed by post-rift decay in subsidence, time scales: 1-10 Myr In early stage, sedimentation cannot keep up with subsidence	Initial heating event, followed by very rapid decay in heat flow	Extensional faulting limited to basin formation phase; during post-rift absence of faulting
ICB	Symmetrical	Width: 500-1000 km; depth: up to 10 km	Slow subsidence, punctuated by periods of faster subsidence, possibly related to large-scale tectonic events; Characteristic time scales: 500-800 Myr	In absence of understanding of basin formation mechanism no prediction for initial heat flow; Heat flow at later stage dominated by burial history	Very low level of faulting throughout tectonic history

8 **Table A1**

9 Notations and physical values common for all experiments (Turcotte and Schubert, 2002; Schubert
10 *et al.*, 2001)

11	Parameter	Values and units	Definition
12	σ, τ	Pa, MPa	stress (complete, deviatoric)
13	P	Pa, MPa	pressure
14	u	m, mm	displacement vector
15	v	m s^{-1} , mm an^{-1}	velocity vector
16	$\dot{\varepsilon}$	s^{-1}	strain rate
17	μ	10^{19} - 10^{25} Pa s	effective viscosity ($\tau/\dot{\varepsilon}$)
18	T	$^{\circ}\text{C}$, K	temperature
19	h_c	40 km	Moho depth
20	h_l	100 - 250 km	thickness of lithosphere
21	D	100 - 200 km	plume diameter
22	ρ	3330 kg m^{-3}	density of mantle lithosphere
23	ρ_m	3340 kg m^{-3}	reference deep mantle density
24	ρ_p	$\rho_m + \Delta\rho_{\text{ch}} + \alpha\rho_m\Delta T$	plume density
25	$\Delta\rho_{\text{ch}}$	$0\text{-}25 \text{ kg m}^{-3}$	chemical density contrast
26	g	9.8 m s^{-2}	acceleration due to gravity
27	C_p	$10^3 \text{ J Kg}^{-1} \text{ }^{\circ}\text{C}^{-1}$	specific heat
28	ΔT	250°C	initial temperature contrast plume - background
29	α	$3 \times 10^{-5} \text{ }^{\circ}\text{C}^{-1}$	thermal expansion coefficient at 0 km depth
30	β	$8 \times 10^{-12} \text{ Pa}^{-1}$	isothermal compressibility

32

Table A2. Specific rheology and related thermal parameters. Compilation by Burov *et al.* (2001). ρ is density; Q , n , A are material-dependent parameters of ductile flow laws (Kirby & Kronenberg, 1987; Kohlstedt *et al.*, 1995). Other parameters from Turcotte & Schubert (2002).

Parameter	Value
All rocks	
λ , G Lamé elastic constants ($\lambda = G$)	30 GPa (above 250 km depth)
λ , G Lamé elastic constants ($\lambda = G$)	60 GPa (below 250 km depth)
ϕ friction angle (Mohr-Coulomb criterion)	30°
C_0 cohesion (Mohr-Coulomb criterion)	20 MPa
<u>Specific upper or weak (quartz) lower-crust properties</u>	
ρ (upper crust)	2700 kg m ⁻³
ρ (lower crust)	2900 kg m ⁻³
n	2.4
A	6.7×10^{-6} MPa ⁻ⁿ ·s ⁻¹
Q	1.56×10^5 kJ·mol ⁻¹
<u>Specific strong lower crust properties (diabase or basalt)</u>	
ρ	2980 kg m ⁻³
n	3.4
A	2×10^{-4} MPa ⁻ⁿ ·s ⁻¹
Q	2.6×10^5 kJ·mol ⁻¹
<u>Specific mantle properties (olivine)</u>	
ρ (lithosphere)	3330 kg m ⁻³
n	3
A	1×10^4 MPa ⁻ⁿ ·s ⁻¹
Q	5.2×10^5 kJ·mol ⁻¹
<u>Thermal model</u>	
Surface temperature (0 km depth)	0 °C
Temperature at the bottom of thermal lithosphere	1330 °C
Temperature at 660 km depth	2000 °C
Thermal conductivity of crust k	2.5 Wm ⁻¹ °C ⁻¹
Thermal conductivity of mantle k	3.5 Wm ⁻¹ °C ⁻¹
Thermal diffusivity of mantle χ	10 ⁻⁶ m ² ·s ⁻¹
Surface radiogenic heat production H_s	9.5×10^{-10} W kg ⁻¹
Radiogenic heat production decay depth h_r	10 km
Thermo-tectonic age of the lithosphere a	60 (young) to 1000 Ma (old)

1
2
3
4
5
6
7
8
9
10
11
12
13
14
15
16
17
18
19
20
21
22
23
24
25
26
27
28
29
30
31
32
33
34
35
36
37
38
39
40
41
42
43
44
45
46
47
48
49
50
51
52
53
54
55
56
57
58
59
60

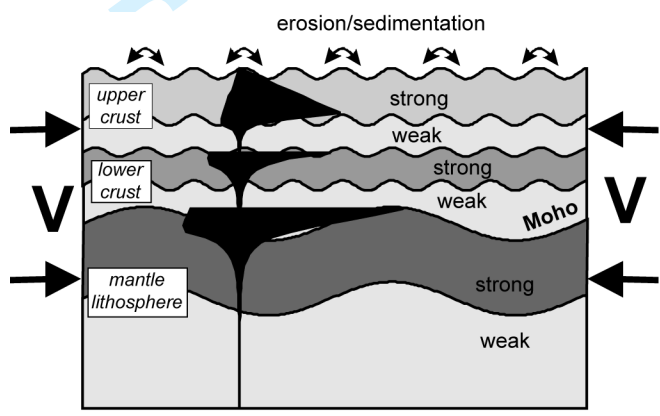


Figure 1

1
2
3
4
5
6
7
8
9
10
11
12
13
14
15
16
17
18
19
20
21
22
23
24
25
26
27
28
29
30
31
32
33
34
35
36
37
38
39
40
41
42
43
44
45
46
47
48
49
50
51
52
53
54
55
56
57
58
59
60

Figure 2

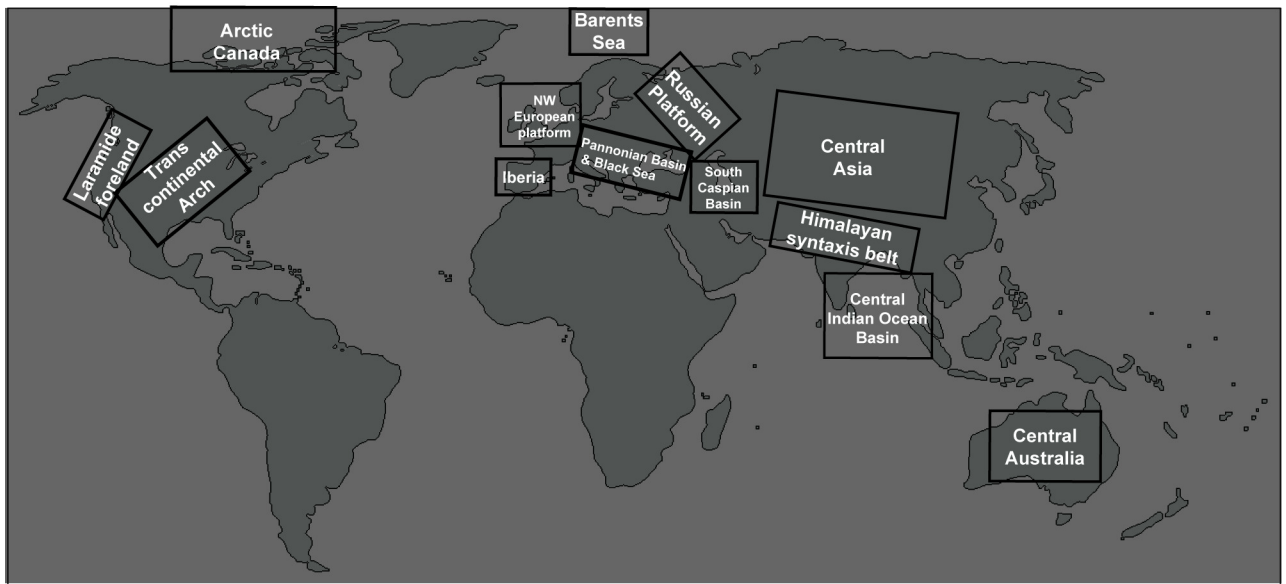
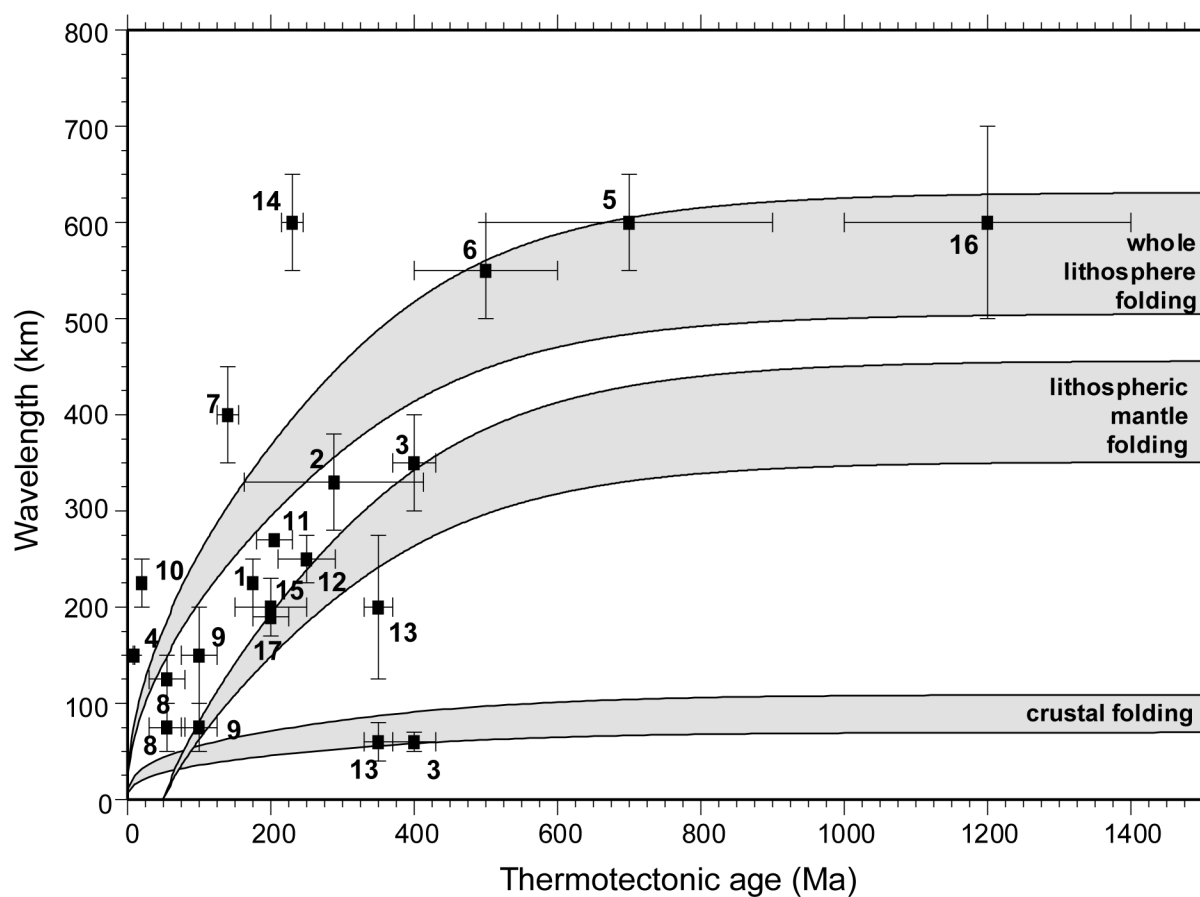
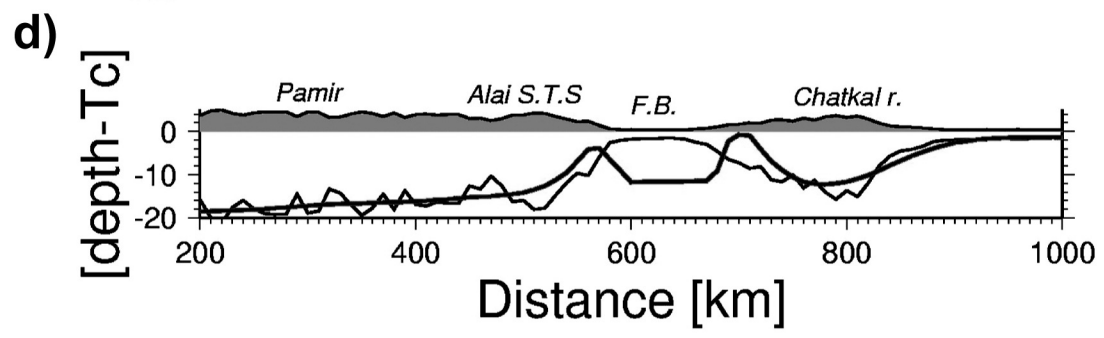
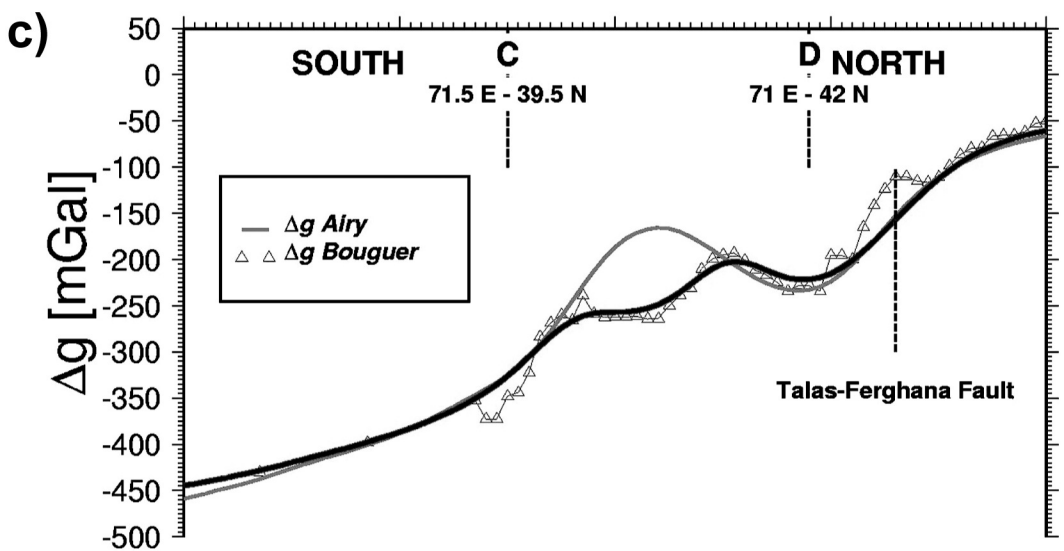
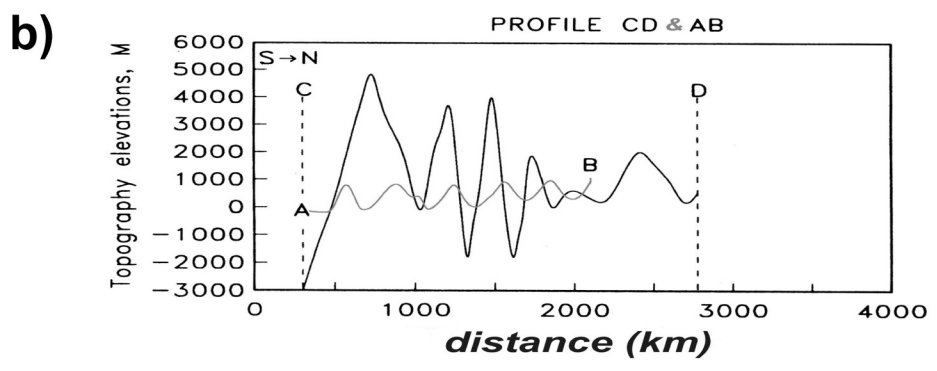
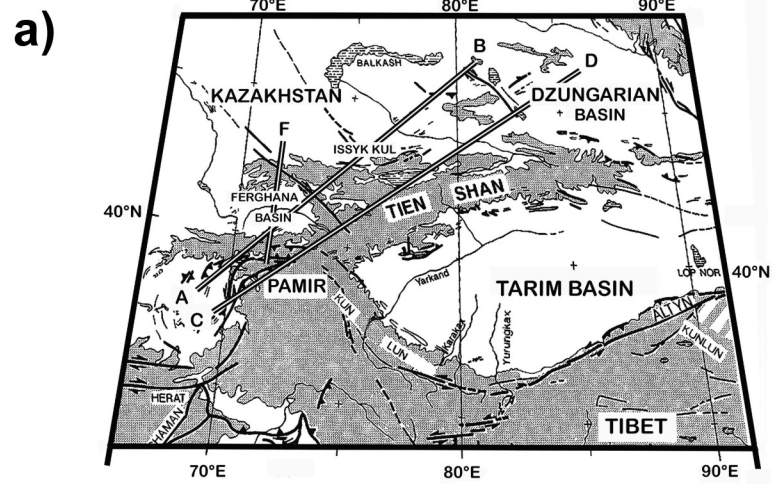


Figure 3



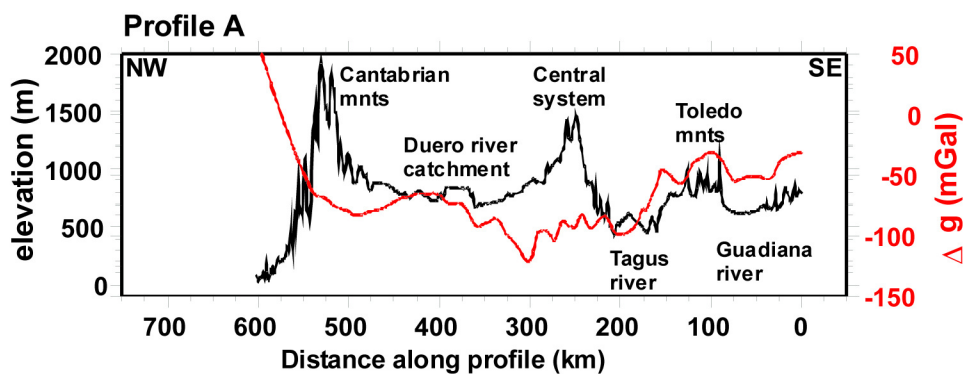
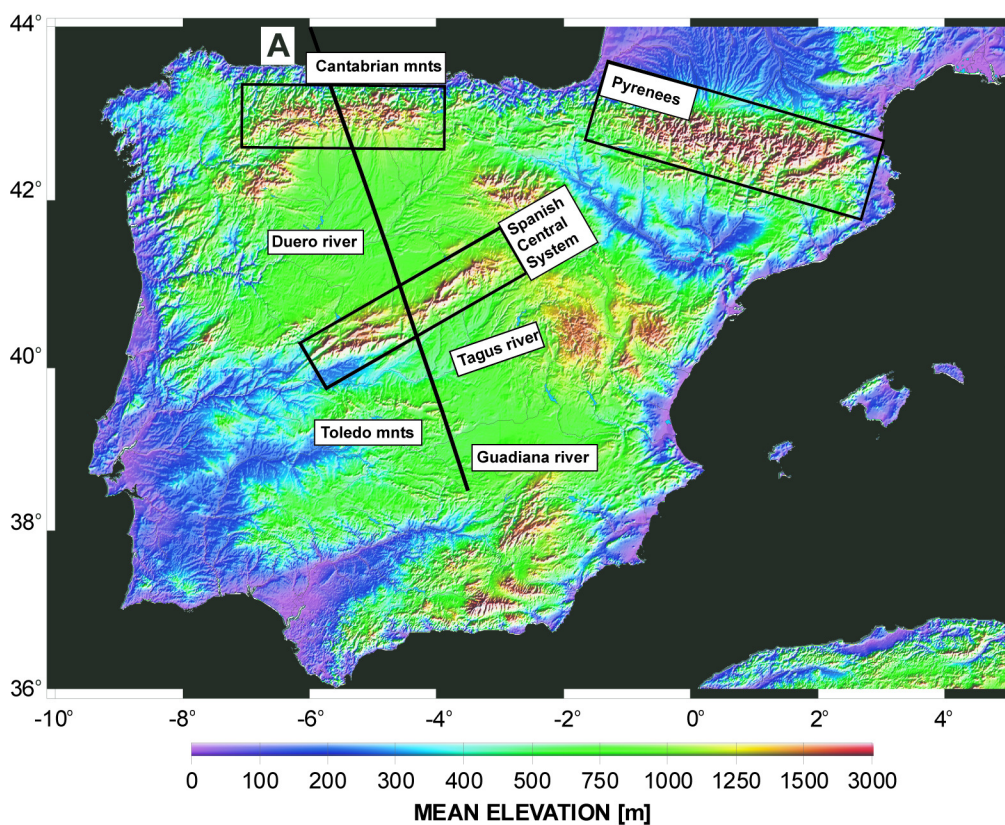
1
2
3
4
5
6
7
8
9
10
11
12
13
14
15
16
17
18
19
20
21
22
23
24
25
26
27
28
29
30
31
32
33
34
35
36
37
38
39
40
41
42
43
44
45
46
47
48
49
50
51
52
53
54
55
56
57
58
59
60

Figure 4



1
2
3
4
5
6
7
8
9
10
11
12
13
14
15
16
17
18
19
20
21
22
23
24
25
26
27
28
29
30
31
32
33
34
35
36
37
38
39
40
41
42
43
44
45
46
47
48
49
50
51
52
53
54
55
56
57
58
59
60

Figure 5a



1
2
3
4
5
6
7
8
9
10
11
12
13
14
15
16
17
18
19
20
21
22
23
24
25
26
27
28
29
30
31
32
33
34
35
36
37
38
39
40
41
42
43
44
45
46
47
48
49
50
51
52
53
54
55
56
57
58
59
60

Figure 5b

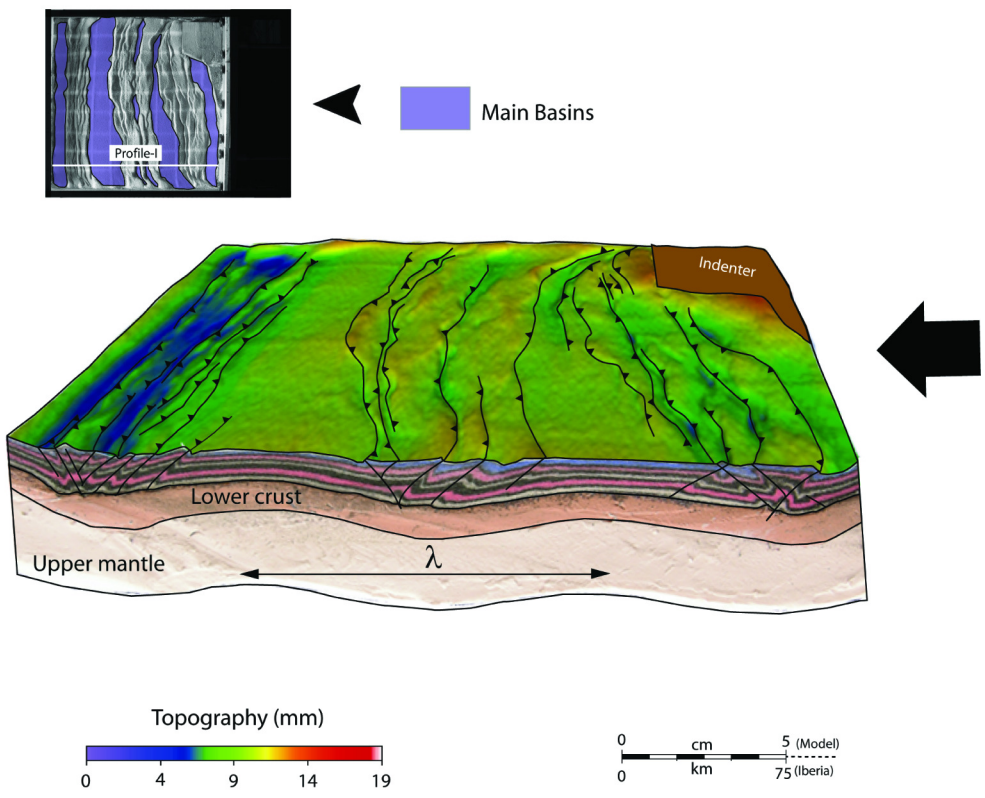
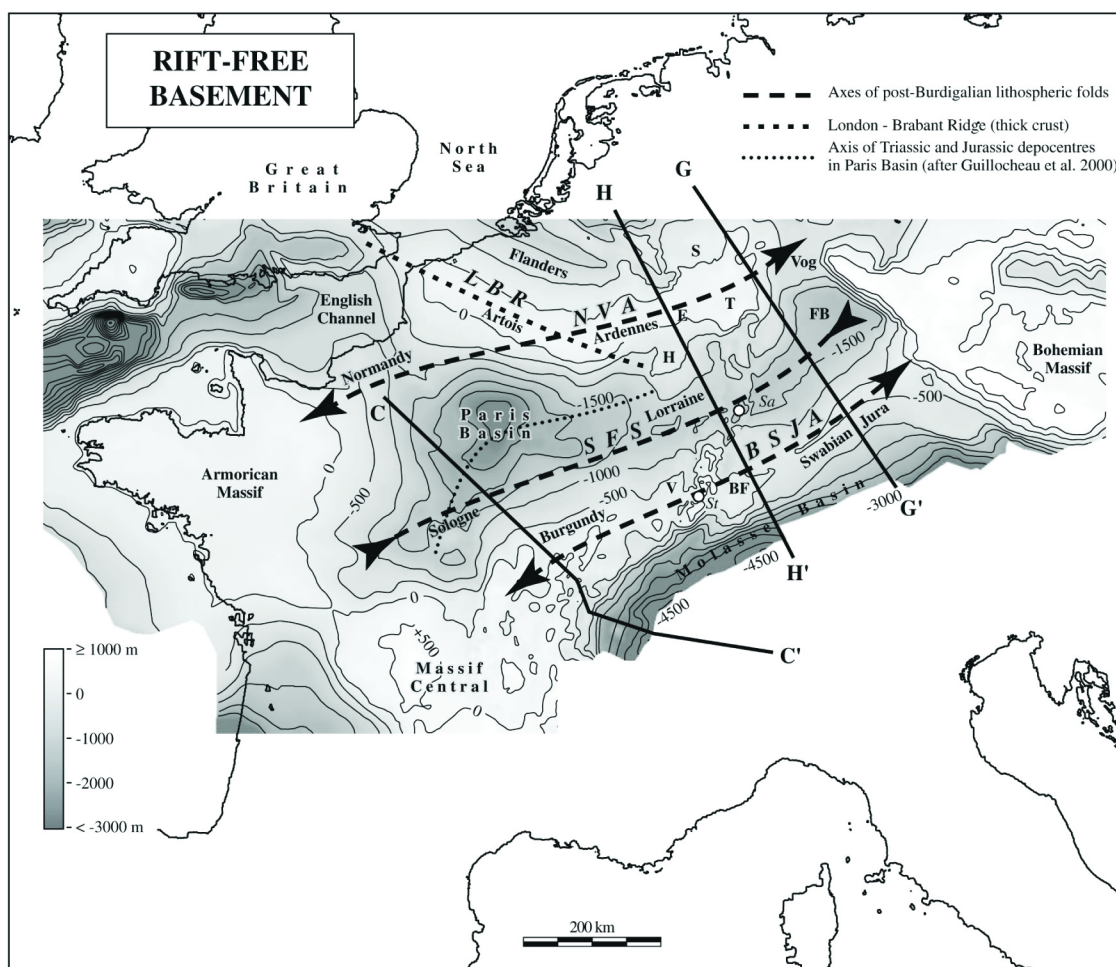
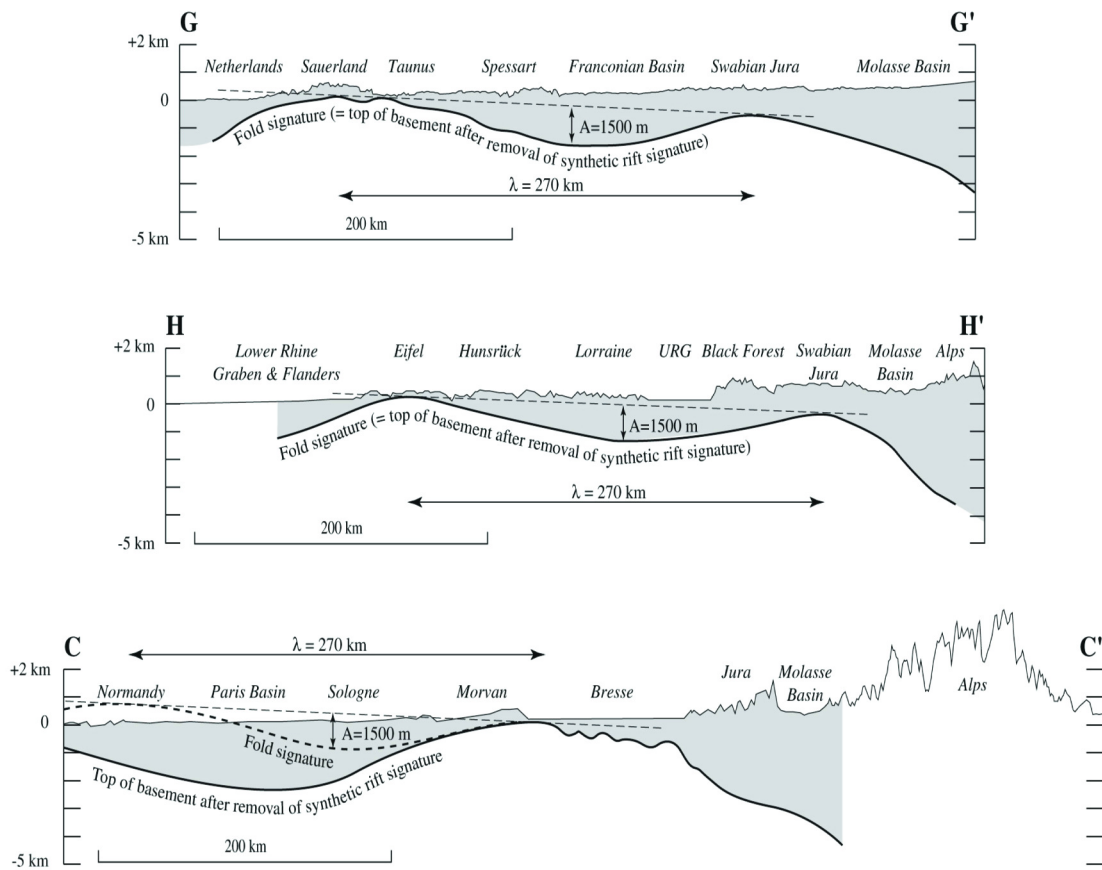


Figure 6a



1
2
3
4
5
6
7
8
9
10
11
12
13
14
15
16
17
18
19
20
21
22
23
24
25
26
27
28
29
30
31
32
33
34
35
36
37
38
39
40
41
42
43
44
45
46
47
48
49
50
51
52
53
54
55
56
57
58
59
60

Figure 6b



1
2
3
4
5
6
7
8
9
10
11
12
13
14
15
16
17
18
19
20
21
22
23
24
25
26
27
28
29
30
31
32
33
34
35
36
37
38
39
40
41
42
43
44
45
46
47
48
49
50
51
52
53
54
55
56
57
58
59
60

1
2
3
4
5
6
7
8
9
10
11
12
13
14
15
16
17
18
19
20
21
22
23
24
25
26
27
28
29
30
31
32
33
34
35
36
37
38
39
40
41
42
43
44
45
46
47
48
49
50
51
52
53
54
55
56
57
58
59
60

Figure 7a

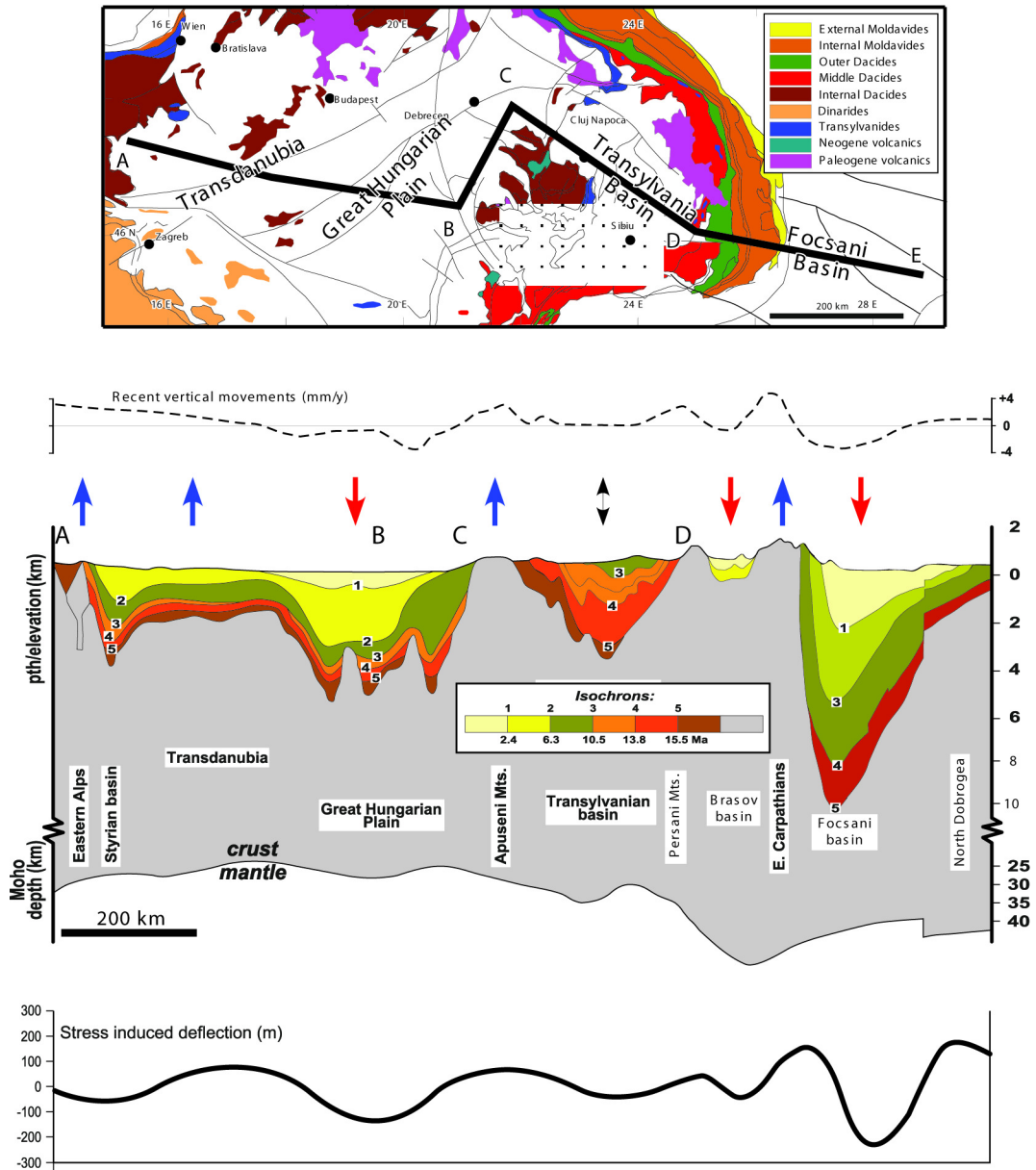
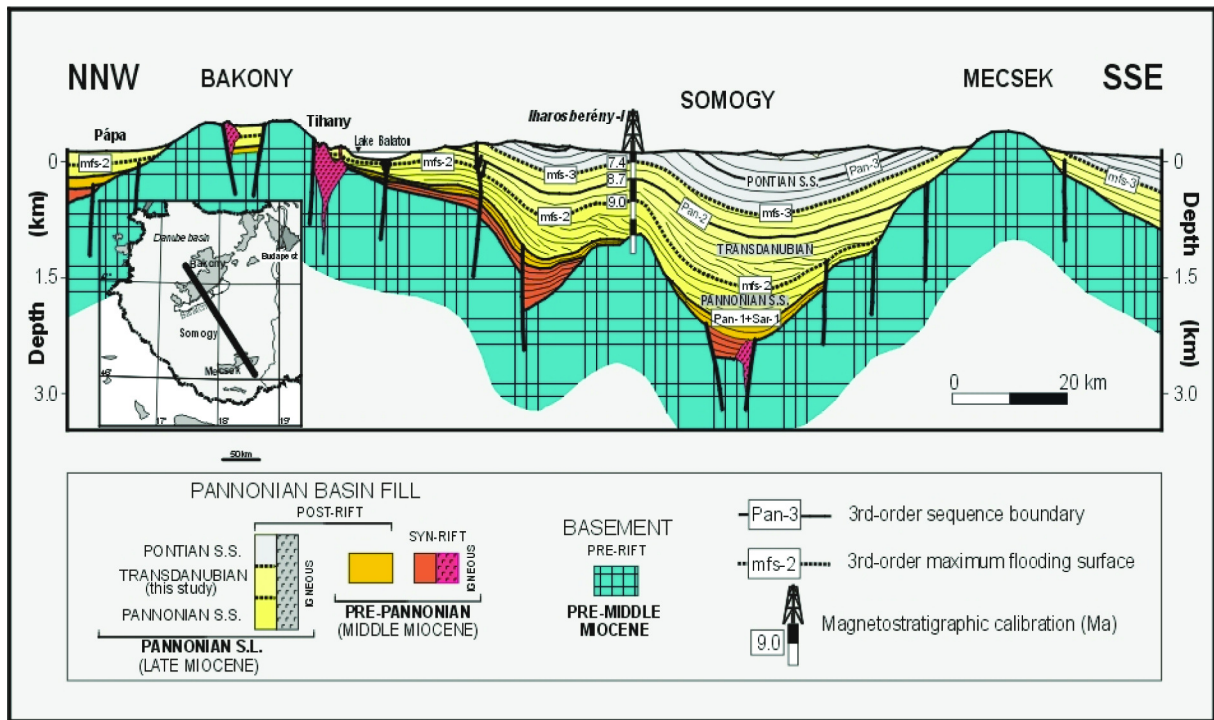


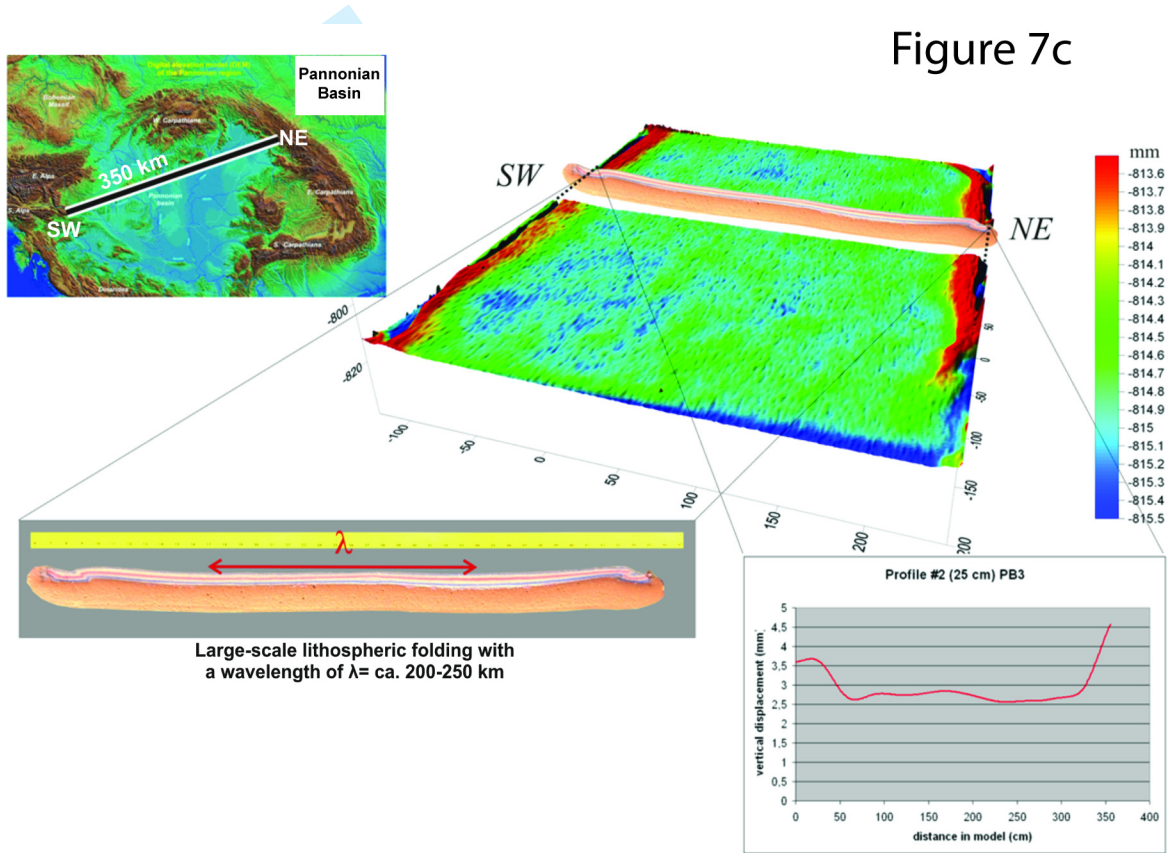
Figure 7b



1
2
3
4
5
6
7
8
9
10
11
12
13
14
15
16
17
18
19
20
21
22
23
24
25
26
27
28
29
30
31
32
33
34
35
36
37
38
39
40
41
42
43
44
45
46
47
48
49
50
51
52
53
54
55
56
57
58
59
60

1
2
3
4
5
6
7
8
9
10
11
12
13
14
15
16
17
18
19
20
21
22
23
24
25
26
27
28
29
30
31
32
33
34
35
36
37
38
39
40
41
42
43
44
45
46
47
48
49
50
51
52
53
54
55
56
57
58
59
60

Figure 7c



1
2
3
4
5
6
7
8
9
10
11
12
13
14
15
16
17
18
19
20
21
22
23
24
25
26
27
28
29
30
31
32
33
34
35
36
37
38
39
40
41
42
43
44
45
46
47
48
49
50
51
52
53
54
55
56
57
58
59
60

Figure 8

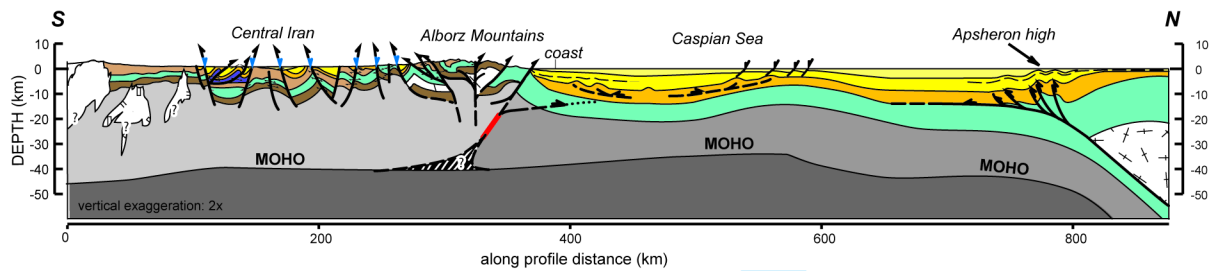
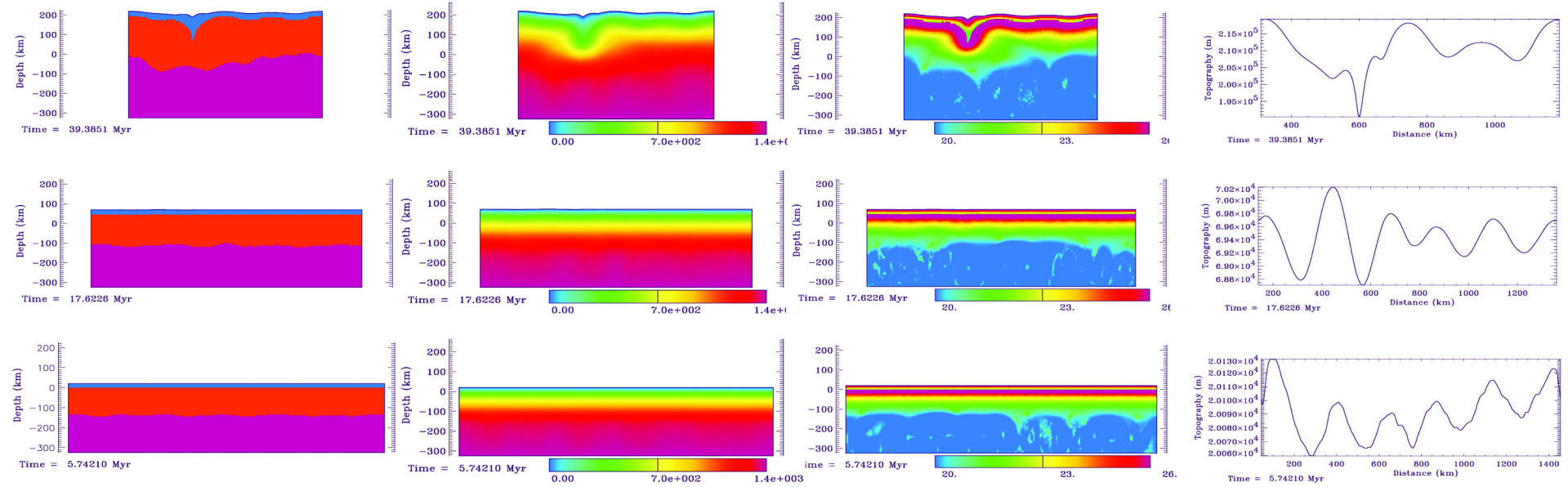
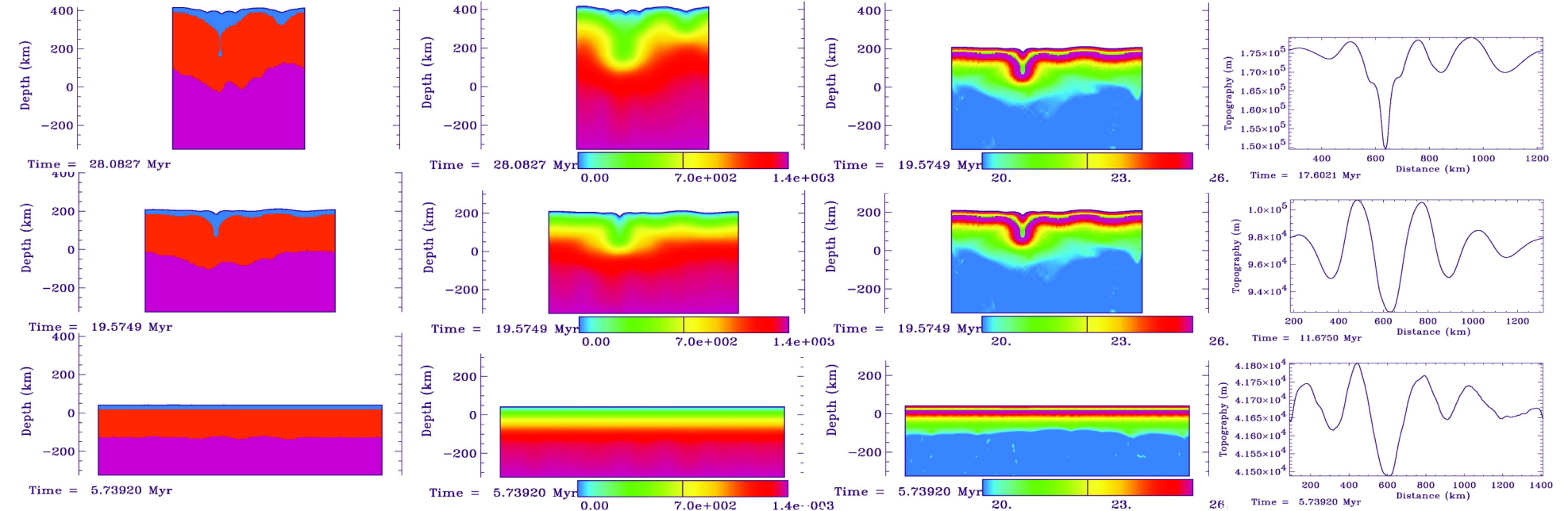


Figure 9

a) $t=150$ Ma, $v=1.5$ cm/yr



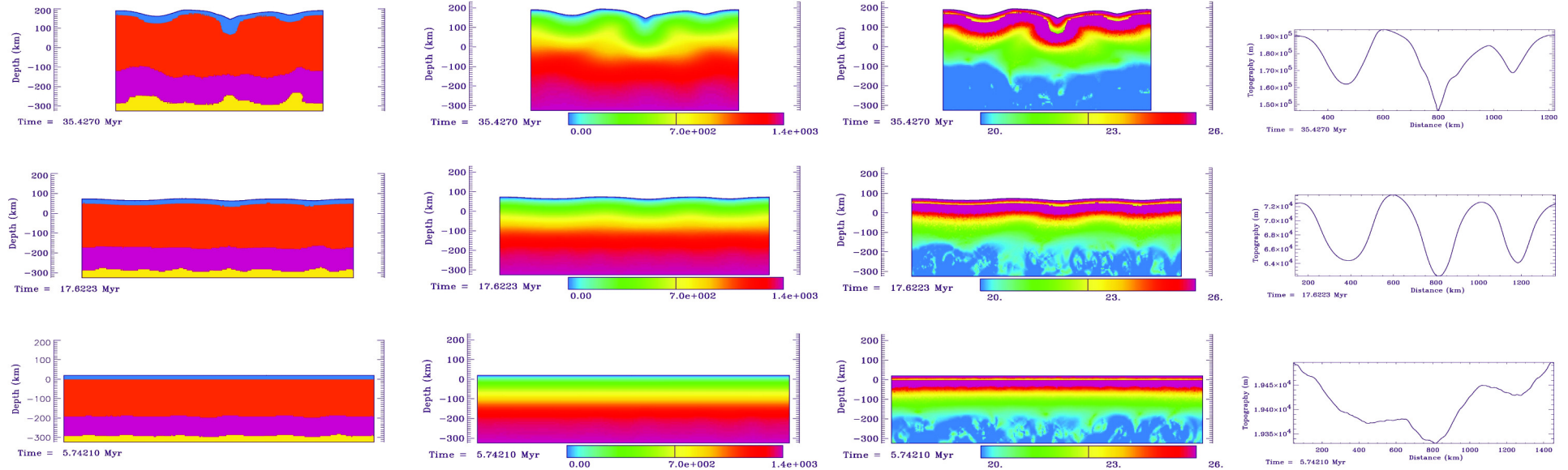
b) $t=150$ Ma, $v=3.0$ cm/yr



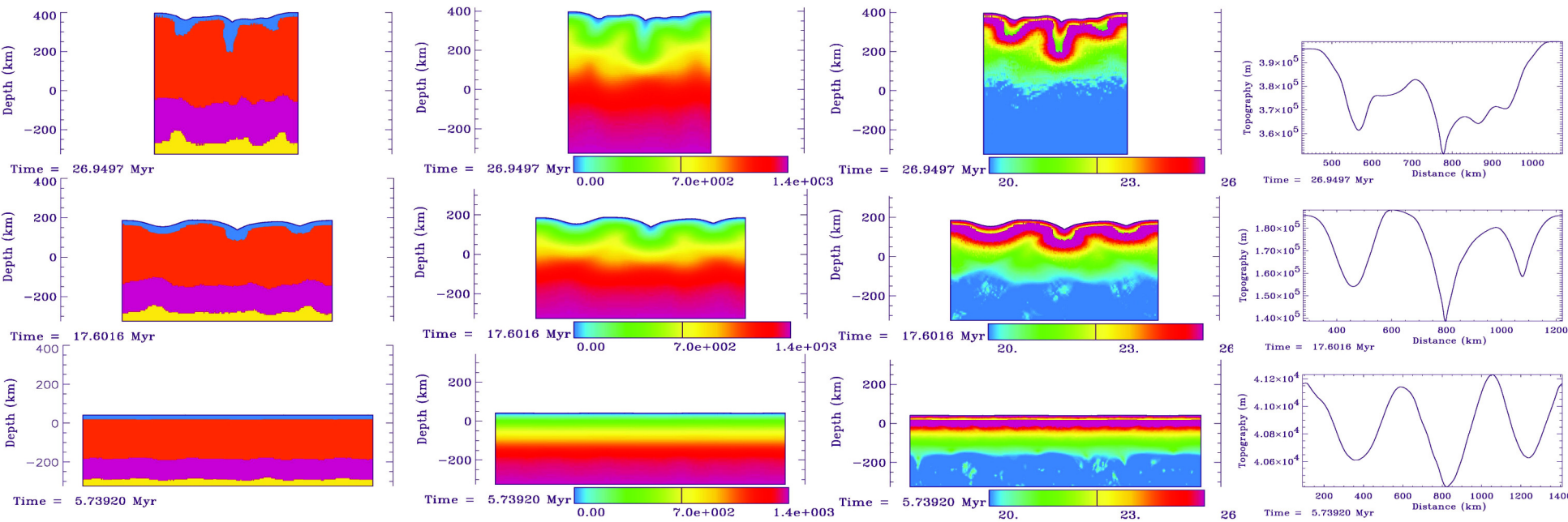
1
2
3
4
5
6
7
8
9
10
11
12
13
14
15
16
17
18
19
20
21
22
23
24
25
26
27
28
29
30
31
32
33
34
35
36
37
38
39
40
41
42
43
44
45
46
47

Figure 10

a) t=300 Ma, v=1.5 cm/yr

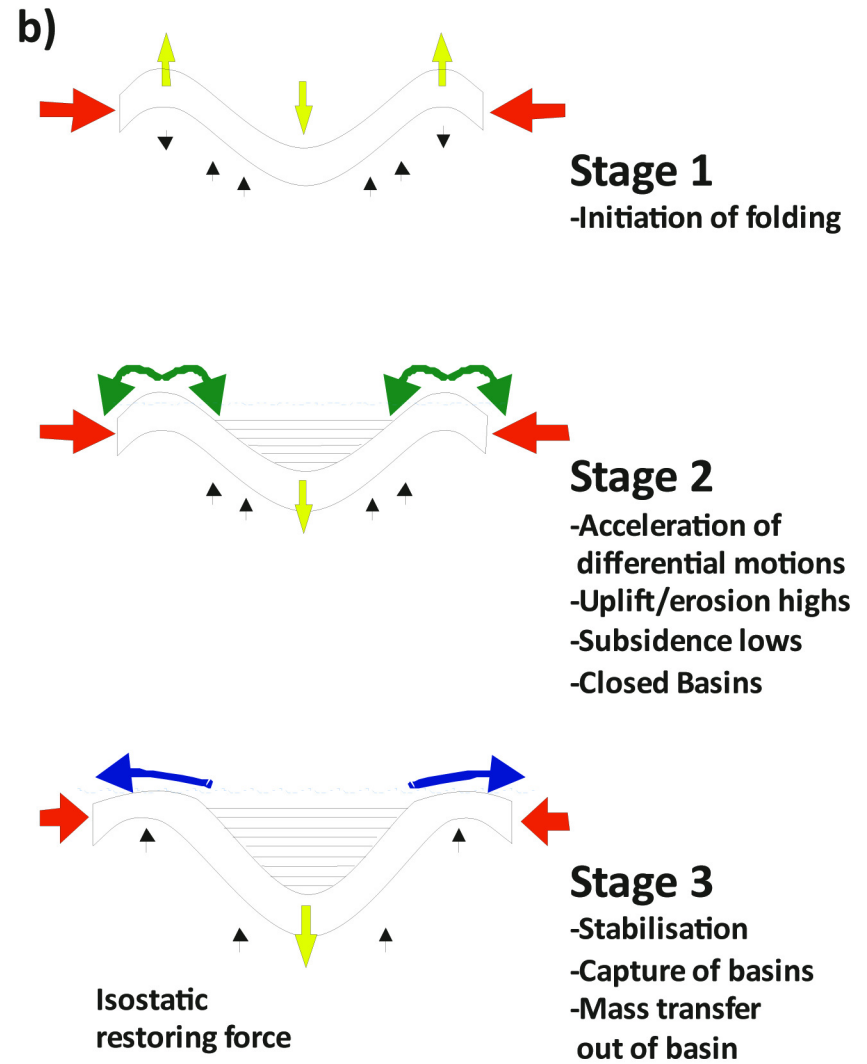
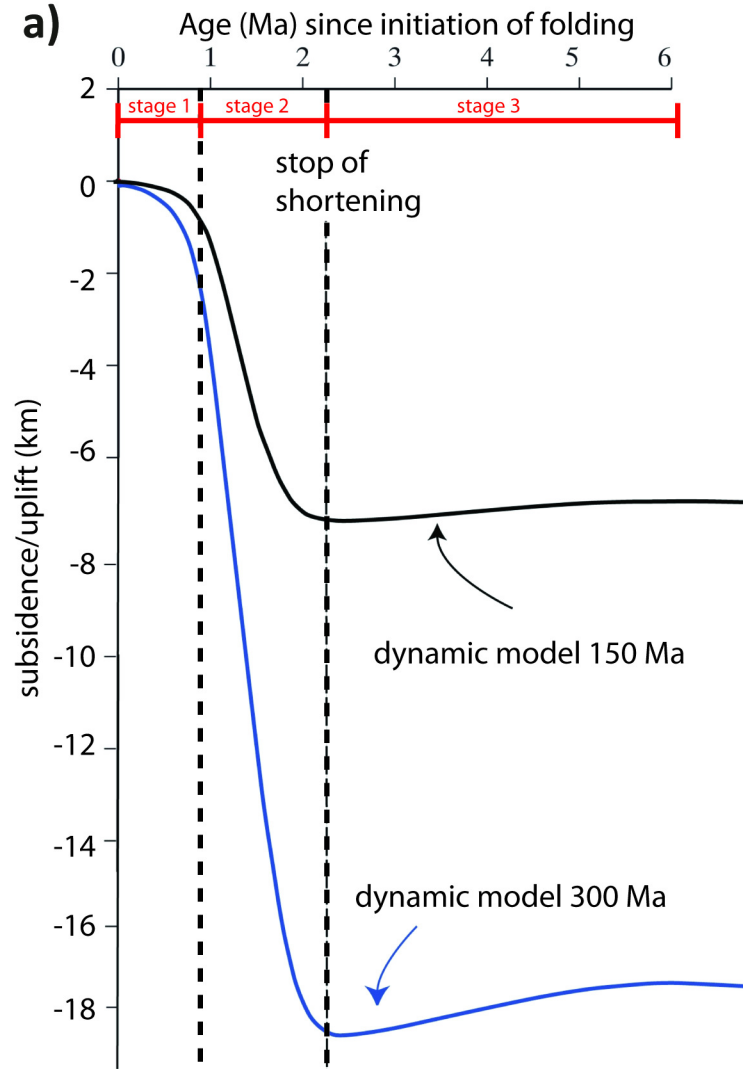


b) t=300 Ma, v=3.0 cm/yr



1
2
3
4
5
6
7
8
9
10
11
12
13
14
15
16
17
18
19
20
21
22
23
24
25
26
27
28
29
30
31
32
33
34
35
36
37
38
39
40
41
42
43
44
45
46
47

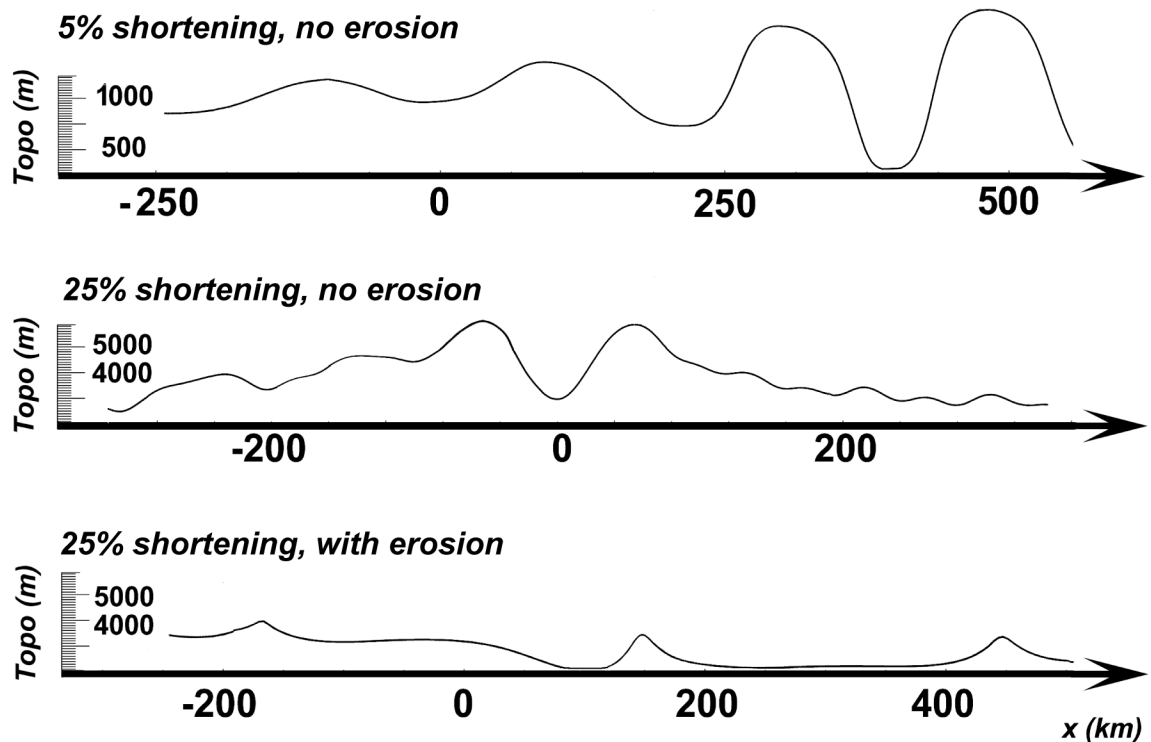
Figure 11



1
2
3
4
5
6
7
8
9
10
11
12
13
14
15
16
17
18
19
20
21
22
23
24
25
26
27
28
29
30
31
32
33
34
35
36
37
38
39
40
41
42
43
44
45
46
47

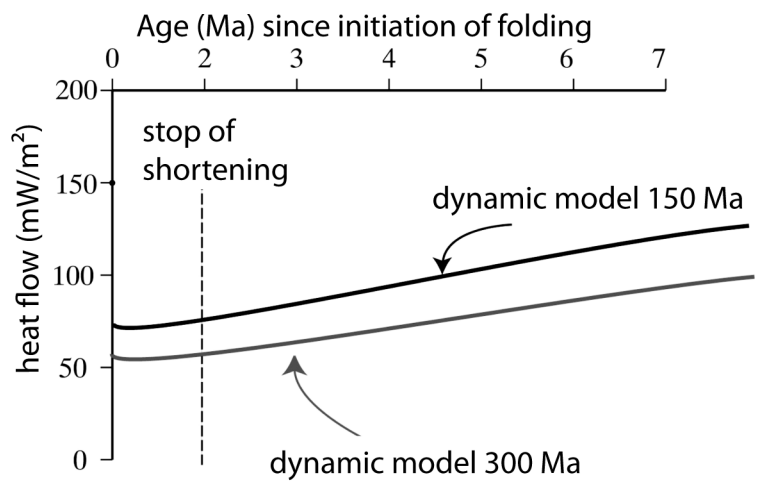
1
2
3
4
5
6
7
8
9
10
11
12
13
14
15
16
17
18
19
20
21
22
23
24
25
26
27
28
29
30
31
32
33
34
35
36
37
38
39
40
41
42
43
44
45
46
47
48
49
50
51
52
53
54
55
56
57
58
59
60

Figure 12



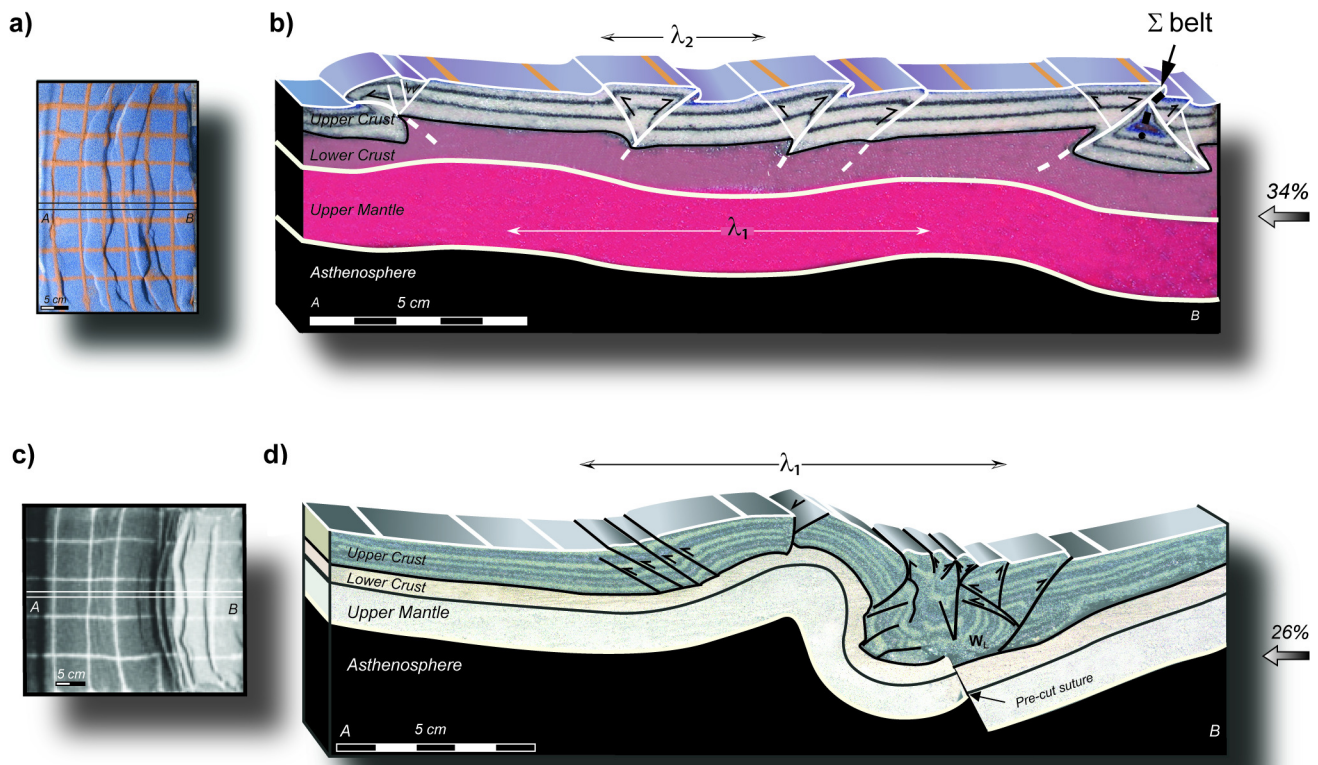
1
2
3
4
5
6
7
8
9
10
11
12
13
14
15
16
17
18
19
20
21
22
23
24
25
26
27
28
29
30
31
32
33
34
35
36
37
38
39
40
41
42
43
44
45
46
47
48
49
50
51
52
53
54
55
56
57
58
59
60

Figure 13



1
2
3
4
5
6
7
8
9
10
11
12
13
14
15
16
17
18
19
20
21
22
23
24
25
26
27
28
29
30
31
32
33
34
35
36
37
38
39
40
41
42
43
44
45
46
47
48
49
50
51
52
53
54
55
56
57
58
59
60

Figure 14



1
2
3
4
5
6
7
8
9
10
11
12
13
14
15
16
17
18
19
20
21
22
23
24
25
26
27
28
29
30
31
32
33
34
35
36
37
38
39
40
41
42
43
44
45
46
47
48
49
50
51
52
53
54
55
56
57
58
59
60

Figure 15

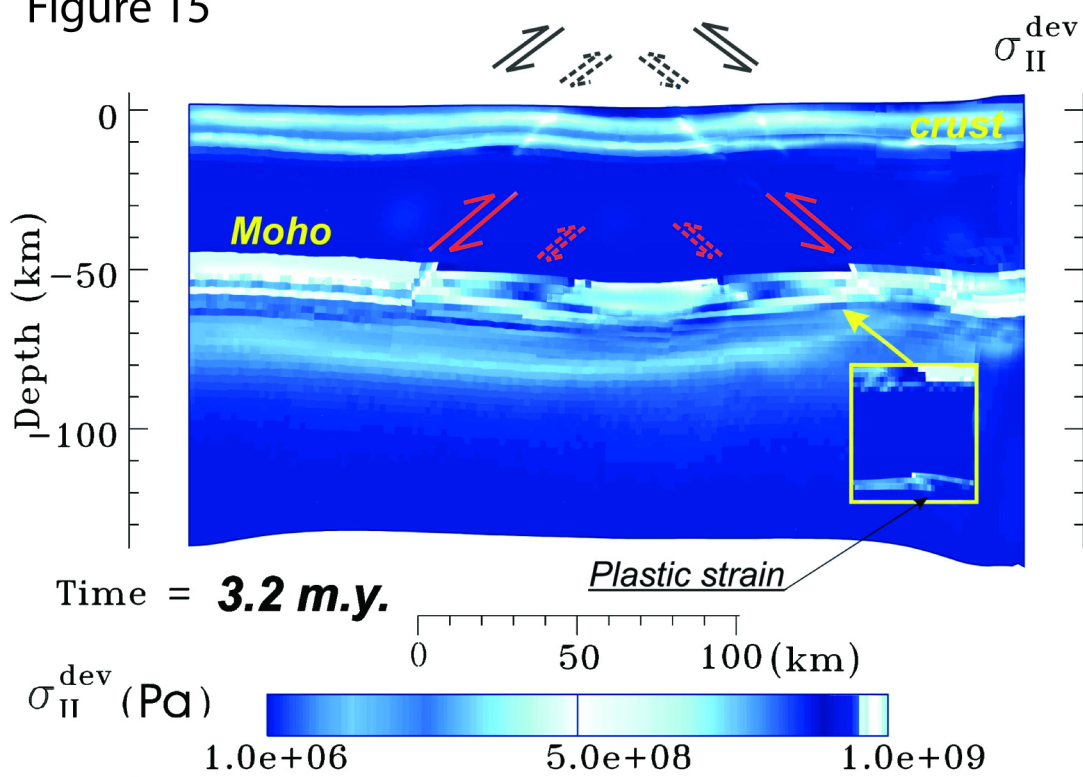


Figure 16

